Order Number 8909154

Bond between aggregate and fly ash cements

Jashimuddin, Jahangir, Ph.D.

Iowa State University, 1988

U·M·I
300 N. Zeeb Rd.
Ann Arbor, MI 48106

Bond between aggregate and fly ash cements

by

Jahangir Jashimuddin

A Dissertation Submitted to the

Graduate Faculty in Partial Fulfillment of the

Requirements for the Degree of

DOCTOR OF PHILOSOPHY

Department: Civil and Construction Engineering
Major: Geotechnical Engineering

Approved:

Signature was redacted for privacy.

In Charge of Major Work

Signature was redacted for privacy.

For the Major Department

Signature was redacted for privacy.

For the Graduate College

Iowa State University
Ames, Iowa

1988

TABLE OF CONTENTS

LIST OF TABLES

LIST OF FIGURES

In the Name of God the Compassionate, the Merciful

INTRODUCTION

Bond strength between fly ash derived cements and aggregate is a critical factor in controlling strength and duribility of fly ash stabilized road bases.

Combination of lime and portland cement with fly ash has been tested as a road base stabilizer for several years. However, recent abundance of high calcium cementitious fly ashes from modern power plants offers potential for new stabilization techniques using fly ash alone.

Past research on bond strength was limited to portland cement; no research was done on fly ash cement-aggregate bond. Also most of the previous research concentrated on mechanical measurement of bond strength, but did little to explain its fundamental nature.

This research reports an evaluation and explanation of bond between fly ash cement and limestone aggregate, with Type I portland cement as a control. Experimental variables were fly ash type, additives, water-cement ratio and age. Parameters of evaluation were bond strength and interface characterization by compound composition, elemental distribution, and pore size distribution. Bond strength of fly ash cements with and without additives was measured and compared to bond strength of Type I portland cement. Correlations were found between bond strength and interface chemical composition.

SCOPE AND OBJECTIVES

The strength of concrete depends upon the strength of the paste, the strength of the coarse aggregate, and the strength of the paste-aggregate interface. There is considerable evidence to indicate that the interface is the weakest region of concrete because of the inevitable presence of flaws and cracks.

In general, bond failure occurs before the failure of either the paste or aggregate. The bond region is weak because cracks invariably exist at the paste-aggregate interface even for continuously moist cured concrete and even before the application of any external load because of drying shrinkage. However, no information on bond strengths between aggregate and fly ash can be found in the literature.

This investigation was designed to obtain information about the magnitude of bond strength, factors favoring good bond strength, substances formed at the interface which might act as chemical "glue", redistribution and diffusion of elements across the interface region, and effect of aggregate-cement paste interaction on the pore size distribution of concrete.

The scope of this research includes the following:

1. Measurement of bond strength between limestone aggregate and fly ash as centered on four factors: (i) type of cement; (ii) effect

of additive; (iii) water-cement ratio of cement paste and (iv) age of cement paste.

2. X-ray diffraction investigation of limestone, cement paste and the interface region, to find which reaction product(s) results from limestone and paste interaction.
3. Electron microprobe analysis at paste-aggregate interface regions to investigate redistribution of elements.
4. Studies of pore size distribution to evaluate physical character of paste-aggregate interaction.

LITERATURE REVIEW

Because no research has been reported in the literature on fly ash cement and aggregate bonding, the review is mainly limited to portland cement-aggregate bonds.

Bond between Aggregate and Cement Paste

General

Bonds may be thought of as the force required to separate two solid components in concrete at their interface. The bond strength depends on the strengths of the cement paste, coarse aggregate, and paste-aggregate interface. A knowledge of the strength of each link and the factors which control each link will enable the researcher to locate the weakest point and concentrate on eliminating the cause of weakness. The three links have not, however, received equal attention from research workers. In particular, the large volume of work relating to the cement matrices can be contrasted with the limited number of investigations designed to show how strongly the matrix adheres to the aggregate [27].

The cement-aggregate bond results from some mechanical interlocking of cement hydration products with the aggregate surface and chemical reaction between aggregate and cement paste. Various studies of the morphological nature of the bond have provided evidence of mechanical interlocking. Other researchers have investigated the

chemical nature of the bond to determine whether chemical reactions occur and to what extent such reactions contribute to bond strength. The degree to which the bond results from each of these processes is not known [31].

Strength and durability of concrete are of most concern to the user. Because the strength of the cement-aggregate bond is generally less than the strength of either the paste or the aggregate, the bond would seem to be a weak link in the development of concrete strength. Studies have been done to investigate the influence of bond on the strength of concrete; however, few studies have addressed the role of cement aggregate bond in the freeze-thaw aspect of concrete durability. Valenta [36] suggested that a reduction in the incidence of bond cracks would decrease the permeability and, hence, improve the durability of concrete.

Structure and properties of the contact layer

Concrete mechanical behavior is a function of the following phases [2]:

1. binder continuous matrix;
2. discontinuous skeleton of the aggregate; and
3. matrix-aggregate contact region.

The behavior of the matrix-aggregate contact region plays an important role for both tensile and compressive strengths. In general, the pattern of concrete fracture follows the contact surface

zone, which represents the weakest chain link. The contact zone consists of a matrix layer and an adjacent aggregate layer; the two layers are separated by a contact surface (Fig. 1a). Physical forces and interactions may exist between the matrix and the aggregate (Fig. 1b). These forces are generated by the adhesive and interlocking forces, as well as by matrix-aggregate interpenetration subsequent to cement paste shrinkage. At this condition, any break occurring in the aggregate-matrix link implies the overtaking of this physical link by a surface crossing the matrix only.

Chemical interaction also takes place between aggregate and matrix, where layers of certain thickness are affected both in the aggregate and the matrix (Fig. 1c); internal cohesive forces develop inside these layers. Owing to new products formed by reactions at the aggregate surface, the interface between aggregate and matrix becomes diffuse and uncertain; the reaction products are generated by epitaxial overgrowth on the surface of the aggregate crystals.

In general, both physical forces (adhesion and interlocking) and chemical interaction (reaction product and epitaxial growth) contribute to bond strength.

Physical forces, which predominate in inert aggregates, essentially depend on aggregate topography and roughness (Fig. 1b). Thus, concrete prepared with polished aggregates such as feldspar or mica (as in granite) is most likely to break at the aggregate-matrix interface irrespective of the strength of the matrix. Microcracks

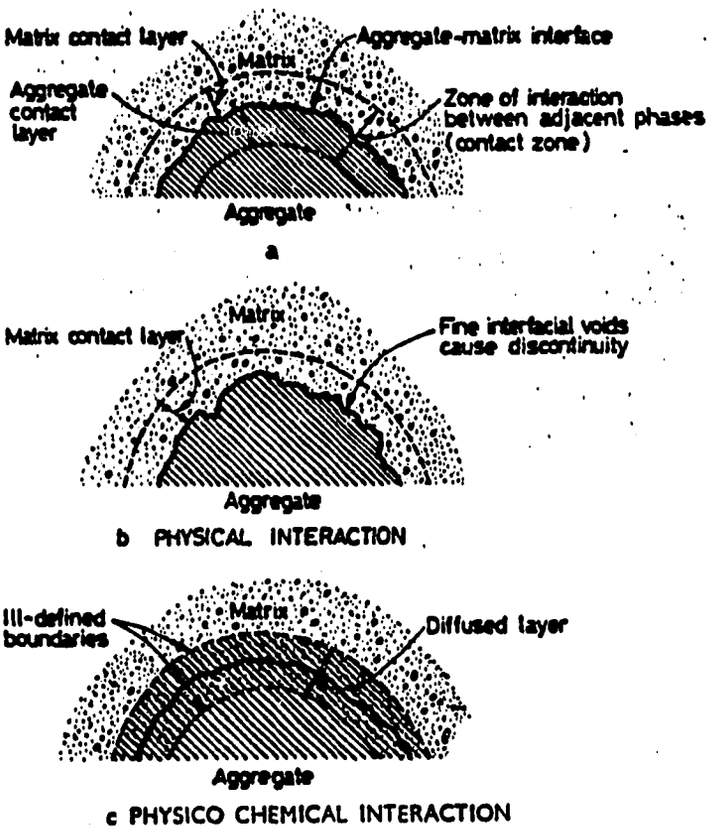

Figure 1. Diagrammatic representation of interactions at the aggregate-matrix interface [2]

start to develop where the maximum value of the force that the interface can stand is exceeded. The fine voids developed over the aggregate surface represent structural breaks in the continuity, and presents an opportunity for the accumulation of a liquid interface phase in favorable conditions. If concrete is submitted to freeze-thaw action or to aggressive chemical agents, the liquid phase changes its volume. This leads to an additional stress on the aggregate-matrix interface; hence, the microcracks will be opened further by overwhelming the existing adhesion forces. The type of cement also plays an important role; cements which subsequent to hydration generate idiomorphic crystals in the contact region are less resistant to aggressive actions than the cements which produce a gel-like mass, wherein a fine crystallization process is initiated.

The intensity of the microcracking process at the matrix-aggregate interface is a function of the following factors: cement type, aggregate mineralogical nature and geometry, water content and concrete hardening conditions.

As for the effects of the aggregate mineralogical nature, the best results are obtained by using calcites and dolomites with freshly crushed surfaces. Aggregate shape, surface structure and stiffness are all factors affecting the strength of the aggregate-matrix bond, mainly because they act as potential stress raisers.

As for the effects due to hardening conditions, it should be

mentioned that, in certain cases, at the end of the autoclaving process subsequent to severe heat treatment, strongly microcracked concretes result. Avram [2] found a drop in the ultrasonic pulse velocity through such concrete, although its compressive strength was practically unchanged in quasi-static loading conditions. On the other hand, such a concrete will most probably have low fatigue and tensile strengths, as well as a lower durability.

Most aggregates show a certain physico-chemical interaction with the cement matrix as well. From the micro-hardness measurements, Lyubimova and Pinus [21] showed that aggregates can be divided into two classes:

1. Those producing a strong contact layer over the matrix surface while the aggregate surface is left practically unchanged; however, at about 50 um from the contact surface, the strength of the matrix mass is considerably lower (Fig. 2a); and
2. Those producing weaker contact layers both on the aggregate and on the matrix surfaces (Fig. 2b).

The first class includes siliceous rocks such as quartzite and such minerals as feldspar and labradorite; the second includes carbonate rocks such as limestone, marble and dolomite and such mineral as calcite.

The explanation of this phenomenon is that, in the presence of cement, the chemical reactions of the two kinds of rocks are

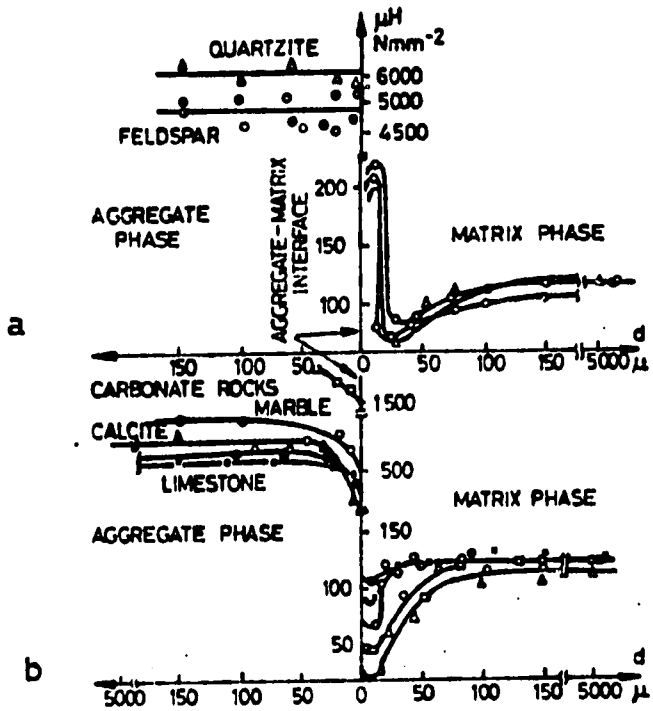

Figure 2. Variation of microhardness values in the aggregate-matrix contact area [21]

different. As already known, at common temperatures, all siliceous materials can absorb calcium hydroxide which, in the case of cement, results from hydration reactions, thus forming hydrated calcium silicate. The elimination of a silicon dioxide layer from the aggregate surface and the production of a compound having higher bonding performances are responsible for the higher hardness of the cement layer (Fig. 2a). This, however, is an extremely slow reaction, which can go on for centuries. It is also the reason why, when under load, early concretes are more prone to microcracking at the matrix-aggregate interface than the older ones [13]. There are also cases when aggregates prove to be inactive. This is due to a layer of crystalline calcium hydroxide deposited over the aggregate surface, thus preventing good cohesion between matrix and aggregate.

Carbonates react, too, with cement hydration products; the contact surface thus built up being characterized by a lower hardness (Fig. 2b). It seems that the main reaction takes place between the carbonates and tri-calcium hydroaluminate, thus forming a complex of monocarbonated tri-calcium aluminate:

$$3CaO.Al_2O_3 + CaCO_3 + 11H_2O = 3CaO.Al_2O_3.CaCO_3.11H_2O$$

If permanently exposed to atmospheric action, carboaluminates might break down into calcium carbonate and alumina. However, this process is only a superficial one, which saves the durability of the concrete.

Another phenomenon which sometimes helps the development of bonds between matrix and aggregate is epitaxial growth, a result of

compatibility between crystalline lattices of aggregates and products of cement hydration. The best examples are such carbonates as limestone rocks; in contact with cement hydration products, they form crystalline portlandite and favor epitaxial overgrowth over the aggregate crystalline lattice. With aggregates which favor epitaxial overgrowth, the structure of the crystalline lattice prevents the formation of liquid or gaseous interface phases over the matrix-aggregate contact surface. Avram [2] speculated that concretes produced with such aggregates would develop a freeze-thaw resistance higher than those produced with aggregates exclusively based on weak physical or chemical bonds. Thus, calcite, in spite of its cleavage planes, is likely to be a better freezing-resistant aggregate than quartz, precisely because it favors epitaxial overgrowth.

Another example of favorable action due to epitaxial overgrowth is supplied by concrete prepared with chalky limestone which displays a compressive strength better than the concrete prepared with whinstone, a much more resistant rock.

Still another example of epitaxial overgrowth is supplied by aluminous cements and limestone aggregates. In such a case, the monocalcium hydroaluminate from cement hydration and its reaction with the calcium carbonate aggregate yields tetracalcium hydroaluminate and calcium carboaluminate [2].

Porosity, humidity and grain geometry of aggregates influence

the nature of matrix contact layer. Porous aggregates, depending on the water content and environmental humidity, may cause a permanent change in humidity at the interface. Aggregate surface drying will lead to an increased cohesive strength.

The amount of cement affects the strength of concrete. Insufficient cement dosage will make the cement matrix the weakest link of the system; whereas in cement rich concrete, the weakest link will be the matrix-aggregate interface.

Thermodynamic nature of adhesion

Predictions of the mechanical behavior of the paste-aggregate bond can be made from the knowledge of physico-chemistry, or surface chemistry of adhesive and adherent, rather than formal mechanics.

The mechanical properties of a bond depend on its surface properties, not on its bulk properties. The source of all surface forces is unbalanced chemical bonds (or surface discontinuities) manifested as surface tension and adsorption. Surface tension is the surface stress (force per unit length), which tends to reduce surface area and is caused by the reversible work required to create a unit area of new surface. In general, surface energy (ergs/cm^2) is numerically equal to surface tension (dyne/cm). If g is surface tension, A is surface area and F^S is the free energy of the surface, free energy change being associated with the creation of a new surface, dA, in magnitude (Fig. 3) can by given by [11]:

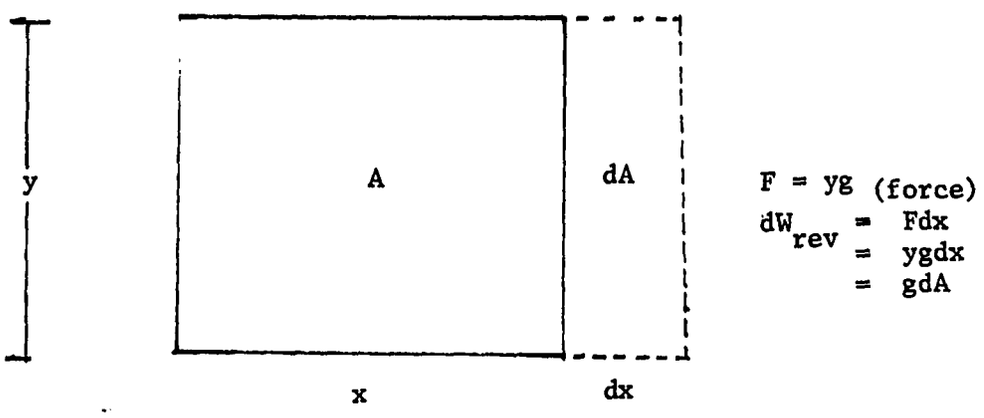

Figure 3. Schematic representation of creating an infinitely small new surface area [11]

$$d(AF^s) = gdA \tag{1}$$

For an isotropic material and solving for g

$$g = F^s + \frac{dF^s}{dA} \cdot A \tag{2}$$

If

$$\frac{dF^s}{dA} = 0 \tag{3}$$

then

$$g = F^s \tag{4}$$

Tabor [35] explained bond energy in terms of surface energy. He considered the simplest, most idealized case of two atomically flat surfaces brought into contact over a specified interfacial area. Suppose that surface energies of two solid surfaces are g_1 and g_2, respectively. After they are brought into contact, their interfacial energy (i.e., $g_{1,2}$) will not equal $g_1 + g_2$. Because the surface atoms will acquire new neighboring atoms, their surface energy will fall; hence, $g_{1,2} < g_1 + g_2$. In the limiting case, if two identical solids are brought into contact, the interface will become identical to the bulk material and $g_{1,2}$ will be zero. More generally, $g_{1,2}$ will always be less than $g_1 + g_2$; therefore

$$g_{1,2} = g_1 + g_2 - D \tag{5}$$

This lowering of energy (D) is equal to the reversible work performed

in creating or destroying the unit area of a joint, whereby:

$$w = g_1 + g_2 - g_{1,2} \tag{6}$$

The work done is really the total surface energy (E^S), related to free surface energy by the following thermodynamic relation:

$$E^S = g - T\frac{dg}{dT} \tag{7}$$

where

$$\frac{dg}{dT} = -S^S \text{ (surface entropy)} \tag{8}$$

The total surface energy (E^S) generally is larger than the surface free energy. Frequently, it is the more informative of the two quantities, and as a good approximation, it is equal to total surface enthalpy.

For simplicity, we may ignore the entropy term $T\frac{(dg)}{dT}$ or alternatively, assume that all experiments are carried out at absolute zero. The temperature independence of E^S generally does hold for substances not too close to the critical temperature, at which surface tension becomes zero. Because most experiments are done at room temperature, and also cement paste and aggregate have high critical temperatures, the difference between g and E^S should not be great.

Measurements of surface energy may be obtained experimentally from heats of solution. Surface energy appears as heat of solution

the interface and in the bulk of the cement paste and this observed morphology has been related to mechanical properties of the bond.

Suzuki and Mizukami [33,34], using a scanning electron microscope, examined cement hydration products grown on the surface of aggregates in contact with cement paste. Although they were unable to identify the hydration products, they found that the quantity or crystallinity of the products correlated roughly with measured bond strength.

Several investigators have observed epitaxial growth of calcium hydroxide on the surface of the calcite aggregate. Struble et al. [32] cited the work of Bertacchi, which showed evidence of a chemical reaction involving the calcite and concluded that the bond strength was due to a combination of chemical reactions and the epitaxial growth of $Ca(OH)_2$ on the calcite surface.

In a study of the bond between cement paste and calcite, Alexander et al. [1] reported the work of Farran who described an aureole of hydrated cement paste surrounding the calcite where cement hydration products were less dense than in the mass of paste, suggesting that the aureole would provide less mechanical resistance.

From a study across the cement-aggregate interface, Lyubimova and Pinus [21] concluded that quartz grains were covered with a layer of epitaxic calcium silicate hydrate (C-S-H). Later SEM studies by Hadley (reported by Struble et al. [32]) and Barnes et al. [3,4]

when the solid interface is destroyed by dissolving; with accurate calorimetry, it is possible to measure energy amounting to a few tenths of a calorie.

In order to know the specific interface energy, the surface area must be determined by some other means. Among various experimental methods available are nitrogen adsorption, vapor adsorption, and mercury porosimetric methods. With solids, direct measurement of g_1 and g_2 is possible; however, there is no satisfactory method of determining $g_{1,2}$ directly. Most of the existing information is derived from experiments between a solid and a liquid, or between two liquids, or in experiments where a vapor is adsorbed on a solid.

Considerable literature search revealed no reference that explained the paste-aggregate bond in terms of surface energy. The theoretical bond strength can be calculated from the possible values of the free surface energy. However, actual strength is much lower than the theoretical strength, because of the presence of flaws and impurities at the interface.

Research on Nature of Cement-Aggregate Bond

Morphological nature of the bond

Studies of the morphological aspects of the cement-aggregate bond typically involve examination by microscope (light or SEM) of the hydration product at the interface. Some investigators have looked for differences between the morphology of the hydration products at

indicated a more complicated interface between cement paste and glass or quartz. They suggested the following sequence of interface formations:

1. A calcium hydroxide film is deposited with the c axis perpendicular to the surface.
2. The film is covered with a layer of elongated C-S-H particles, producing an appearance similar to a hair brush.
3. Larger calcium hydroxide crystals precipitate with their c axes parallel to the surface.
4. Space-filling secondary calcium hydroxide crystals form near the interface.

Iwasaki and Tomiyama [17] investigated the adhesion film between cement paste and various aggregate materials, and suggested the following sequence of formations:

1. Ettringite needles are precipitated on the aggregate surface.
2. Calcium hydroxide plates precipitate.
3. The film thickens and becomes more dense.

Chemical nature of bond

The following empirical evidence of chemical reaction at the interface was reviewed by Alexander et al. [1]:

1. Despite the rough correlation between bond and cement paste strength, there is enough variability with different brands of

Type I cement to suggest that the chemical composition of the cement affects bond strength.

2. The bond strengths for different rocks with the same surface texture vary by more than a factor of two.
3. Bond strength and failure patterns appear to depend on time and temperature of curing.
4. For siliceous rocks, the more acid rocks develop the highest bond strengths. The bond strengths of extrusive rocks are directly proportional to their silica content.

Several investigators have provided indirect evidence of chemical reactions between cement and aggregate. Lyubimova and Pinus [21] found that chemical reactions of cement paste with quartz caused the formation of epitaxial C-S-H; Scholer [31] suggested that siliceous aggregate produces more chemical bonding than other aggregates.

A pozzolanic reaction between cement and siliceous rocks was suggested by Alexander et al. [1]. Similarly, Struble et al. [32] reported the work of Schweite, which showed that C-S-H could form from chemical reactions between quartz and a calcium hydroxide solution and suggested that a similar reaction might occur in concrete (involving calcium hydroxide that occurs in voids around quartz grains).

Two types of chemical reactions have been suggested for carbonate aggregates. One is the transformation of calcite at the surface into

calcium hydroxide, suggested by Farran (reported by Alexander et al. [1]). Evidence for such attack included observation of corrosion of calcite surfaces by Farran, and a decrease in the intensity of the 3.04 A° X-ray diffraction peak for calcite by Buck and Dolch [7]. Similar evidence was provided by Chatterji and Jeffrey [8], who reported etching of aggregate grains, especially limestone.

The other type of chemical reaction possible between cement and carbonate aggregate is that with calcium aluminate present in the cement to form a carboaluminate [1,21]. Reaction between calcite and C_3A or C_4AF, was later shown by Cussino and Pintor [10] to produce $3CaO.Al_2O_3.CaCO_3.11H_2O$.

Mechanical nature of bond

The shape and surface texture of the aggregate play an important part in cement-aggregate bond, because there is a considerable amount of mechanical interlocking between the aggregate and the matrix phase. Mindess [22] stated that flexural and tensile strength of concretes made with rough aggregates may be 30% higher than those made with smooth aggregates.

The bond region is generally weaker than the paste or the aggregate phase because of the existence of cracks at the paste-aggregate interface. These cracks are due to bleeding and segregation and to volume changes of the cement paste during setting and hydration. During drying, the aggregate particles tend to restrain

shrinkage of cement paste because of their higher elastic modulus. This induces shear and tensile forces at the interface, which increase with increasing particle size. Under load, the difference in elastic moduli between the aggregate and the cement paste will lead to still more cracking.

As mentioned earlier, a wide range of bond strength of cement with various aggregates has been used as indirect evidence of chemical reactions between cement and rock types. However, as pointed out by Ozol [24], these differences could alternatively be explained by different roughness factors of various aggregates. An important aspect of bond strength with different aggregates is the true surface area each aggregate presents for bonding, regardless of whether the bond is primarily due to mechanical interlocking of cement hydration products with the aggregate surface or to chemical reaction between aggregate and paste [24].

Influence of Bond on Concrete Strength and Durability

Some investigations have shown a relationship between bond strength and concrete strength. Alexander et al. [1] reported a linear correlation (by multiple regression analysis) between concrete strength (compressive and tensile) and paste and bond strengths, where the coefficient of paste strength was approximately double that of bond strength. The regression equation is:

$$Y = b_0 + b_1 m_1 + b_2 m_2$$

where

For modulus of rupture : $b_0 = 290$, $b_1 = 0.318$, $b_2 = 0.162$

For compressive strength: $b_0 = 480$, $b_1 = 2.08$, $b_2 = 1.02$

m_1 = modulus of rupture of paste (psi); and

m_2 = modulus of rupture of aggregate-cement bond (psi).

Based on measurements of microcracking in concrete during compressive tests, Scholer [31] hypothesized that the cement-aggregate bond influenced concrete strength by controlling the amount of microcracking necessary for failure. Patten [25] suggested that at high stress levels, poor bond allows cracks to propagate more rapidly, hastening failure.

Little has been published on the role of the bond in portland cement concrete durability. Valenta [36] measured flexural strength and durability (the number of freeze-thaw cycles to produce a 50% reduction in flexural strength of the bond) of bonds between cement paste and fractured and smooth surfaces of various rock types. Durability was greater with the fractured surface than with the smooth surface, indicating that mechanical interlocking increases durability.

Cussino and Pintor [10] investigated the role of bond on sulfate attack. They measured compressive and flexural strength of concrete specimens made with five types of cements, and calcareous and silicious aggregates. The specimens were cured in plain water and in

water containing sulphate. Sulfate attack was shown to be less for calcareous than for siliceous aggregates; they attributed this result to the chemical reaction of cement paste with calcareous aggregates involving transformation of monosulphoaluminate into carboaluminate and ettringite.

TENSILE BOND STRENGTH TEST

Bond strength was measured with a test patterned after ASTM C-190; the mold is shown in Figure 4. A tensile testing machine was used for measuring strength and an automatic, diamond-blade masonry saw was used to cut aggregate. Guidance was also taken from the test method developed by Hsu and Slate [16].

Specimen Preparation

A limestone block from Indiana was cut into 1 x 1 x 1-3/8 inch prisms to fit accurately into one-half of the briquette mold shown in Figure 4. The prisms then were washed with water and carbon tetrachloride solution to remove dirt and oil, placed in a 200 F oven for 24 hours to evaporate the carbon tetrachloride, and then washed in water. Next, one face (bonding face, 1 x 1 inch) of each prism was polished with 600 grit sand paper and then washed again. The prisms were soaked in water for a minimum period of 24 hours, then wiped with a saturated cloth to obtain a saturated surface dry condition, before making the specimen.

Cement pastes prepared from two fly ashes (Neal #2 and Neal #4) were used. Neal #2 is a high calcium, slightly cementitious ash; Neal #4 is a high calcium, cementitious ash. ASTM Type I portland cement was used for comparison with fly ash.

Trace additives for fly ashes were selected on the basis of their

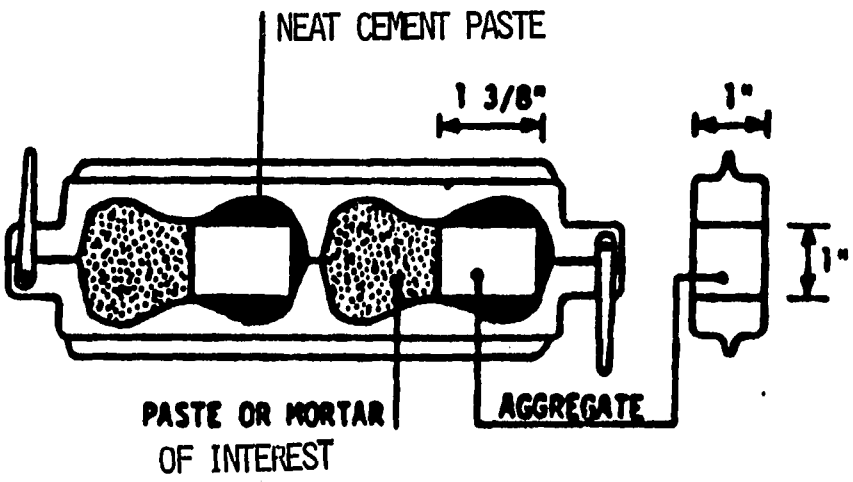

Figure 4. Diagram of mold device used to prepare tensile bond strength specimens

ability to control set times and increase strength [5,29]. Two Neal #4 fly ash pastes were prepared, one plain (i.e., having no additive) and one having for its trace additive a 3% fertilizer grade di-ammonium phosphate. Two Neal #2 pastes also were prepared, one plain and the other having for its trace additive a 2% fertilizer grade ammonium nitrate.

Water-cement ratios of 0.24, 0.30 and 0.36 by weight were chosen. These ratios were selected because ratios less than 0.24 make a paste which is too dry for molding, while ratios greater than 0.36 make one which bleeds considerably because it is too wet. Tests were done at the end of 7, 14 and 28 days of curing.

For tests of the bond strength of cement paste and aggregate, specimens were prepared as shown in Figure 4. Paste strength and rock strength tests were conducted using specimens made from cement paste only and rock only.

To mold the specimens, a prism of limestone aggregate was placed into one-half of the mold; the bonding face of the prism was placed in the middle of the mold, as shown in Figure 4. The space between the wall of the mold and the aggregate prism (only in the half in which the prism is placed) was filled with portland cement paste having a water-cement ratio of about 0.30, taking care to ensure the bonding face of the prism was clear of the portland cement paste. The other half of the mold then was filled with the appropriate cement pastes, including the space between the wall of the mold and the bonding face

of the aggregate.

After molding, the specimens were placed in a moist-cure room having an average temperature of 72 degrees F and a relative humidity of 100 percent. After 24 hours, the mold was removed and the specimens were stored in the moist cure room until testing.

Results

Results were obtained from a total of 450 specimens with each value in the tables being average for five observations. One standard deviation is reported next to the appropriate mean.

Results for cement paste-aggregate bond strength and paste tensile strength are reported in Tables 1-3 as a function of water-cement ratio and age. Strengths from the three testing ages are averaged and presented as a function of w/c ratio in Table 4. Similarly, Table 5 represents average strength (over three w/c ratios) as a function of age. Graphs showing how bond and paste strengths for each cement vary with age and water-cement ratio are also shown in Figures 5-9. Bar graphs showing the effect of additives for each testing age are shown in Figures 10 and 11.

Factors influencing strength are water-cement ratio, age, and additives. Test results show that tensile strength decreases with increasing water-cement ratios; all three cements showed the same trend. Test results also showed that strength invariably increased

Table 1. Slightly cementitious Neal #2 fly ash-limestone tensile bond strength and paste tensile strength with three variables (cement type, water/cement ratio of paste matrix, and age).

Surface Roughness: Smooth (polished with 600 grit sandpaper)				
	Cement Type	**Neal #2 Fly Ash**		
Age (days)	W/C Ratio	0.24	0.30	0.36
7	Bond strength,	30.7 (5.9)[a]	18.1 (7.0)	12.1 (7.9)
14	psi	40.2 (9.1)	23.8 (9.8)	16.6 (8.7)
28		50.1 (6.1)	30.2 (5.0)	27.9 (9.0)
7	Paste strength,	38.0 (8.1)	23.9 (7.8)	16.6 (9.1)
14	psi	55.6 (13.1)	33.2 (11.0)	26.0 (8.0)
28		69.1 (8.9)	46.8 (6.5)	33.7 (8.4)
	Cement Type	**Neal #2 Fly Ash + 2% Ammonium Nitrate**		
Age (days)	W/C Ratio	0.24	0.30	0.36
7	Bond strength,	28.5 (6.1)	22.5 (9.1)	18.1 (10.8)
14	psi	42.6 (7.4)	23.6 (10.5)	22.8 (8.0)
28		48.5 (6.0)	33.6 (9.8)	26.5 (8.3)
7	Paste strength,	40.3 (8.9)	33.7 (9.6)	26.2 (10.4)
14	psi	68.3 (9.3)	48.5 (9.1)	34.3 (8.7)
28		88.8 (8.2)	69.7 (8.1)	46.7 (8.7)

[a]Number in parentheses is one standard deviation.

Table 2. Cementitious Neal #4 fly ash-tensile bond strength and paste tensile strength with three variables (cement type, water/cement ratio of paste matrix, and age)

Surface roughness: Smooth (polished with 600 grit sandpaper)				
	Cement Type	Neal #4 Fly Ash		
Age (days)	W/C Ratio	0.24	0.30	0.36
7	Bond strength,	53.4 (12.0)[a]	41.1 (9.2)	29.1 (6.3)
14	psi	72.9 (8.8)	57.2 (8.8)	54.4 (5.9)
28		96.0 (8.4)	85.1 (10.9)	60.0 (7.9)
7	Paste strength,	75.7 (12.6)	59.9 (9.3)	40.1 (8.5)
14	psi	102.5 (13.6)	88.0 (11.0)	60.3 (7.3)
28		119.3 (15.0)	99.4 (13.4)	78.4 (12.6)
	Cement Type	Neal #4 Fly Ash + 3% Ammonium Phosphate		
Age (days)	W/C Ratio	0.24	0.30	0.36
7	Bond strength,	64.0 (10.3)	51.7 (10.5)	33.4 (6.7)
14	psi	87.5 (11.7)	64.5 (10.6)	48.4 (8.4)
28		122.0 (11.4)	95.3 (8.4)	68.1 (9.6)
7	Paste strength,	82.2 (11.2)	65.0 (12.7)	45.3 (9.0)
14	psi	117.8 (17.7)	92.2 (10.6)	69.2 (12.6)
28		187.1 (15.9)	122.3 (12.3)	90.0 (11.3)

[a]Number in parentheses is one standard deviation.

Table 3. Type I portland cement-limestone tensile bond strength and paste tensile strength with three variables (cement type, water/cement ratio of paste matrix, and age)

Surface Roughness: Smooth (polished with 600 grit sandpaper)				
Cement Type		Type I Portland Cement		
Age (days)	W/C Ratio	0.24	0.30	0.36
7	Bond strength,	480 (51)[a]	474 (56)	414 (65)
14	psi.	526 (45)	487 (77)	396 (58)
28		596 (58)	515 (65)	439 (71)
7	Paste strength,	893 (44)	842 (39)	717 (78)
14	psi	1090 (105)	895 (43)	752 (41)
28		1130 (85)	905 (42)	760 (96)

[a]Number in parentheses is one standard deviation.

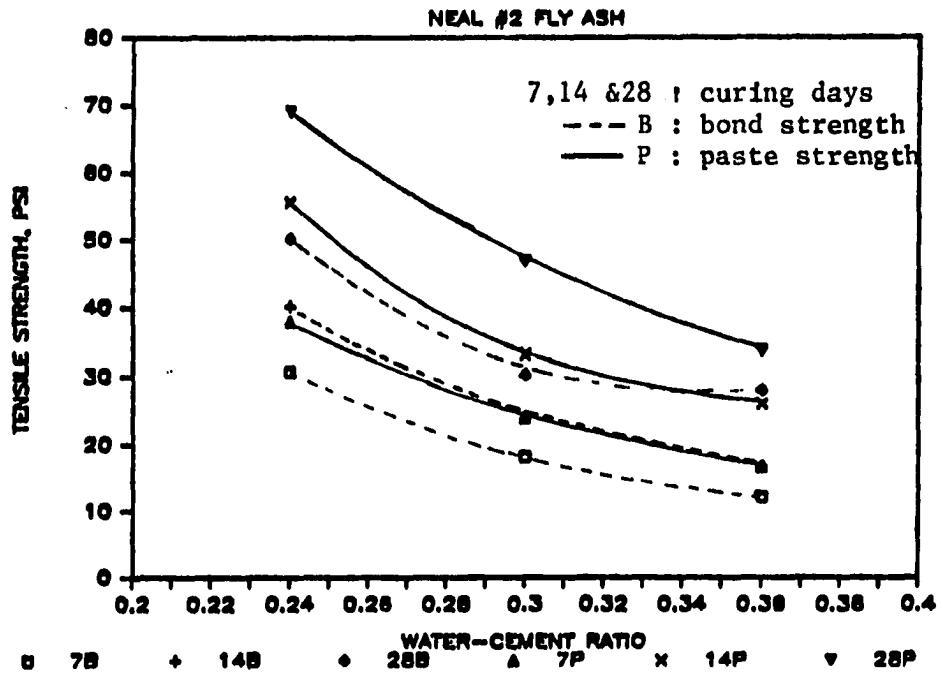

Figure 5. Bond and paste strength for Neal #2 fly ash

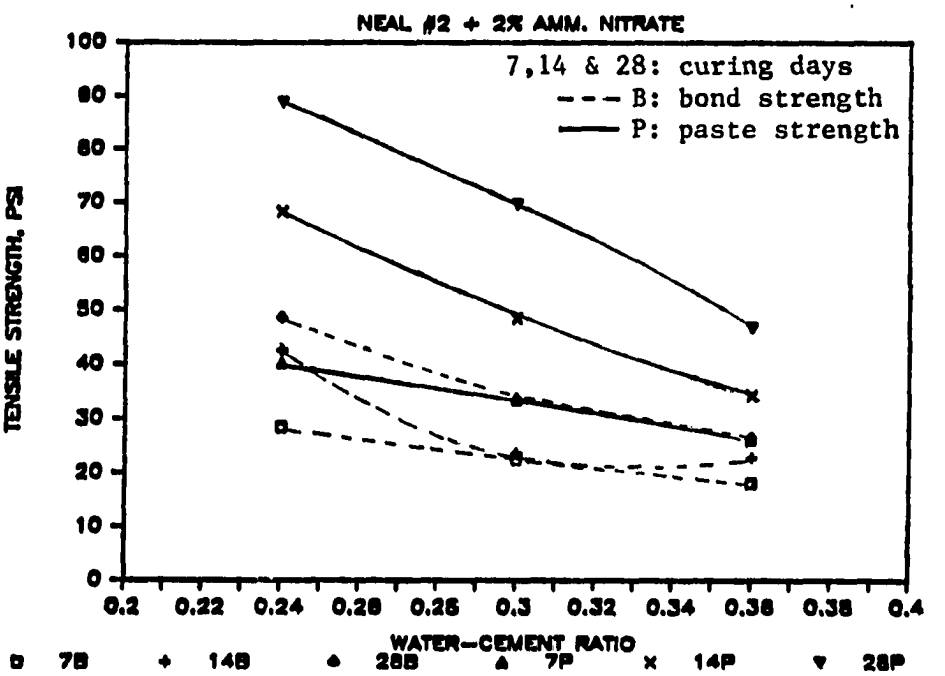

Figure 6. Bond and paste strength for 2% ammonium nitrate treated Neal #2 fly ash

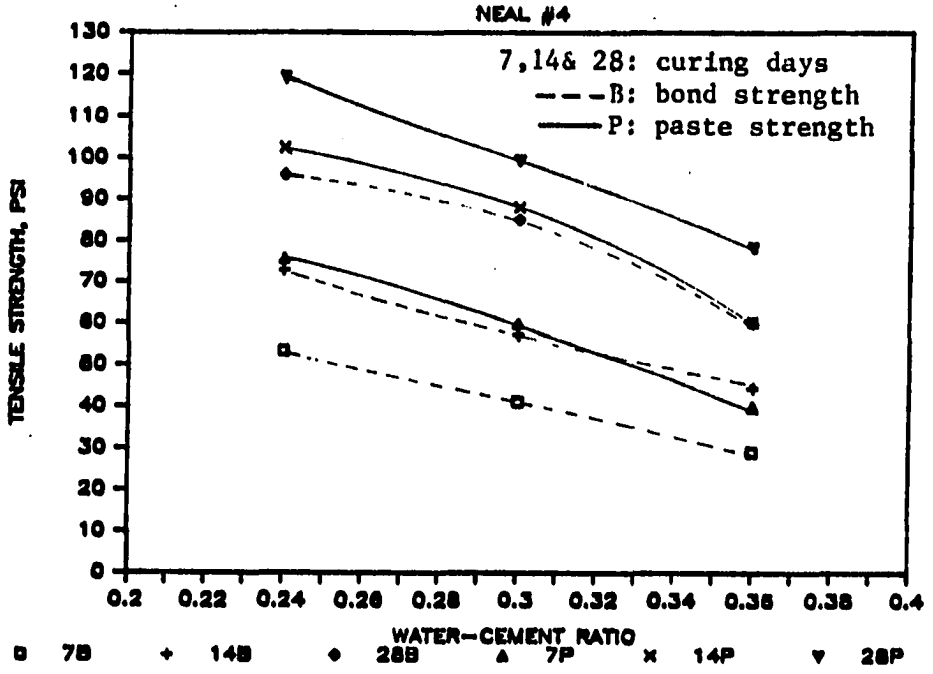

Figure 7. Bond and paste strength for Neal #4 fly ash

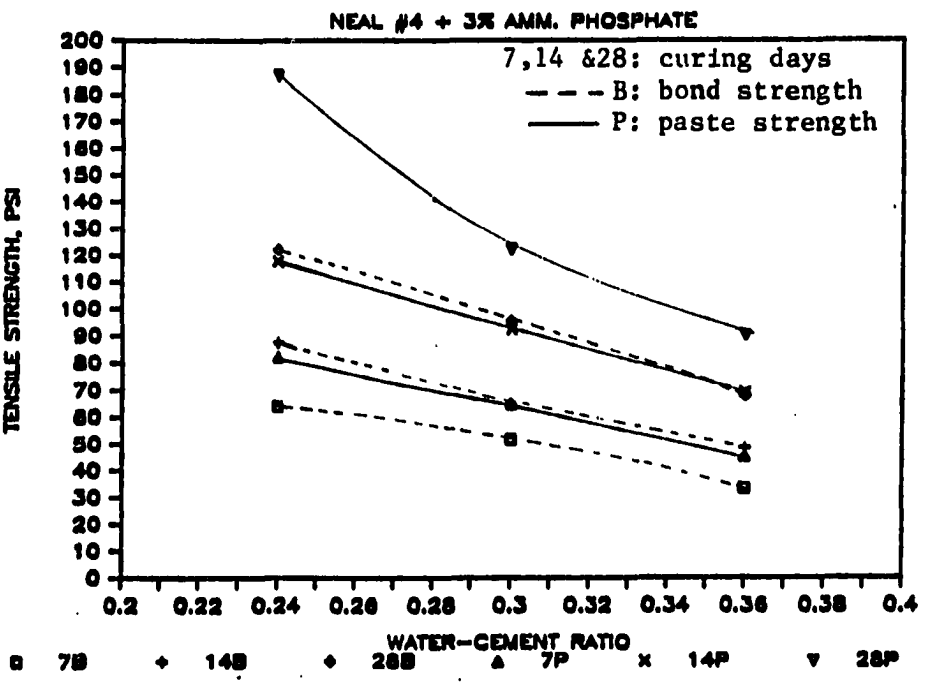

Figure 8. Bond and paste strength for 3% ammonium phosphate treated Neal #4 fly ash

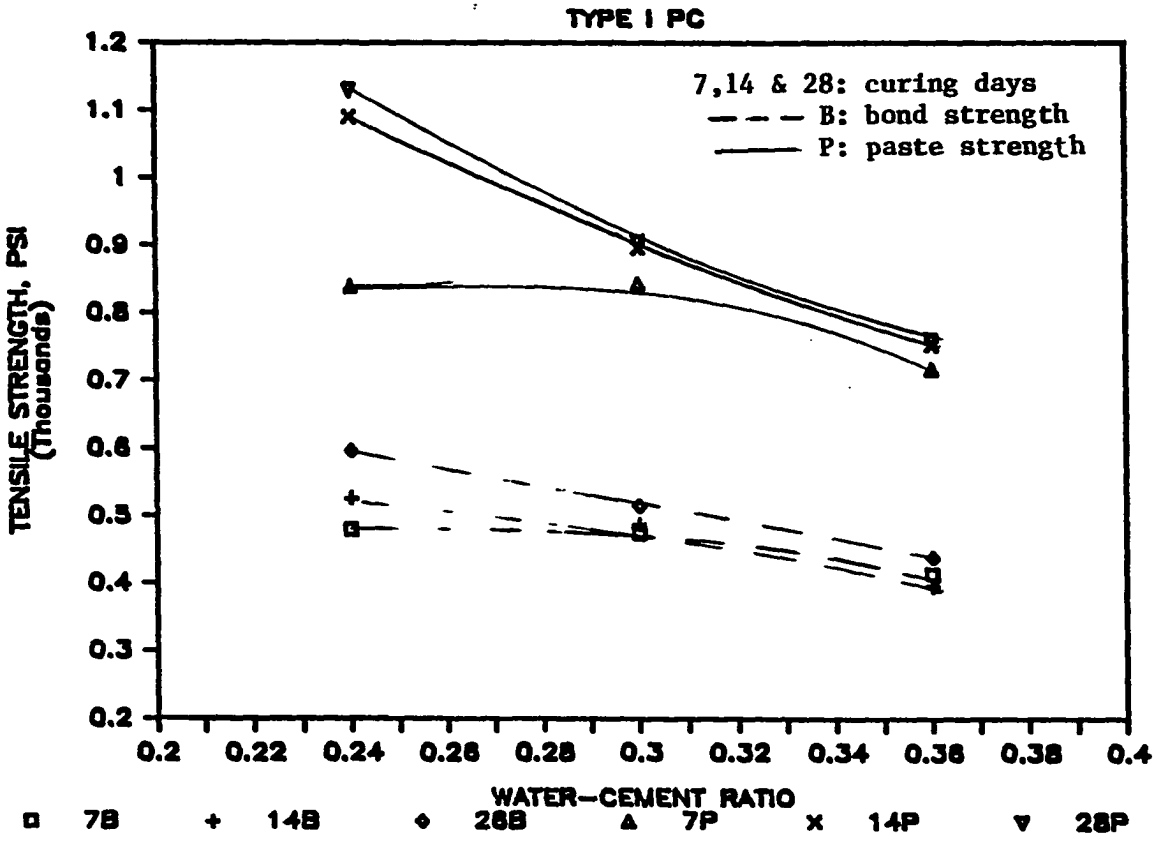

Figure 9. Bond and paste strength for Type I portland cement.

Table 4. Average bond and paste strength as a function of water/cement ratio

	Average Bond Strength (psi)			Average Paste Strength (psi)		
Water/Cement Ratio	0.24	0.30	0.36	0.24	0.30	0.36
Neal #2 Fly Ash						
Strength[a]	40.3	24.2	18.9	54.2	34.6	25.4
Ratio[b]	1.00	0.60	0.47	1.00	0.64	0.47
Neal #2 Fly Ash+ 2% Ammonium Nitrate						
Strength	39.9	26.6	22.5	65.8	50.6	35.7
Ratio	1.00	0.67	0.56	1.00	0.77	0.54
Neal #4 Fly Ash						
Strength	74.1	61.1	44.5	99.2	82.4	59.6
Ratio	1.00	0.82	0.60	1.00	0.83	0.60
Neal #4 Fly Ash+ 3% Ammonium Phosphate						
Strength	91.2	70.5	50	129	93.2	68.2
Ratio	1.00	0.77	0.55	1.00	0.72	0.53
Type I Portland Cement						
Strength	534	492	416	1020	880	743
Ratio	1.00	0.92	0.78	1.00	0.86	0.73

[a]Overall average of 7, 14 and 28 day strength.
[b]Fraction of strength at the w/c ratio of 0.24.

Table 5. Average bond and paste strength as a function of age

	Average Bond Strength (psi)			Average Paste Strength (psi)		
Age (days)	7	14	28	7	14	28
Neal #2 Fly Ash						
Strength[a]	20.3	26.3	36.1	26.2	38.3	49.9
Ratio[b]	1.00	1.33	1.78	1.00	1.46	1.90
Neal #2 Fly Ash+ 2% Ammonium Nitrate						
Strength	23.0	29.7	36.2	33.4	50.4	68.4
Ratio	1.00	1.29	1.57	1.00	1.51	2.05
Neal #4 Fly Ash						
Strength	41.2	58.2	80.4	58.6	83.6	99.0
Ratio	1.00	1.41	1.95	1.00	1.43	1.69
Neal #4 Fly Ash+ 3% Ammonium Phosphate						
Strength	49.7	66.8	95.1	64.2	93.1	133.1
Ratio	1.00	1.35	1.91	1.00	1.45	2.07
Type I Portland Cement						
Strength	456	469	516	799	912	932
Ratio	1.00	1.01	1.13	1.00	1.14	1.17

[a]Overall average strengths at W/C ratios of 0.24, 0.30 and 0.36.
[b]Fraction of average 7 day strengths.

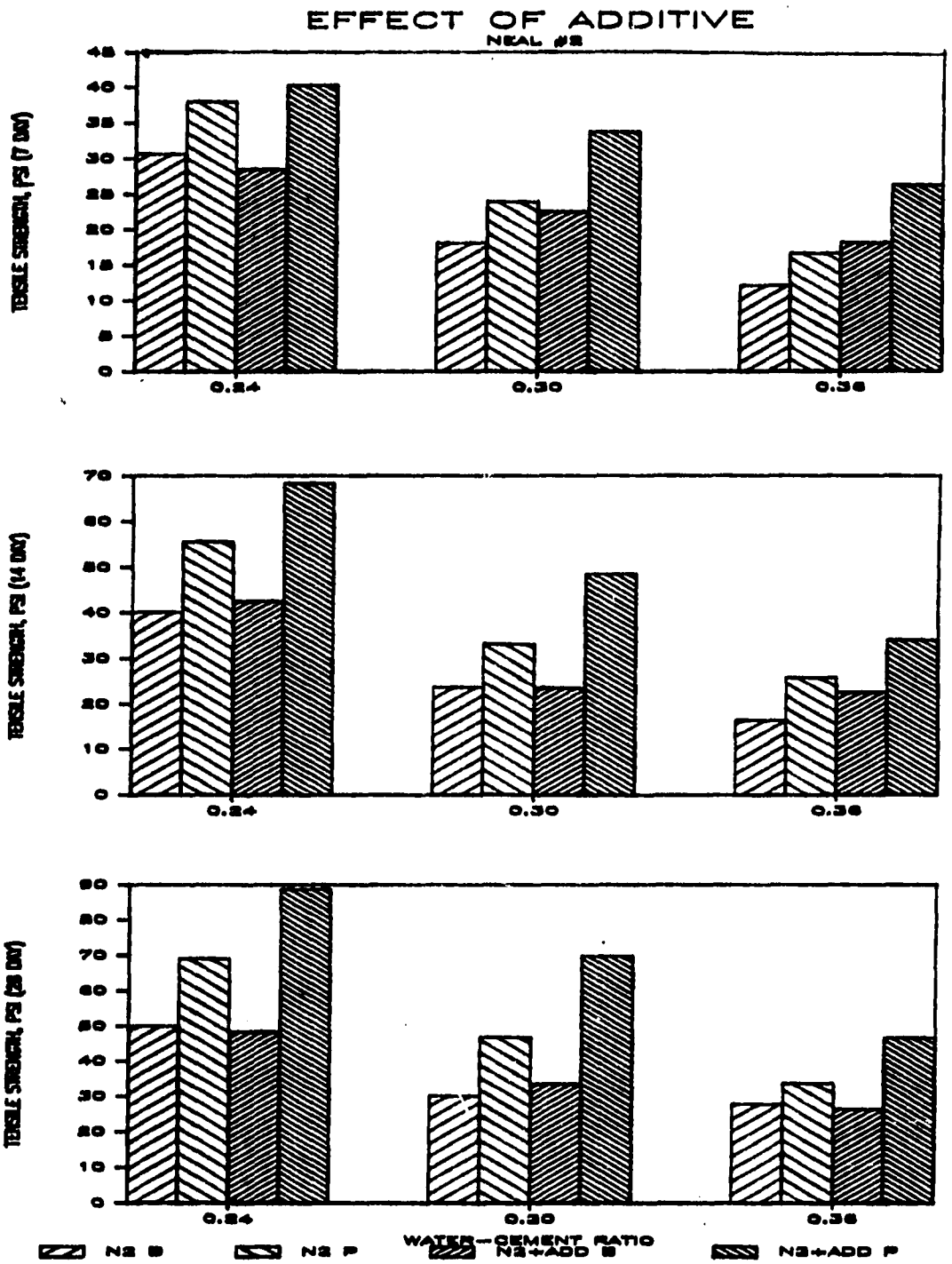

N2: Neal #2; ADD: 2% Ammonium nitrate; B: Bond; P: Paste

Figure 10. Bond and paste strength of Neal #2 fly ash - comparison of treated and untreated case

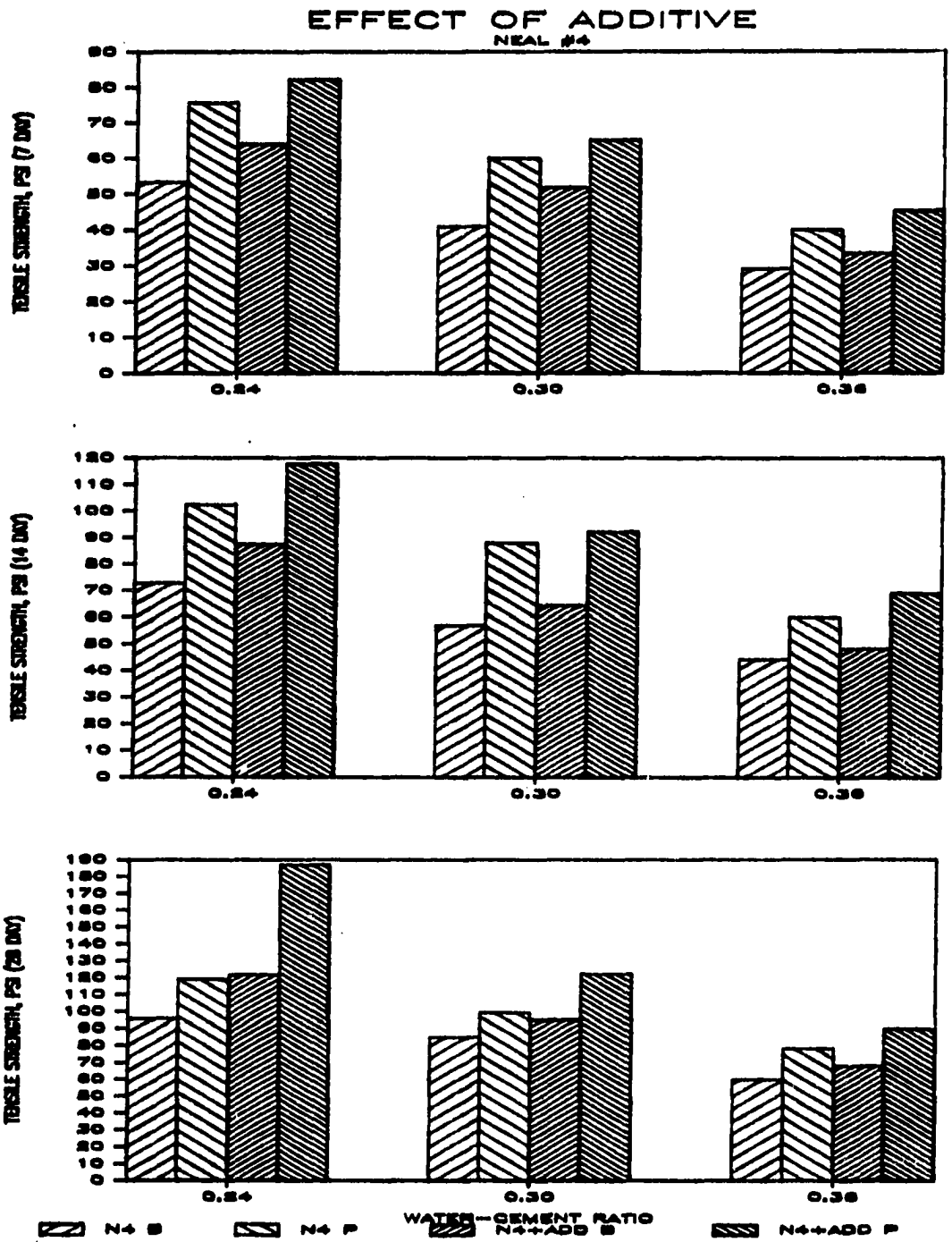

N4: Neal #4; ADD: 3% Ammonium phosphate; B: Bond; P: Paste

Figure 11. Bond and paste strength of Neal #4 fly ash - comparison of treated and untreated case

with age for all three cements. Both of these results were expected.

Results concerning the effects of additive on strength showed the use of 3% ammonium phosphate definitely increases bond and paste strength for the cementitious Neal #4 fly ash at all ages. Results for the slightly cementitious Neal #2 ash were less definite, in that the effect of 2% ammonium nitrate on bond strength was rather erratic (sporadic increases and decreases in strength were observed) even though distinct increases in paste strength were seen.

Statistical Analysis

Analysis using a general linear model was conducted to determine the statistical significance of the effect of water-cement ratio, curing period and trace additive on strength. The analytic technique used ("analysis of covariance") combines the features of analysis of variance and regression. The model is described below:

$$\text{strength}_{ijk} = \mu + \text{add}_i + \text{type}_j + (\text{add} * \text{type})_{ij} + \beta_1 \cdot WC + \beta_2 \cdot \text{day} + \varepsilon_{ijk}$$

where

μ is the overall mean with the following parameters:

add = treatment with trace additive or plain

type = bond or paste strength

add * type = interaction between additive and type

WC = water-cement ratio

day = curing period

β_1 and β_2 are regression coefficients, and

ε is the random variability component of strength.

It was assumed that the data were from random samples of independent observation from a normally distributed population.

Additive and type were used as qualitative independent variables, whereas water-cement ratio and day were used as quantitative independent varibles. The Statistical Analysis System (SAS) was used to evaluate the model.

The hypothesis specification is:

H_o: parameter = 0, H_A: at least one of the parameter is not zero;

$\alpha = 0.05$

The null hypothesis (H_o) implies that the effect of independent variables on strength is not significant. The alternate hypothesis (H_A) is that the assumed model is correct, i.e. there is significant effect of independent variables on strength. Level of significance was set at 95%, or $\alpha = 0.05$.

F tests and T tests are used to evaluate the adequacy of the model and significance testing. Working on the assumption that H_o is true, test statistics (F and T values) are calculated from the data as an index or measure of discrepencies from H_o.

F values are the ratio of the variances of the parameters to the error variance. The null hypothesis is rejected if the F value

exceeds $F_c = F$ (degree of freedom of parameter, degree of freedom of error variance, $\alpha/2$). T values are the ratio of the difference in calculated and hypothesized parameter values to the sample standard deviation. If the T value exceeds $T_c = T$ (degree of freedom of parameter, $\alpha/2$), then H_o is rejected. The p value (also called the actual significance level or the exceedence probability) is the probability of randomly obtaining a test statistic value more extreme than that calculated from the sample. For this investigation, H_o is rejected when p value is less than 0.05.

The analysis of the linear model for the three cements is presented in Tables 6 through 10. It can be seen that the regression was significant; the probability (p value) of obtaining an F greater than the F calculated was 0.0001. Effects of type, water-cement ratio and curing time on strength were also significant; also, the effect of additive was significant for Neal #2 and Neal #4 fly ashes (no additive was used for portland cement); additive-type interaction was significant only in Neal #2 fly ash. After studying the T values and the associated p values in Tables 6-10 the following observations can be made:

1) adding 2% ammonium nitrate to Neal #2 fly ash increased paste strength but it did not increase the bond strength;
2) adding 3% ammonium phosphate increased both paste and bond strength for Neal #4 fly ash;

3) bond strength was lower than paste strength for all cements;
4) increasing the water-cement ratio decreased strength;
5) increasing curing time increased strength.

Responses of bond strength and paste strength to additive, water-cement ratio and curing time are examined separately and presented in Tables 7, 9 and 10. Paste strength is more sensitive to additive, changes in water-cement ratio and curing time than bond strength in Neal#2 and portland cement specimens; bond strength is more sensitive in Neal #4 specimen.

T values for the three cements are summarized in Table 11 to compare the behavior of the three cements; the results are summarized below:

1) increases in paste strength of Neal #2 fly ash (due to ammonium nitrate) were more significant than the corresponding increases in Neal #4 paste strength (due to di-ammonium phosphate). However, increases in bond strength of Neal #2 fly ash were insignificant.
2) decreases in strength with increases in water-cement ratio were most pronounced in Neal #4 fly ash, followed by the decreases in Neal #2 and portland cement.
3) increases in strength with curing time were most prominent in Neal #4 fly ash; Neal #2 was second in the response, whereas the effect was rather low in portland cement.

Table 6. Covariance analysis for Neal #2 fly ash

General Linear Models

Dependent Variable: Strength

Source	F Value	PR > F	R^2
Model	96.51	0.0001	0.73497
Additive	24.42	0.0001	
Type	114.93	0.0001	
Additive*Type	13.40	0.0003	
WC	185.13	0.0001	
Day	144.66	0.0001	

H_0: Parameter = 0, H_A: Parameter = 0; α = 0.05

Parameter	T	PR > [T]
Intercept	16.82	0.0001
Additive 2% AN Plain	6.08	0.0001
Type Bond Paste	-4.99	0.0001
Additive*Type 2% AN Bond 3% AN Paste Plain Bond Plain Paste	-3.66	0.0003
WC	-13.61	0.0001
Day	12.03	0.0001

Table 7. Analysis of covariance for Neal #2 - Effect of additive on bond and paste strength

General Linear Model				
Dependent Variable: strength				
H_0: Parameter = 0, H_A: Parameter ≠ 0; α = 0.05				
	Bond		Paste	
Parameter	T	PR ≥ [T]	T	PR ≥ [T]
Intercept	11.39	0.0001	13.00	0.0001
Additive 2% AN Plain	1.07	0.2869	6.00	0.0001
WC	-9.06	0.0001	-11.42	0.0001
Day	6.68	0.0001	11.20	0.0001

Table 8. Covariance analysis for Neal #4 fly ash

General Linear Models

Dependent Variable: Strength

Source	F Value	PR > F	R^2
Model	151.43	0.0001	0.81313
Additive	42.48	0.0001	
Type	114.86	0.0001	
Additive*Type	1.25	0.2651	
WC	267.01	0.0001	
Day	331.17	0.0001	

H_0: Parameter = 0, H_A: Parameter = 0; $\alpha = 0.05$

Parameter	T	PR > [T]
Intercept	21.07	0.0001
Additive 3% DAP Plain	5.42	0.0001
Type Bond Paste	-6.79	0.0001
Additive*Type 3% DAP Bond 3% DAP Paste Plain Bond Plain Paste	-1.12	0.2651
WC	-16.34	0.0001
Day	18.20	0.0001

Table 9. Analysis of covariance for Neal #4 - Effect of additive on bond and paste strength

General Linear Model				
Dependent Variable: strength				
H_0: Parameter = 0, H_A: Parameter ≠ 0; $\alpha = 0.05$				
	Bond		Paste	
Parameter	T	PR ≥ [T]	T	PR ≥ [T]
Intercept	16.45	0.0001	14.32	0.0001
Additive 3% DAP Plain	5.37	0.0001	4.66	0.0001
WC	-13.34	0.0001	-11.68	0.0001
Day	15.65	0.0001	12.51	0.0001

Table 10. Covariance analysis for portland cement

General Linear Models

Dependent Variable: Strength

Source	F Value	PR > F	R^2
Model	226.96	0.0001	0.887859
Type	567.38	0.0001	
WC	97.51	0.0001	
Day	16.00	0.0001	

H_0: Parameter = 0, H_A: Parameter = 0; α = 0.05

Parameter	T	PR > [T]
Intercept	23.94	0.0001
Type (Bond Paste)	-23.82	0.0001
WC	-9.82	0.0001
Day	4.00	0.0001

	Bond		Paste	
Parameter	T	PR > [T]	T	PR > T
WC	-5.37	0.0001	-9.75	0.0001
Day	2.87	0.0063	3.44	0.0001

Table 11. Comparison of T values among Neal #2 fly ash, Neal #4 fly ash and portland cement

General Linear Model						
Dependent Variable: strength						
H_0: Parameter = 0, H_A: Parameter = 0; α = 0.05						
	Bond			Paste		
	Neal #2	Neal #4	Portland Cement	Neal #2	Neal #4	Portland Cement
Parameter	T	T	T	T	T	T
Additive 2% AN/3% DAP Plain	1.07	5.37	-	6.00	4.36	-
WC	-9.06	-13.34	-5.37	-11.42	-11.68	-9.95
Day	6.68	15.65	2.87	11.20	12.51	3.44

Discussion

The above findings indicate that quality control is extremely important for producing strong bonds; amount of water must be controlled and adequate curing time must be provided. Fly ashes need more strict quality control than portland cement.

Although ammonium nitrate increases the paste strength of Neal #2 fly ash, it did not significantly increase bond strength. Aggregate and paste were completely separated at the contact surface after the tensile test. This suggests a lack of physico-chemical interaction between the paste and the aggregate.

Ammonium phosphate has beneficial effects on the strength of Neal #4 fly ash; both bond and paste strength increase considerably. The failure surface was an irregular cross section through the paste phase indicating physico-chemical interactions between the cement paste and the aggregate. The thickness of the paste layer adhering to the aggregate after the tensile test was also greater for the ammonium phosphate treated specimens than it was for the untreated ones. Therefore, paste strength is a controlling factor in developing strong composites.

The failure surface in portland cement bond specimens was occurring partially through the aggregate phase. Therefore, strength of aggregate also plays an important role in determining the bond strength.

X-RAY DIFFRACTION EXAMINATION

X-ray diffraction tests were performed to investigate the nature of the interface between the cement paste and the aggregate and to identify any reaction product(s) that might form. These reaction products can be correlated to the measured bond strength.

A General Electric x-ray diffractometer with a copper target in the x-ray tube was used. An excitation voltage of 50 kv and a filament current of 16 ma were used.

This investigation was limited to the specimens made from Neal #4 fly ash (plain and ammonium phosphate treated); a portland cement specimen was also examined for comparison.

Procedure

Limestone from Indiana was cut roughly into 1" x 1-1/2" x 1/8" slabs. One face (1" x 1-1/2") of the slab was polished successively with 5 um, 3 um, 1 um and 0.5 um polishing cloths. Then a layer of about 1/8" thick cement paste (water-cement ratio = 0.24) was spread carefully over the polished stone surface. The specimens were allowed to hydrate for 120 days in the humidity room; they were air-dried before conducting the x-ray diffraction tests.

The cement side of the specimen was polished into a smooth surface using a fine crocus cloth, after which x-ray diffraction testing was performed. After the test, the specimen was removed from

the diffractometer; the cement surface was then further polished to expose a new surface and a second test was performed on the new surface. By successively polishing the sample newer surfaces closer to the aggregate boundary were exposed. Diffraction tests were conducted at each surface and the process was continued until a diffraction pattern for the aggregate was obtained. In this way, the chemical compound in the paste-aggregate interface region was obtained. X-ray diffractograms are presented in Appendix B.

Results

Portland cement paste specimen

Appendix B-1 is the diffractograms from the portland cement-limestone boundary. More than twenty tests were done, but for convenience in presentation only seven are shown. These seven diffractograms were chosen to give a representative picture of the chemical compound profiles across the paste-aggregate interface.

Trace 1 is for the paste surface, about 1 mm away from the limestone where no paste-aggregate interaction products appear. Traces 2 and 3 also represent the paste phase, but become successively closer to the aggregate surface. The principal hydration products of the paste phase are $Ca(OH)_2$ (L), ettringite (E), calcium-silicate-hydrate (CSH) and calcium-silicate-hydrate II (CSH II). Mineral powder diffraction files compiled by the Joint Committee on Powder

Diffraction Standards (JCPDS) [18] and the Highway Research Board (HRB) Special Report 127 [23] were used to identify chemical compounds. Crystalline compounds are indicated by well defined peaks; poorly crystalline and amorphous compounds are indicated by the halo (a gentle hump or rise in the background response) on a diffraction trace.

Traces 4 and 5 have diffraction patterns from both the paste and the stone phases, although both are at a much reduced intensity. Traces 6 and 7 are for pure limestone.

An examination of all the traces indicate that numbers 4 and 5 are most likely to be for the interface region. A halo observed in the 12 to 20 degree two theta range on the trace 5, marked (X), was not observed in the paste or in the limestone. It was not possible to positively identify the compound even after considerable searching of the JCPDS files.

The intensity of $Ca(OH)_2$ shows some interesting characteristics as it approaches the interface. Intensities for all the diffracting planes reduce gradually from the paste phase towards the interface region, but the ratio of intensity of 001 plane (18 degree two theta) to 101 plane (34 degree two theta) increases from about 0.5 to 1, which indicate that $Ca(OH)_2$ crystals form with an orientation tendency with the C-axis perpendicular to the limestone surface. A general overview of crystallography is presented in Appendix C.

Ettringite is also seen at the interface, although at a reduced intensity from the bulk phase.

The halo observed in the paste phase in the range of 26 to 38 degree two theta is due to poorly crystalline CSH. This halo decreases in intensity towards the interface, indicating that the interface is deficient in cementitious amorphous CSH gel.

Neal #4 fly ash

Appendix B-2 is the diffractograms from the Neal #4 fly ash-limestone boundary. As in the portland cement specimen, the XRD diffractograms started from the paste phase towards the stone phase through the interface region.

Trace 1 is for the paste surface, about 1 mm away from the limestone surface. Successive traces 2, 3 and 4 are also for the paste phase. Traces 5-9 represent the probable interface region and show diffraction patterns present in both the cement paste and limestone. Traces 10 and 11 are for pure limestone.

The main crystalline hydration product observed on the fly ash side is ettringite (E). There is a decrease in the intensity of ettringite as it approaches the stone surface, but subsequently the intensity increases again as it passes across the interface. Intensity again drops down in stone phase. Higher intensity at the interface region shows higher ettringite concentration.

Intensity of crystalline SiO_2 (Q) decreases within the paste

phase as it approaches the interface region, increases again at the interface and gradually diminishes in the stone phase. This shows that the paste region close to the interface is richer in SiO_2 than the bulk paste phase.

Diamond [12] found a relationship between the diffraction peak of the CSH amorphous halo and CaO content; the position of the diffraction maximum shifts to higher angles with increasing CaO contents of up to 20%, but thereafter remains constant at about 32 degrees two theta. The halos observed in the 18 to 36 degree two theta range are due to amorphous CSH; the peak was around 32 degrees two theta in the paste phase. It is interesting to note here that the peak position tends to shift to a lower two theta position, around 31 degrees, as it approaches the interface; this may indicate that the CSH gel becomes deficient in calcium and rich in silica. Also, the area of the halo decreases towards the interface, showing lesser amounts of cementitious material.

The halos observed in the 8 to 16 degree two theta range, with the peak at around 12 degrees two theta, are due to the formation of calcium-aluminum-hydrate (CAH) and calcium-aluminum-silicate-hydrate (CASH). It is interesting to note that the area of this halo does not decrease as it moves towards the interface, but the peak position shifts from 12 degrees two theta to 10 degree two theta. This may indicate that concentrations of CAH and CASH remain more or less uniform throughout the paste phase; but CAH and CASH become poorer in

calcium content near the interface, thereby producing weaker cement.

Neal #4 fly ash with 3% ammonium phosphate

X-ray diffractograms are shown in Appendix B-3. Traces 1 and 2 are diffraction patterns from the paste phase, traces 3-9 represent gradual transitions from the paste to the stone through the interface region, and traces 10-12 are for the pure limestone.

Principal hydration products from the paste phase are ettringite (E), monosulfoaluminate (M), stratlingite (S), CSH, CAH and CASH.

The intensity of ettringite remains relatively constant throughout the paste phase; the diffractogram for the paste closer to the limestone boundary (trace 9) also show the same ettringite intensity as in the bulk paste phase. Ettringite intensity gradually drops down throughout the aggregate phase. This shows that there is no excess concentration of ettringite at the interface.

Monosulfoaluminate and stratlingite show more distinct diffraction peaks in the bulk phase than in the interface, showing thereby that the interface is deficient in those two compounds.

Crystalline SiO_2 intensity at first increases and then decreases towards the interface, showing that the interface is deficient in SiO_2. It is interesting to note here that the diffraction peaks of SiO_2 have a higher intensity than that observed in the plain Neal #4 fly ash specimen.

CSH halos form in the 18 to 36 degree two theta range, with peaks

at around 32 degrees two theta. The intensity and peak position of the halos remain relatively unchanged throughout the paste phase; the intensity reduces slowly at the interface. The intensity of CSH amorphous halo is very high compared to the untreated specimen, indicating that cementitious CSH gel plays a very important role in the bonding process. This gel has higher cementing properties because it does not become deficient in calcium, enabling it to produce higher bond strength.

CAH and CASH halos form in the 8 to 12 degree two theta range, with peaks at around 9 degrees two theta. It is interesting to note that the intensity increases towards the interface, unlike CSH; but the peak position remains relatively unchanged.

Discussion

There is evidence of chemical reaction between the cement pastes and the limestone aggregate. The paste-aggregate irterface region is found to be distinctly different in compound composition and crystal orientation from the paste or aggregate.

The portland cement-limestone interface is composed mainly of crystalline $Ca(OH)_2$ and ettringite. It is deficient in amorphous CSH. One important finding is that the crystal orientation at the interface is different from the bulk paste phase; $Ca(OH)_2$ crystals form with an orientation tendency with their C-axis perpendicular to the limestone

surface. This may favor the epitaxial overgrowth of $Ca(OH)_2$ on the limestone surface, promoting very high bond strength. In fact, the bond was so strong that the aggregate ruptured during the tensile test and the bond remained intact.

The Neal #4 fly ash-limestone interface is composed mainly of ettringite; the ettringite concentration in this region is higher than in the paste. The CSH present at the interface is deficient in calcium, and much smaller in quantity when compared to the paste. The CAH and CASH present at the interface are also deficient in calcium. Ettringite concentration at the interface, and depletion of calcium from CSH, CAH and CASH may be responsible for the lower bond strength of the plain Neal #4 fly ash specimens when compared to the bond strength of ammonium phosphate treated Neal #4 fly ash specimens.

Ammonium phosphate treated Neal #4 fly ash-limestone interface does not show excess concentration of ettringite as compared to the paste. Also, there is not any depletion of calcium from CSH, CAH and CASH present at the interface region. The presence of CSH, CAH and CASH at the interface region of the ammonium phosphate treated specimens is possibly responsible for the stronger bond, as compared to the bond in the plain Neal #4 fly ash-limestone specimens.

ELEMENTAL ANALYSIS ACROSS PASTE-AGGREGATE INTERFACE BY ELECTRON MICROPROBE

Electron microprobe (EMP) tests were performed to obtain quantitative elemental analyses across the paste-aggregate interface. The data are used to explain measured bond strength and to supplement interpretation of x-ray diffraction analysis.

Procedure

Composite specimens were prepared the same way as for x-ray diffraction testing and cured for 15 months, then broken in the middle to expose a fresh paste-aggregate boundary. The exposed surface was polished, impregnated with resin, and polished again. Next, the specimens were oven dried at 60° C for 24 hours and an approximately 150-200 A° thick carbon coating was applied.

Specimens of plain cement paste were prepared by molding the pastes (W/C ratio = 0.24) in plastic rings of 1" diameter x 3/4" high and cured in a humidity room until tested. An aggregate specimen was prepared by cutting the rock into a slab measuring 1" x 1/4" x 3/4". Polishing and carbon coating was done in the same manner as in the composite specimens.

Plain paste and rock specimens were tested by directing the electron beam at random spots on the test surface. For composite specimens, the electron beam was shot at various spots along three

randomly selected traverses across the paste-aggregate interface, starting at 300 um on the limestone side to 1000 um into the paste.

A preliminary analysis was performed by a scanning electron microscope (SEM) equipped with an energy dispersive spectrometer (EDS) to determine the physical boundary of the interface region. The rock sides of composite specimens showed very little variation in elemental composition; therefore, only eight EMP locations in the limestone up to 300 um away from the paste-aggregate contact surface were tested. Because the pastes had considerable variation in elemental composition, twenty locations up to 1000 um away from the paste-aggregate contact surface were necessary to define unaltered material. Interface regions were tested at much closer intervals than the bulk paste or aggregate phases to investigate elemental composition of the interface in detail.

Results

Elemental compositions of the Indiana limestone, portland cement paste and Neal #4 fly ash are in the Table 12. Elemental composition of Neal #4 fly ash compares very well with that in Table 13 obtained by Bergeson [5] from x-ray fluorescence tests. A typical elemental composition across the paste-aggregate interface of a composite specimen is in Figure 12; each value shown is the average of three measurements. Discussion of the result is limited to the three major

Table 12. Elemental composition of Indiana limestone, Type I portland cement (Monarch brand) and Neal #4 fly ash

Elemental Composition (%)	Indiana Limestone	Portland Cement	Neal #4 Fly Ash
Number of Tests	16	9	10
SiO_2	0.06 (0.03)[a]	23.66 (1.84)	31.83 (2.29)
TiO_2	0.00 (0.01)	0.18 (0.16)	0.89 (0.40)
Al_2O_3	0.19 (0.27)	5.51 (1.19)	18.05 (1.76)
FeO	0.04 (0.03)	2.08 (0.31)	5.95 (0.95)
MgO	2.17 (0.36)	3.03 (0.71)	6.19 (1.34)
CaO	53.17 (1.40)	61.68 (1.49)	29.64 (2.51)
BaO	0.03 (0.03)	0.13 (0.11)	0.85 (0.45)
Na_2O	0.02 (0.09)	0.27 (0.34)	1.52 (1.10)
K_2O	0.02 (0.03)	0.84 (0.83)	0.31 (0.18)
P_2O_5	0.45 (0.07)	0.41 (0.12)	1.30 (0.54)
SO_3	0.09 (0.06)	2.02 (0.85)	3.34 (0.54)
Total	56.23 (1.35)	100	100

[a]Number in parentheses is one standard deviation.

Table 13. Elemental composition of Neal #4 fly ash

Elemental Composition (%)	Actual	Literature[a]
SiO_2	31.83	32.1
TiO_2	0.89	1.2
Al_2O_3	18.05	19.7
FeO	5.95	5.8
MgO	6.19	7.7
CaO	29.64	29.5
BaO	0.85	-
Na_2O	1.52	2.2
K_2O	0.31	0.3
P_2O_5	1.30	-
SO_3	3.34	-
Total	100	98.5

[a]After Bergeson [5].

elements such as CaO, SiO_2 and Al_2O_3. The rest of the elements did not show any significant distribution pattern; however, the results are shown in Appendix D.

Bergeson [5] applied concepts from glass chemistry to the Iowa fly ashes that the reactivity of the glassy phase of fly ashes can be characterized by an index which is the ratio of glass formers to modifiers, expressed by $(SiO_2+Al_2O_3)/(CaO+MgO)$. Comparing the elemental former/modifier ratio with the glassy phase former/modifier ratio, Bergeson [5] found a linear relationship and suggested that data from elemental analysis can be utilized to characterize the glassy phase of a fly ash. He also suggested that the lower the ratio the more reactive the glass structure would be, and found that fly ashes having lower ratio show higher compressive strength. It will be seen later that this concept can be used in explaining the bond strength and the nature of tensile failure.

Limestone-portland cement paste specimen

Elemental composition across the paste-aggregate interface is shown in Figure 12. The following observations are made:

1) Diffusion of CaO from 0-100 um of the aggregate region and from 70-170 um of the paste region towards the paste region near the aggregate boundary (0-50 um).
2) Diffusion of SiO_2 from the paste side near the aggregate boundary

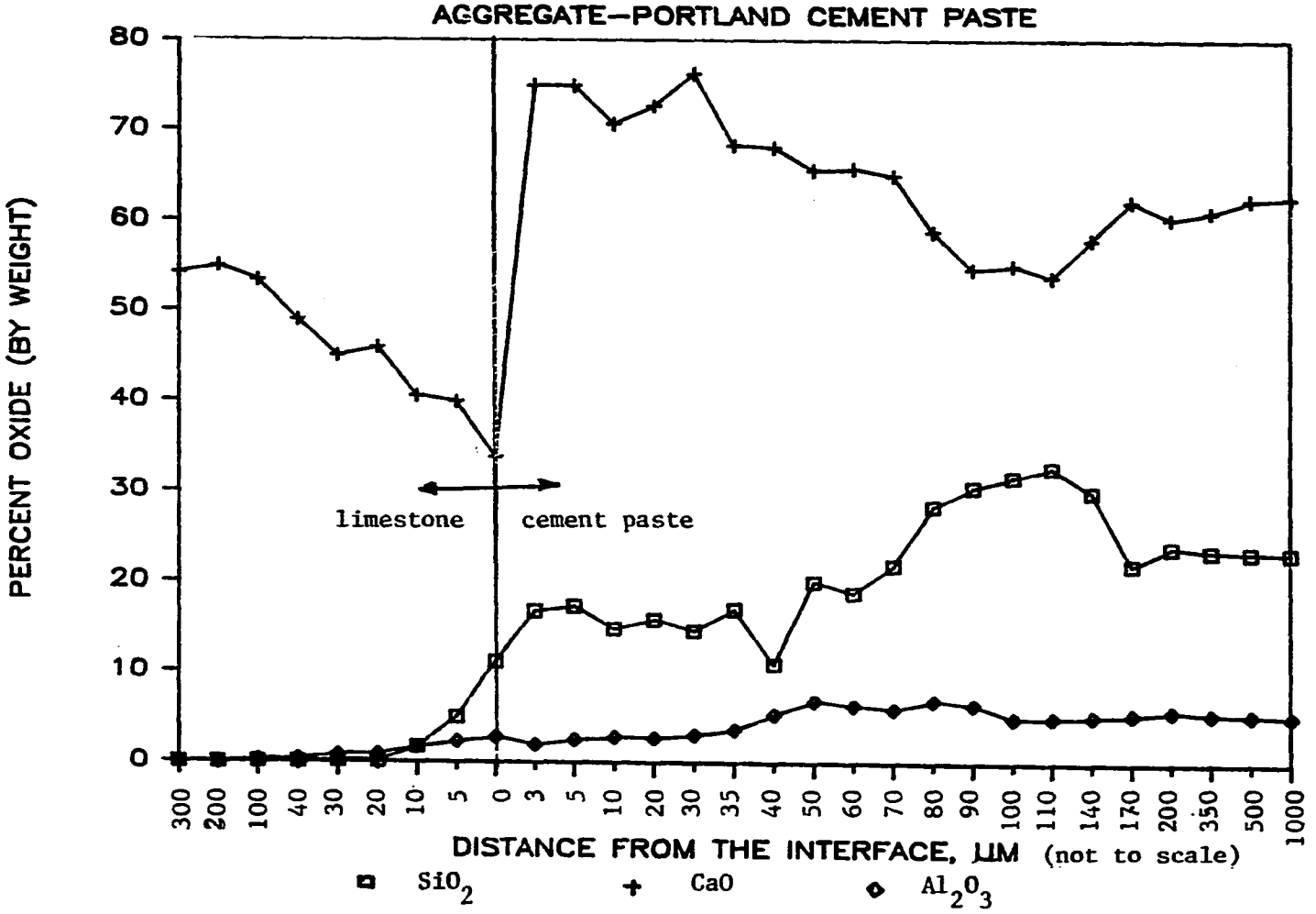

Figure 12. Elemental composition across the limestone-portland cement paste interface

(0-70 um) towards 70-170 um of the paste region and 0-20 um of the limestone region.

3) Diffusion of Al_2O_3 from the paste side near the aggregate boundary (0-40 um) towards the aggregate side (0-30 mm) and 40-100 um of the paste region.

The above observations indicate that the elemental composition of the interface region is distinctly different from the bulk aggregate or paste phases. Interphase diffusion of elements between the portland cement paste and the limestone is clearly evident. The paste side near the aggregate boundary becomes rich in CaO, but becomes deficient in SiO_2 and Al_2O_3, this supports the finding from the x-ray tests that the interface region is composed mainly of $Ca(OH)_2$, a calcium rich compound, and deficient in CSH. The accumulation of excess calcium at the interface may be responsible for the strong bond observed (average 28 day strength is 596 psi at the W/C ratio of 0.24). Penetration of SiO_2 and Al_2O_3 into the calcite crystal may be an indication of a chemical reaction between cement paste and limestone.

Limestone-Neal #4 fly ash paste specimen

Elemental composition across the paste-aggregate interface is shown in Figure 13. With the exception of a slight diffusion of CaO

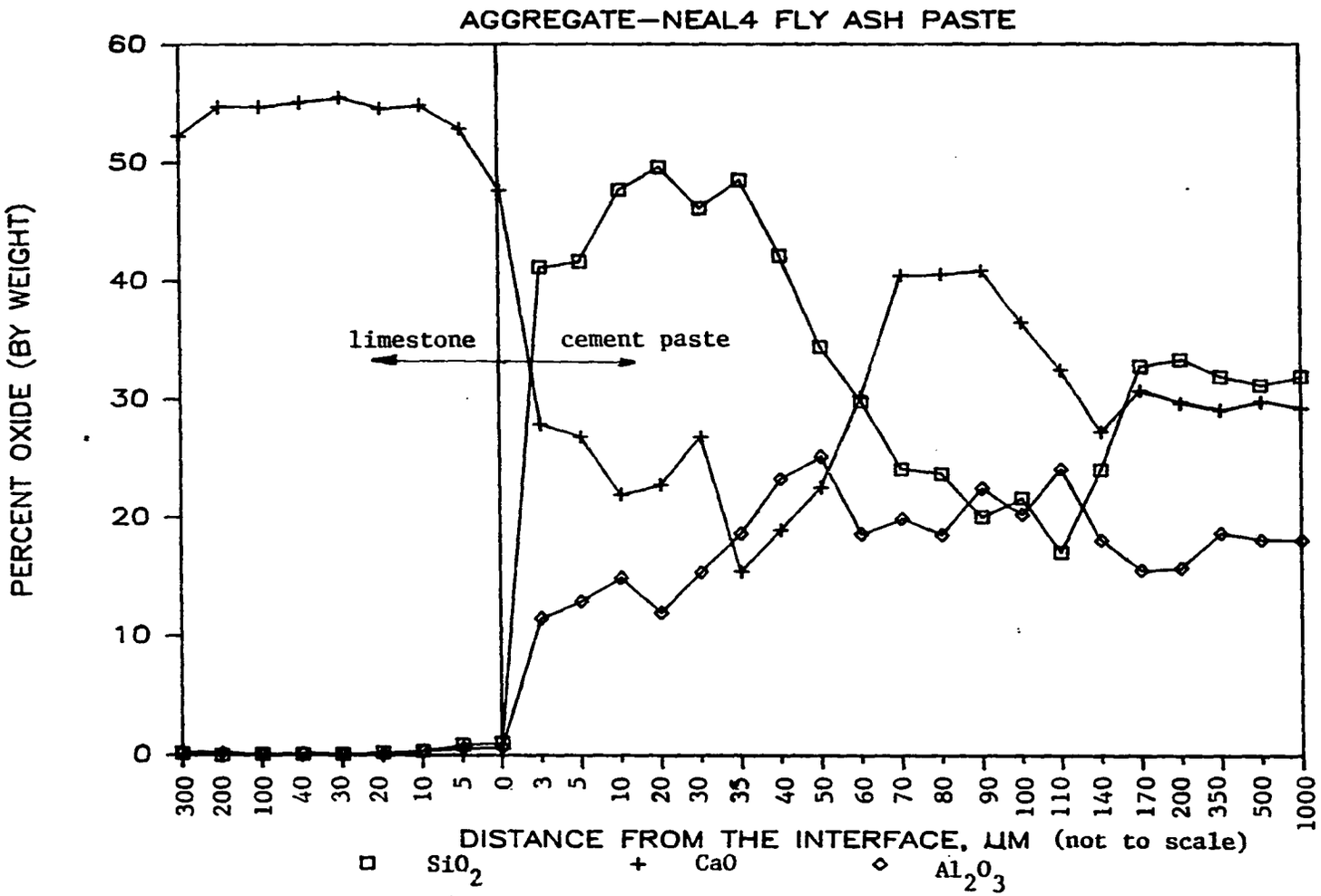

Figure 13. Elemental composition across the limestone-Neal #4 fly ash paste interface

from the limestone side towards the paste side, there is very little interphase elemental diffusion. The following observations mainly are limited to the paste:

1) Diffusion of CaO from the aggregate side (0-10 um) and from the paste side (0 to 50 um) towards 60-170 um of the paste region. The paste-aggregate contact region thus becomes deficient in CaO.
2) Diffusion of SiO_2 from 60-170 um of the paste region towards 0-60 um of the paste side near the aggregate boundary.
3) Diffusion of Al_2O_3 from 0-35 um and from 140-300 um of the paste region towards 35-140 um of the paste region.

Redistribution of elements within the paste phase is clearly evident. The paste region closer to the aggregate boundary becomes richer in SiO_2 and deficient in CaO and Al_2O_3 when compared to the bulk paste phase, indicating an inferior bonding quality (average 28 day bond strength of plain fly ash specimens is 96 psi at the W/C ratio of 0.24 against the corresponding bond strength of 122 psi of ammonium phosphate treated fly ash specimens). These results support findings of the x-ray diffraction tests that calcium-silicate-hydrate, calcium-aluminate-hydrate and calcium-aluminate-silicate-hydrate present at the paste-aggregate contact region are deficient in calcium.

The elemental $(SiO_2+Al_2O_3)/(CaO+MgO)$ ratio of the paste, Figure

14, is higher near the aggregate boundary (0-50 um) than it is in the bulk paste phase, meaning that the fly ash glassy phase was chemically less reactive there. Because the silica-rich paste predominates, the cementing property of this region is inferior to the bulk phase and the region (0-50 um) is weaker through which bond failure is likely to occur.

Limestone-Neal #4 (3% ammonium phosphate treated) fly ash paste specimen

Elemental composition across the paste-aggregate interface is shown in Figure 15. There is very little evidence of interphase elemental diffusion. Redistribution of elements within the paste took place, however. The following observation is mainly limited to the paste phase:

1) Diffusion of CaO from the 50-200 um of the paste region towards the paste region near the aggregate boundary (0-50 um).
2) Diffusion of SiO_2 from 0-50 um of the paste region towards 50-110 um of the paste region.
3) Diffusion of Al_2O_3 from 0-100 um of the paste region towards 100-200 um of the paste region.

The paste side closer to the aggregate boundary (0-50 um) is rich in high calcium cementitious compounds; this supports findings from

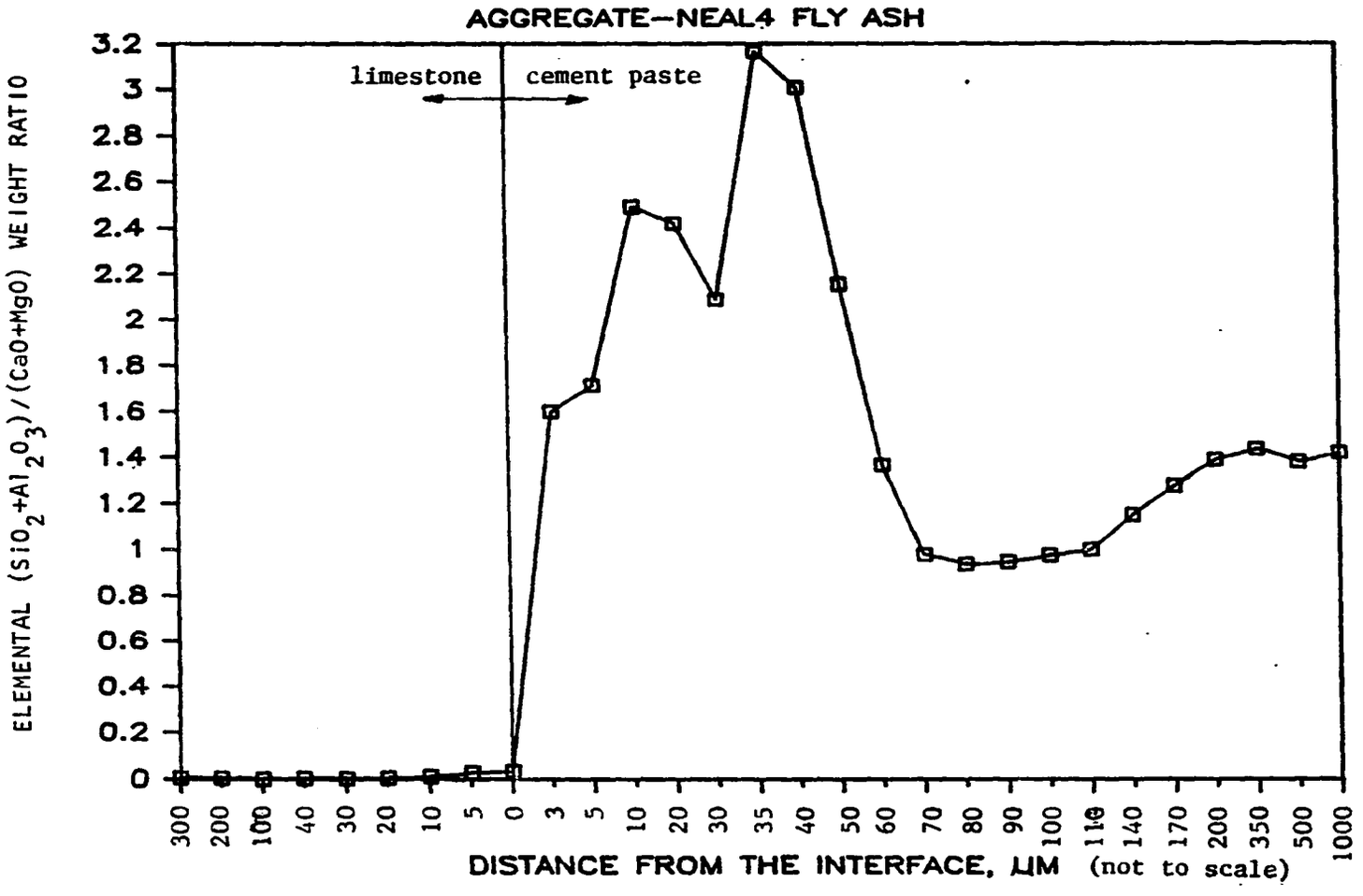

Figure 14. Elemental $(SiO_2+Al_2O_3)/(CaO+MgO)$ weight ratio of Neal #4 fly ash at the contact region

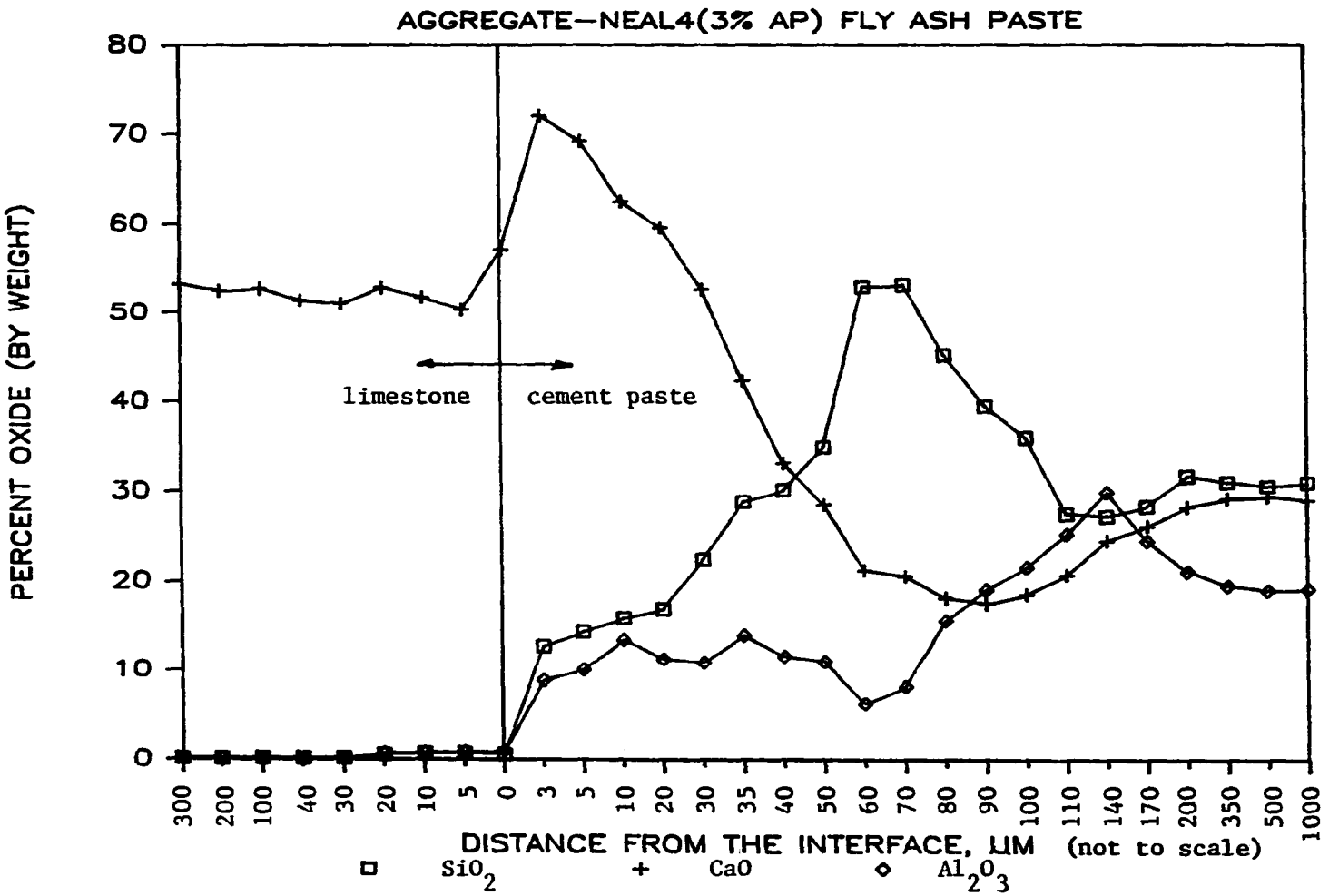

Figure 15. Elemental composition across the limestone-ammonium phosphate treated Neal #4 fly ash paste interface

the x-ray diffraction test that the contact region is composed of calcium rich calcium-silicate-hydrate, calcium-aluminate-hydrate and calcium-aluminum-silicate-hydrate compounds. The presence of these cementitious gels makes the bond between the cement paste and the aggregate very strong. Tensile failure is likely to occur outside this region. An intermediate region in the paste (50-350 um) offers a weaker zone through which bond failure is more likely to take place.

The elemental $(SiO_2+Al_2O_3)/(CaO+MgO)$ ratio of the ammonium phosphate treated Neal#4 fly ash paste, Figure 16, is lower in the region closer to the aggregate boundary (0-50 um) and higher in the 50-350 um region than it is in the bulk paste phase, meaning that the fly ash glassy phase was chemically more reactive at the interface and therefore capable of producing strong bonds.

Discussion

The cement paste-aggregate interface is distinctly different from the bulk paste or aggregate. Evidence exists of interphase elemental diffusion and also of redistribution of elements within the paste. Both the magnitude of bond strength and the location of the failure zone correlate with the nature of the elemental distribution at the interface.

The limestone-portland cement specimen shows that a paste

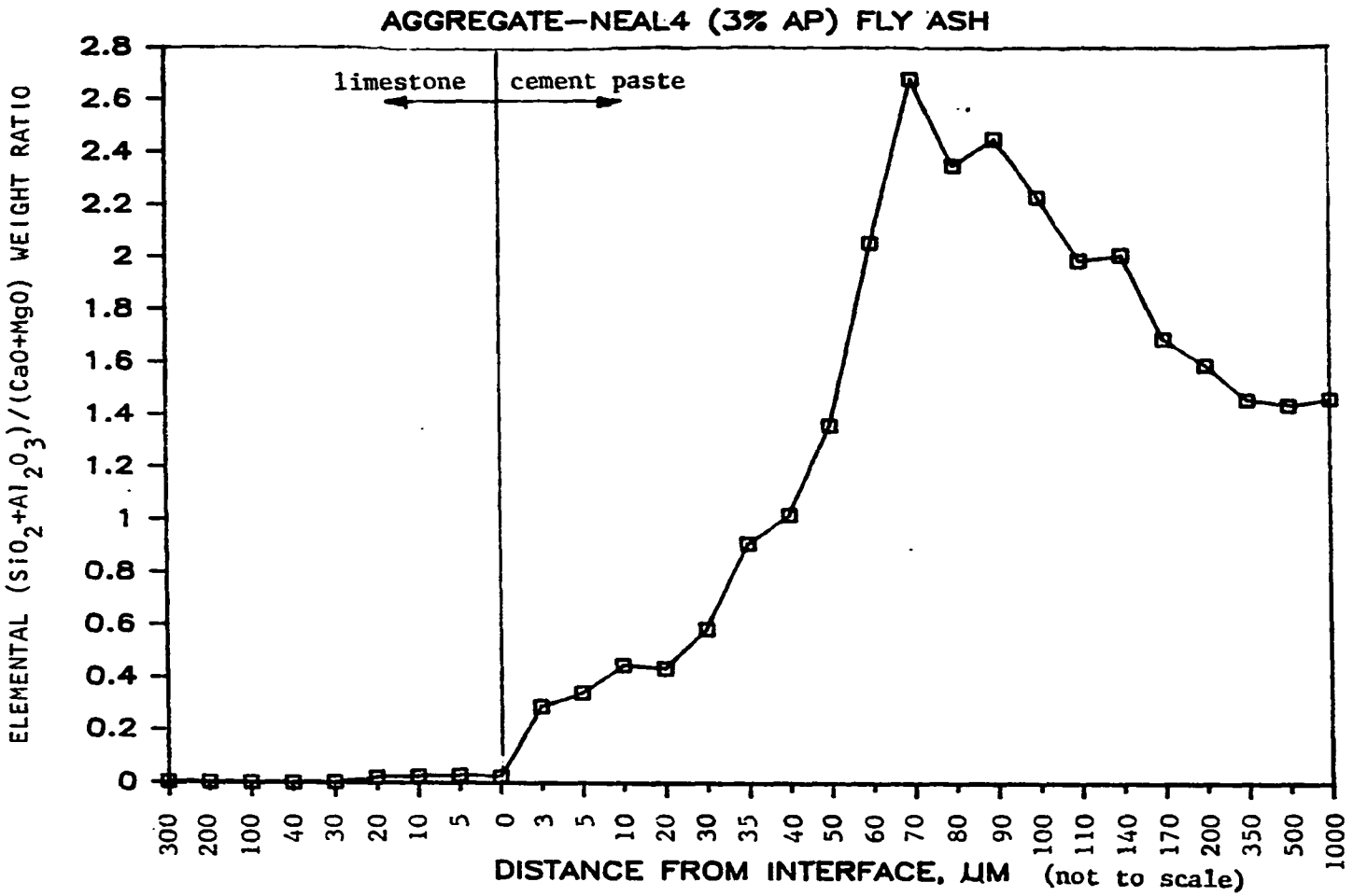

Figure 16. Elemental (SiO_2+Al_2O_3)/(CaO+MgO) weight ratio of ammonium phosphate treated Neal #4 fly ash at the contact region

region adjacent to the aggregate boundary becomes richer in calcium and deficient in silica and alumina content; calcium leaches out from the limestone towards the cement paste, and silica and alumina from the paste diffuse towards the limestone. Bond strength is very high due to the accumulation of excess calcium in the paste closer to the aggregate boundary, whereas the limestone becomes weaker through leaching of calcium as evidenced by the rupturing of aggregates during the tensile tests.

The limestone-Neal #4 fly ash specimen shows very little interphase elemental diffusion; redistribution of elements within the paste takes place, however. The paste, in contact with the aggregate, becomes richer in silica and deficient in calcium and alumina content, thereby making this region weaker. The glassy phase of Neal #4 fly ash at the paste-aggregate contact region was less reactive when compared to that of the bulk phase and may be responsible for low bond strength. Failure of plain Neal #4 fly ash specimens takes place through the paste very close to the aggregate boundary.

Ammonium phosphate treated Neal #4 fly ash specimen shows redistribution of elements within the paste but it does not show interphase elemental diffusion. Accumulation of excess calcium in the paste near the aggregate boundary, and diffusion of silica and alumina from the interface towards the bulk paste is observed. Also, the glassy phase of the fly ash at the aggregate boundary was more reactive than that of the bulk phase; this may be responsible for promoting

bonding superior to that of plain fly ash specimens. Tensile failure takes place through the paste away from the aggregate boundary, where it may be deficient in calcium and relatively rich in silica.

The improved bond strength of Neal #4 fly ash specimens after the addition of ammonium phosphate may be due to a change in elemental distribution and increased reactivity of the fly ash glassy phase at the aggregate boundary. The failure zone in plain fly ash specimens is through the paste, very close to the aggregate boundary as evidenced by a thin layer of paste sticking to the aggregate surface; that layer becomes much thicker after the addition of ammonium phosphate, visually indicating a stronger bond between the paste and the aggregate.

CEMENT PASTE-AGGREGATE REACTION AND ITS INFLUENCE ON THE PORE SIZE DISTRIBUTION OF CONCRETE

Studies of the pore size distribution were performed to evaluate the physical character of paste-aggregate interaction. This study is important because strength and durability of concrete are greatly influenced by pore structure of concrete.

Procedure

Indiana limestone, portland cement, and plain and 3% ammonium phosphate treated Neal #4 fly ash were used to make composite specimens. Limestone blocks, about 3/8" X 3/8" X 1-1/8" in size, were shaped by filing them to the form of half cylinders, measuring about 1/8 " in radius and about 1" long. The flat surface along the longitudinal axis was polished with a number 600 grit sandpaper. To make reacted composite specimens (i.e., those in which aggregate and cement paste remain in contact during curing), the cement paste (w/c = 0.24) was placed on the flat surface of the limestone in such a way that the specimens were full cylinders in shape. For unreacted composite specimens, the limestone was prepared as described above, except that no cement paste was placed on the flat limestone surface; instead, the cement paste was molded in a half cylinder form, similar to that of limestone, in a petri dish and was allowed to cure separately. All specimens were cured for 14, 28 and 90 days and oven

dried at 105° C for a period of 48 hours before porosimeter testing.

Pore structures were evaluated using a Quantachrome SP 2000 mercury intrusion porosimeter. Pressures of up to 60,000 psi were used to force mercury, a nonwetting liquid, into smaller and smaller sized pores. The volume intruded was recorded and plotted over the range of pore sizes. The porosimeter was used to scan over 0-1200, 0 to 6000 and 0-60,000 psi pressure ranges to obtain information on all pore sizes up to 18 angstroms radius.

At first, pore size distribution was obtained for reacted composite specimens; the amount of stone and paste in each specimen is shown in Table 14. Then, the companion unreacted specimens (containing the same amount of stone and paste) were tested to obtain the pore-size distribution.

Reacted composite specimens made with plain Neal #4 paste were found to split off at the paste-aggregate contact surface during oven drying before the mercury porosimeter tests. Because of the sample preparation problem and lack of resources it was decided to exclude Neal #4 fly ash specimens from porosimeter testing.

Results

The experimental pore size distribution data in this work are presented in the form of cumulative pore size distribution curves, the pore volume parameter being expressed as percent of the total specimen

Table 14. Mercury porosimeter specimens

Specimen Designation	Age Days	Weight (gm) Stone	Cement Paste	Total
Neal #4 Fly Ash + 3% Ammonium Phosphate				
A1	14	1.16	0.51	1.67
A2	14	1.17	0.44	1.61
A3	28	1.19	0.56	1.75
A4	28	1.11	1.04	2.15
A5	28	1.34	0.69	2.03
A6	90	1.07	0.68	1.75
A7	90	0.97	0.60	1.57
A8	90	1.24	0.51	1.75
Portland Cement				
B1	14	1.02	0.63	1.65
B2	14	1.52	1.09	2.61
B3	28	1.20	0.63	1.83
B4	28	1.28	0.82	2.10
B5	90	1.34	0.52	1.86
B6	90	1.18	0.72	1.90

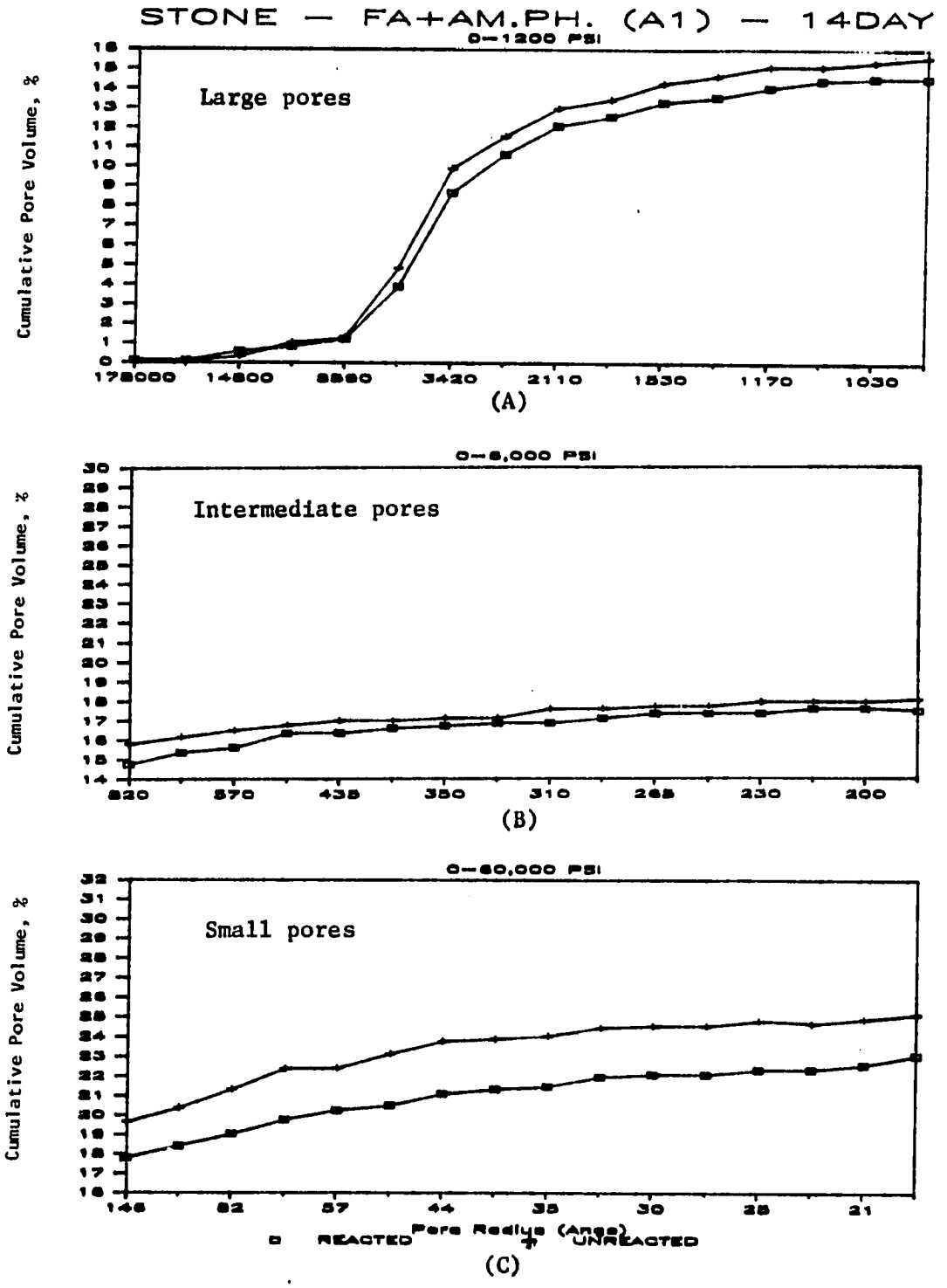

Figure 17. A typical cumulative pore size distribution of limestone-cement paste composite specimens (reacted and unreacted)

volume. The results are presented for 14, 28 and 90 day cured composite specimens, both reacted and unreacted, in Appendix E. A typical representation of cumulative pore size distribution curves, such as Figure 17, shows three sets of intrusion tests. Figure 17a shows results for large capillaries from 178,000 to 889 angstroms, a pressure range of 0-1200 psi. Figure 17b shows results for intermediate capillaries from 820 to 190 angstroms, a pressure range of 0-6000 psi. Finally, Figure 17c shows results for small capillaries from 146 to 18 angstroms, a pressure range of 0 to 60,000 psi. Pore size designations (i.e., "large," "intermediate," and "small") are rather arbitrary and will be used hereinafter for convenience in comparison.

Neal #4 fly ash (treated with ammonium phosphate) specimens

The cumulative pore volume was smaller in reacted specimens than in unreacted ones, showing a reduction in porosity in all the pore size ranges. The nature of the reduction in porosity is time dependent, being most prominent in large and small capillaries after 14 day curing. The 28 day cured specimens, in general, showed a comparable reduction in pore volumes of all pore sizes. As the curing was continued, after 90 days, reduction in pore volumes of large and intermediate size capillaries was more than that of small capillaries.

Portland cement specimens

The results are, in general, similar in nature to the fly ash specimens; reacted specimens showed smaller cumulative pore volumes than the unreacted ones. However, there are also some differences in the nature of reduction in pore volumes. The pore volumes of large capillaries were affected least, regardless of curing periods. At the early stages of curing, after 14 days and also after 28 days, reduction in pore volumes of the small and the intermediate size capillaries were comparable. However, as curing was continued, after 90 days, pore volumes of intermediate size capillaries were reduced most.

Discussion

The important finding of this investigation is that the interaction between the limestone and ammonium phosphate treated Neal #4 fly ash and portland cement pastes causes a reduction in the porosity of the paste-aggregate composite specimens over a wide range of pore sizes. Although there is a slight difference in the responses from Neal #4 fly ash and portland cement generally, they are in good agreement.

The nature of the reduction in porosity is time dependent. Ammonium phosphate treated Neal #4 fly ash specimens showed the reduction in pore volumes of large (178,000 - 889 angstrom radius) and

small (146 - 18 angstrom radius) capillaries to be more prominent compared to the intermediate (820 - 190 angstrom radius) size capillaries, after a curing period of 14 days. Then, capillaries of all sizes experienced a more or less uniform reduction in pore volumes at the end of 28 days. As the hydration continued, after 90 days, reduction in pore volumes of the large and intermediate size capillaries is more pronounced than the that of the small size capillaries.

By contrast, portland cement specimens showed that, regardless of curing periods, the pore volume of the large capillaries is affected least. At the early stages of hydration, such as after 14 days and also after 28 days of curing, reduction in pore volumes of the small and intermediate size capillaries are comparable. After a longer curing time, at the end of 90 days, pore volumes of the intermediate capillaries are reduced most.

Although the reason for reduction in the porosity of the reacted composite specimen due to cement paste-aggregate interaction is speculative, the following mechanisms may be presented as possible explanations.

It is possible to accumulate cement hydration product in the pore spaces of the aggregate. Dissolution of the carbonate phase may also take place by the etching action of cement pastes, resulting in the blocking of pore spaces of the aggregate. Barnes et al. [4] reported aggregate pore filling by secondary $Ca(OH)_2$ crystals.

Limestone may contract volumetrically when it is placed in contact with cement pastes which normally have high pH values. Lemish and Moore [20] showed that contraction of certain carbonate rocks does take place in the alkaline environment.

Results from the x-ray diffraction tests indicated that the portland cement-aggregate interface is composed of highly ordered $Ca(OH)_2$; the interface region becomes more structured than the bulk paste phase which may result in a denser configuration.

Predominance of amorphous calcium-silicate-hydrate (CSH), calcium-aluminate-hydrate (CAH) and calcium-aluminate-silicate-hydrate (CASH) at the ammonium phosphate treated Neal #4 fly ash-limestone interface may produce a denser interface region because of their gel-like structure.

Regardless of the mechanism, reduction in pore volumes due to the paste-aggregate interaction can cause a multitude of effects in concrete behavior. The reduction in pore volumes may increase strength and decrease permeability. Reduced permeability should improve the durability of concrete against deleterious chemical attack. It is speculated, however, that a decrease in permeability at the interface region may cause generation of increased hydraulic pressure during freezing which can adversely affect the freeze-thaw durability of the cement paste-aggregate bonds.

SUMMARY AND CONCLUSIONS

Tensile Bond Strength Test

1. Ammonium nitrate is not effective in increasing bond strength between slightly cementitious Neal #2 fly ash and limestone, although it increases paste strength.

2. Dibasic ammonium phosphate increased both the bond and paste strengths of the highly cementitious Neal #4 fly ash specimens.

3. Fly ash concretes may require more strict quality control measures and longer curing times than portland cement concrete.

4. The cement paste-aggregate bond failures took place through the contact surface in Neal #2 fly ash, through the paste in Neal #4 fly ash, and through the aggregate in portland cement specimens. It may, therefore, be concluded that paste strength controls the bond strength of highly cementitious fly ash concretes, whereas aggregate strength is a controlling factor in portland cement concretes.

X-ray Diffraction Examination

1. The cement paste-aggregate interface region is distinctly different in chemical composition and crystal orientation when compared to the paste or the aggregate bulk phases.

2. Portland cement paste-limestone bonding mainly results from epitaxial growth of $Ca(OH)_2$ over the aggregate surface, because

crystal lattices of $Ca(OH)_2$ and limestone are compatible.

3. Plain Neal #4 fly ash paste-limestone bonding is mainly due to the growth of ettringite at the aggregate surface. Higher concentrations of ettringite and lower concentrations of calcium-silicate hydrate (CSH, which is also deficient in calcium) at the aggregate boundary may have caused the lower bond strength, in comparison with the ammonium phosphate treated specimens.

4. Ammonium phosphate treated Neal #4 fly ash-limestone bonding is mainly due to the formation of abundant calcium rich calcium-silicate hydrate (CSH) at the interface which makes the bond stronger.

5. In the treated Neal #4 specimen, the concentrations of calcium-aluminate hydrate (CAH) and/or calcium-aluminum-silicate hydrate (CASH) are higher at the interface than in the untreated specimen, and also richer in calcium. The high calcium, cementitious CAH and CASH gels may contribute to stronger bonds.

Electron Microprobe (EMP) Test

1. The elemental composition of the paste-aggregate interface region is different from the paste or the aggregate bulk phases; interphase elemental diffusion and redistribution of elements within the paste phase are evident.

2. The portland cement-limestone specimen showed the diffusion of calcium from the limestone towards the paste and diffusion of

silica and alumina from the paste towards the limestone. Accumulation of excess calcium in the interface may be responsible for very high bond strength; the rupturing of aggregates during tensile tests may indicate that the limestone becomes weaker by leaching out of calcium.

3. The plain Neal #4 fly ash-limestone interface showed lower calcium and alumina concentrations, and higher silica concentration when compared to the bulk paste phase. Addition of ammonium phosphate to the Neal #4 fly ash reversed the trend, and caused an accumulation of excess calcium at the interface; diffusion of silica and alumina towards the bulk paste is also observed. The higher calcium concentrations, an indicator of excess cementitious material, at the interface region produced stronger bonds in treated specimens.

4. The glassy phase chemical state of the plain Neal #4 fly ash at the paste-aggregate interface region was less reactive than that of the treated fly ash, which may be a reason for lower bond strength.

Mercury Porosimeter Test

1. Interaction between the Indiana limestone and ammonium phosphate treated Neal #4 fly ash and portland cement pastes causes a reduction in pore volumes over a wide range of pore sizes, which may cause a decrease in permeability and an increase in strength. Reduced permeabilty at the interface region should improve the resistance to chemical attack, but it is speculated that constriction of pore spaces

may cause increased hydraulic pressure during freezing which can adversely affect the freeze-thaw durability of bonds.

2. The reduction in porosity depends on the degree of hydration of the cement pastes and the type of cement used. The ammonium phosphate treated Neal #4 fly ash-limestone specimens showed that the reduction in pore volumes was more prominent in the 146-18 and 178,00 - 889 angstrom ranges than in the 820 - 190 angtrom range after 14 days of curing; after 28 days, pores of all sizes experienced a uniform reduction; after 90 days, 820 - 190 and 178,00 - 889 angstrom size pores were reduced most.

3. The portland cement-limestone specimens showed, by contrast, that 178,00 - 889 angstrom size pores are affected least regardless of curing time. Reduction in pore volumes of 146 - 18 and 820 - 190 angstrom size pores are comparable after 14 and 28 days of curing. After 90 days 820 - 190 angstrom size pores were reduced most.

To summarize, these investigations provided an insight into the cement paste-limestone interface. Bond strength and the nature of bond both depend on the type of cement used; aggregate type also has an influence. There appears to be a potential for improving bond strength by treating highly cementitious fly ashes with ammonium phosphate; however, the resulting bond strength is still too lower compared to the portland cement paste, so more stringent quality control is warranted when using fly ash concrete.

RECOMMENDATIONS FOR FURTHER STUDY

The following suggestions are made for further research of the cement paste-aggregate bonds.

1. Bond between more fly ash and aggregate types, and its response to a variety of curing times and curing conditions should be studied.

2. Specimens saved from the tensile tests can be examined with a x-ray diffractometer and an SEM to identify the substances formed at the interface.

3. Differential thermal analysis (DTA) can be helpful in identifying the paste-aggregate reaction product(s), where x-ray diffraction tests fail to do so.

4. SEM micrographs and energy or wavelength dispersive x-ray (EDX or WDX) spectra should be obtained simultaneously from selected interface locations to study the interface microstructural detail and its effect on bond.

5. Mercury porosimetry and freeze-thaw durability tests should be performed on identical specimens to correlate pore size distribution to freeze-thaw resistance.

6. Specimens obtained from actual field condition should also be subjected to the various tests mentioned above. The objective will be to examine the microstructural development at the interface and correlate that to the actual field performance.

BIBLIOGRAPHY

1. Alexander, K. M., J. Wardlaw and D. J. Gilbert. "Aggregate-Cement Bond, Cement Paste Strength and the Strength of Concrete." Pp. 59-81 in Proceedings of the International Conference on the Structure of Concrete. London: Cement and Concrete Association, 1968.

2. Avram, C. Concrete Strength and Strains. New York: Elsevier Scientific Publishing Company, 1981.

3. Barnes, B. D., S. Diamond and W. L. Dolch. "The Contact Zone between Portland Cement Paste and Glass 'Aggregate' Surfaces." Cement and Concrete Research, 8(2) (1978), 233-244.

4. Barnes, B. D., S. Diamond and W. L. Dolch. "Micromorphology of the interfacial Zone Around Aggregates in Portland Cement Mortar." Journal of American Ceramic Society, 62(1-2) (1979), 21-24.

5. Bergeson, K. L. "The Glassy Phase and reaction Product of Iowa Fly Ashes." Ph. D. Thesis, Iowa State University, 1986. 121 pages.

6. Bergeson, K. L., J. M. Pitt and T. Demirel. "Increasing Cementitious Properties of Class C Fly Ash." Transportation Research Record, 998 (July 1985), 25-37.

7. Buck, A. D., and W. L. Dolch. "Investigation of a Reaction Involving Nondolomitic Limestone Aggregate in Concrete." Journal of American Concrete Institute, 63(7) (1966), 755-763.

8. Chatterji, S. and J. W. Jeffry. "The Nature of the Bond Between Different Types of Aggregates and Portland Cement." Indian Concrete Journal, 45(8) (1971), 346-349.

9. Cullity, B. D. Elements of X-Ray Diffraction. Second edition. Reading, Massachusetts: Addison-Wesley, 1978.

10. Cussino, L. and G. Pintor. "An Investigation into the Different

Behavior of Silicic and Calcareous Aggregates in Mixes with Regard to the Mineralogical Composition of the Cement." Il Cemento, 4 (1972), 255-268.

11. Demirel, T. "Notes on Soil Behavior." Unpublished, Civil Engineering Department, Iowa State University, 1983.

12. Diamond, S. "On the Glass Structure Present in Low-Calcium and in High-Calcium Fly Ashes." Cement and Concrete Research, 13 (1983), 459-464.

13. Facaoaru, I., G. Stanculescu and N. Tannenbaum. "Studies on the Cracking of Concrete under Uniaxial Stress Fields". Proceedings of the International Conference on Structure and Solid Mechanics, Southamton, 1969. New York: Wiley Interscience, 1971.

14. Fagerlund, G. "Strength and Porosity of Concrete." Proceedings of the International Symposium on Pore Structure and Properties of Materials. RILEM/IUPAC, D51-D53, Prague, 1973.

15. Hsu, T. T. C. and F. O. Slate. "Tensile Bond Strength Between Aggregate and Cement Paste or Mortar." Proceedings, Journal of American Concrete Institute, 60(4) (1963), 465-485.

16. Hsu, T. T. C., F. O. Slate, G. M. Starman and G. Winter. "Microcracknig of Plain Concrete and the Shape of Stress-Strain Curve." Proceedings, Journal of American Concrete Institute, 60(2) (1963), 209-224.

17. Iwasaki, N. and Y. Tomiyama. "Bond and Fracture Mechanism of Interface Between Cement Paste and Aggregate." Review of 30th General Meeting, Cement Association of Japan, 1976, 213-215.

18. Joint Committee on Powder Diffraction Standards (JCPDS). Powder Diffraction File Search Manual for Common Phases, Inorganic and Organic. Swarthmore, Pennsylvania: JCPDS International Center for Diffraction Data.

19. Lea, F. M. The Chemistry of Cement Concrete. New York: Chemical Publishing Company, 1971.

20. Lemish J. and W. J. Moore. "Carbonate Aggregate Reactions: Recent Studies and an Approach to the Problem." Highway Research Record, 45 (1964), 57-71.

21. Lyubimova, T. Yu. and E. R. Pinus. "Crystallization Structure in the Contact Zone Between Aggregate and Cement in Concrete." Colloid Journal of USSR., 24(5) (1962), 491-498.

22. Mindess, S. and J. F. Francis. Concrete. Englewood Cliffs, New Jersey: Prentice-Hall, Inc., 1981.

23. National Academy of Sciences. "Guide to Compounds of Interest in Cement and Concrete Research." Highway Research Board Special Report 127, 1972.

24. Ozol, M. A. "Shape, Surface Texture, Surface Area, and Coatings." American Society for Testing and Materials, STP 169B (1979), 584-628.

25. Patten, B. J. F. "The Effects of Adhesive Bond Between Coarse Aggregate and Mortar on the Physical Properties of Concrete." UNICIV Report No. R-82. University of New South Wales, Australia, 1972.

26. Perry, C. and J. E. Gillott. "The Influence of Mortar-Aggregate Bond Strength on the Behavior of Concrete in Uniaxial Compression." Cement and Concrete Research, 7(5) (1977), 553-664.

27. Philleo, R. E. "The Origin of Strength of Concrete." Symposium on Structure of Portland Cement Paste and Concrete - Highway Research Board. Special Report 90, 1966.

28. Pitt, J. M., T. Demirel, S. Schlorholtz, R. Hammerburg and R. Allenstein. "Final Report: Characterization of Fly Ash For Use in Concrete." Iowa Highway Research Board, Ames, Iowa, Project HR-225,

September 1983.

29. Pitt, J. M., T. Demirel, K. L. Bergeson, J. R. Rohde and J. Jashimuddin. "Final Report: Optimization of Soil Stabilization with Class C Fly Ash." Iowa Highway Research Board, Ames, Iowa, Project HR-260, January 1987.

30. Roy, C. N. R. Solid State Chemistry. New York: Marcel Dekker, Inc., 1974.

31. Scholer, C. F. "The Role of Mortar-Aggregate Bond in the Strength of Concrete." Highway Research Record, 210 (1967), 108-117.

32. Struble, L., J. Skanly and S. Mindess. "A Review of the Cement-Aggregate Bond." Cement and Concrete Research, 10(2) (1980), 277-286.

33. Suzuki, M. and K. Mizukami. "Bond Strength between Cement Paste and Aggregate." Review of 29th General Meeting, Cement Association of Japan, 1975, 94-96.

34. Suzuki, M. and K. Mizukami. "Bond Strength between Cement Paste and Aggregate." Review of 30th General Meeting, Cement Association of Japan, 1976, 211-213.

35. Tabor, D. "Principles of Adhesion - Bonding in Cement and Concrete." Pp. 63-87 in Proceedings of a NATO Advanced Research Institute on Adhesion Problems in the Recycling of Concrete. Editor Pieter C. Kreiger. Paris, France: Saint-Rem-les-Chevreuse, 1980.

36. Valenta O. "The Significance of the Aggregate-Cement Bond for the Durability of Concrete." International Symposium on the Durability of Concrete. Preliminary Report. Nakladatelostoi Ceskoslovenske Akademie Ved, Prague, 1961.

ACKNOWLEDGEMENTS

I am greatly indebted to my major professor Dr. John M. Pitt for his support, patience, encouragement and guidance at every phase of this research. I render special thanks to Dr. Richard Handy, Dr. Ken Bergeson, Dr. Edward Kannel and Dr. Robert Horton Jr. for serving on my Program of Study Committee. I would like to thank Dr. Alfred Kracher for his guidance and help in electron microprobe testing. I also remember my friend Glen (Oren) for his help in SEM testing and his encouragement in pursuing my career goal. Mr. Dave Robson deserves thanks for offering editorial services at various stages of the dissertation writing. Dr. Turgut Demirel, Dr. John Lemish and Dr. Vedat Enustun provided valuable suggestions on various aspects of this research and their effort is gratefully acknowledged.

I am also indebted to my parents without whose concern I would have not been in a position to earn an advanced education; my mother won't settle for anything less than a Ph.D. from me. I wish my father, who was a staunch supporter of higher education, were alive today to see one of his goals fulfilled. My wife Nasreen has been a major source of encouragement during the last four years of my life and no praise is high enough for her endurance during this episode.

All my relatives and friends deserve thanks for everything.

APPENDIX A

TENSILE STRENGTH OF LIMESTONE

1 X 1 3/4 X 12 inch prisms of Indiana limestone were procured from the Rowat Stone Company of Des Moines. The prisms were cut into 1 X 1 3/4 X 4 inch size; they were then hand filed to fit into the mold shown in Figure 4. After that the specimens were soaked in water for at least 24 hours before tensile testing. Tensile strength was measured for six specimens as shown below:

Specimen No.	Strength (psi)
1	587
2	578
3	600
4	622
5	657
6	720

Average strength = 627 psi,
Standard deviation = 49 psi,
Coefficient of variaton = 8 percent.

APPENDIX B

X-RAY DIFFRACTION TRACES

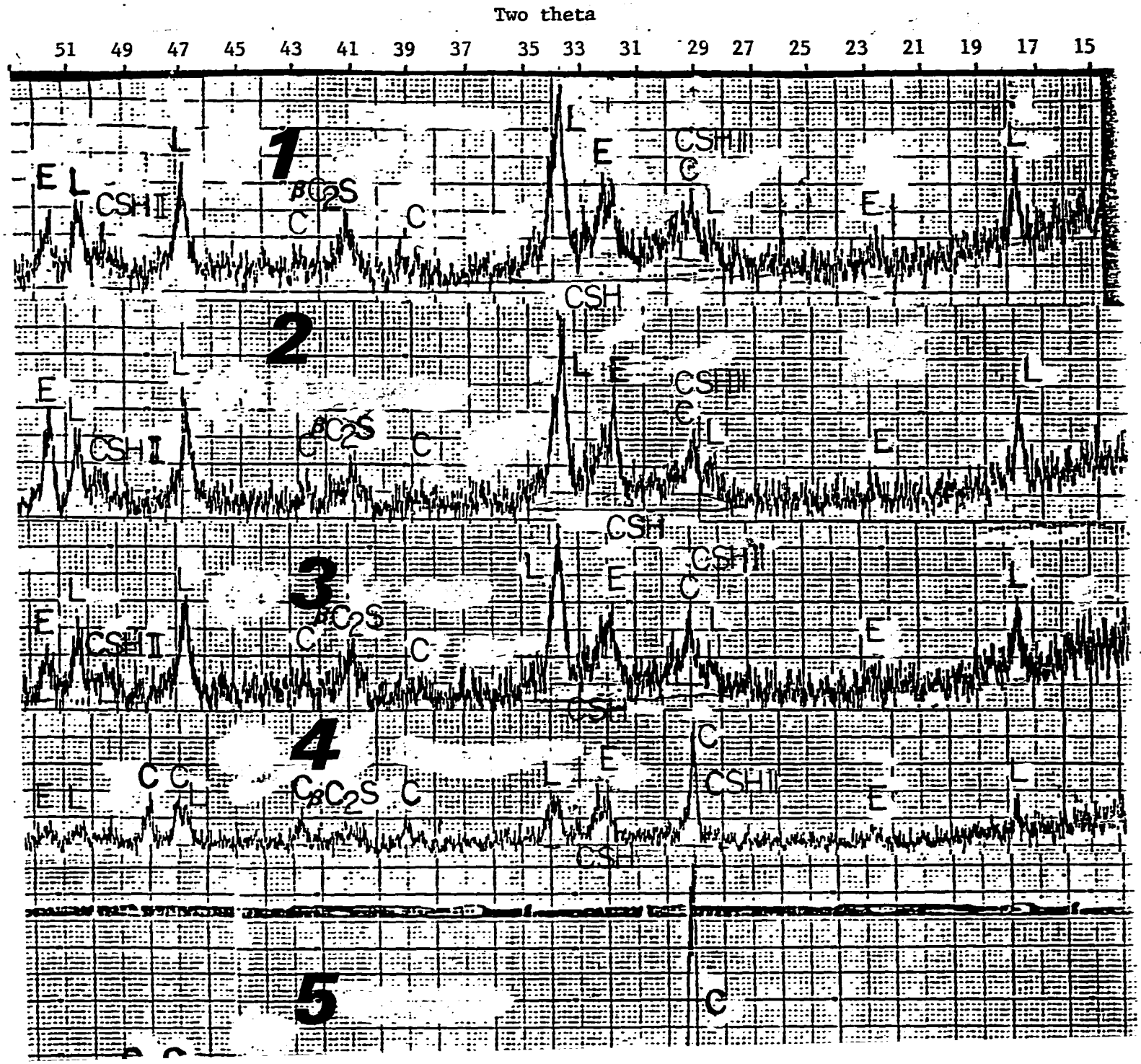
Two theta
51 49 47 45 43 41 39 37 35 33 31 29 27 25 23 21 19 17 15
1
2
3
4
5
CSH II
CSH
C
E
L
βC2S
C3C2S

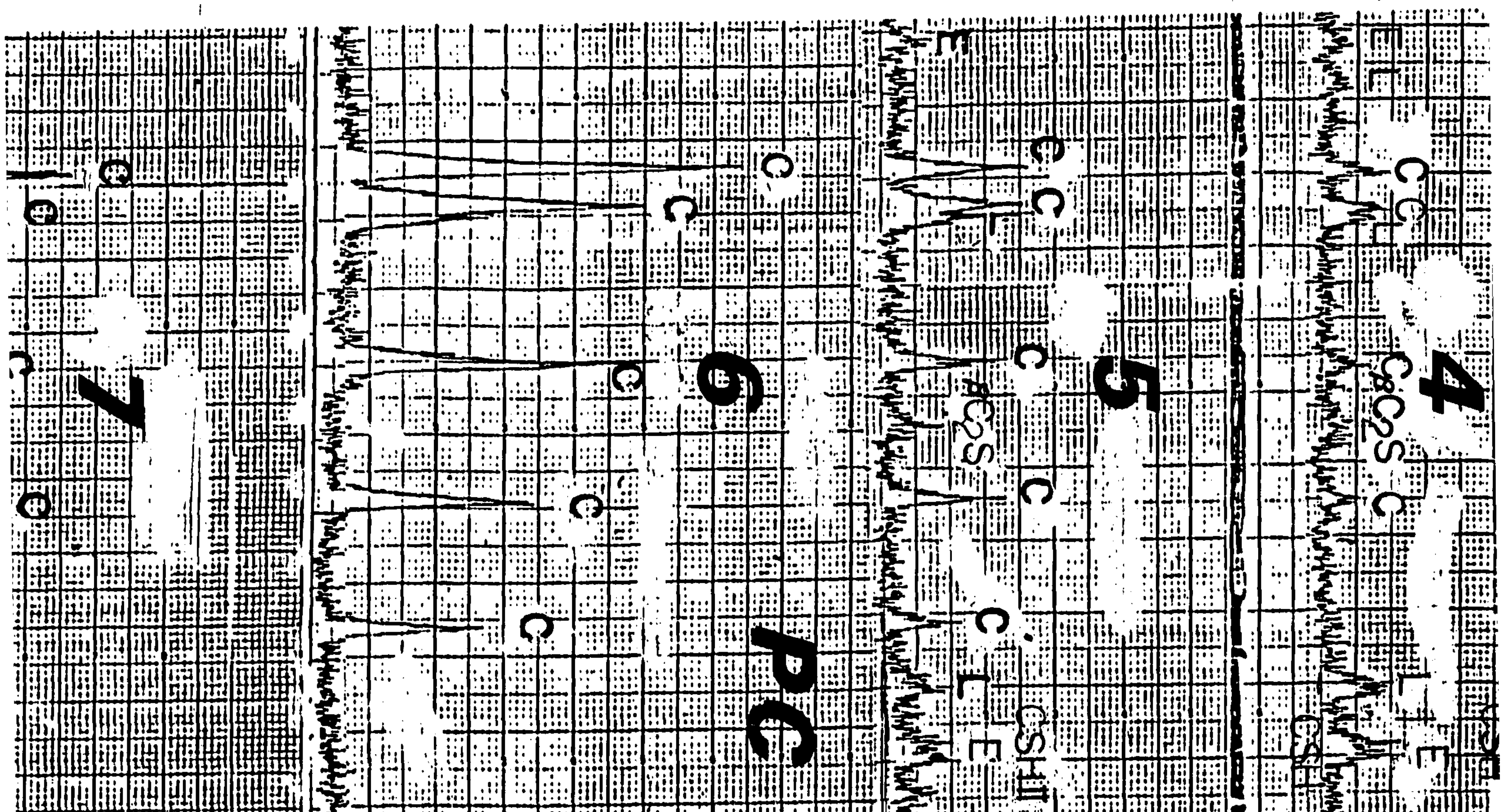
4
5
6
7
PC
CSHI
CSHII

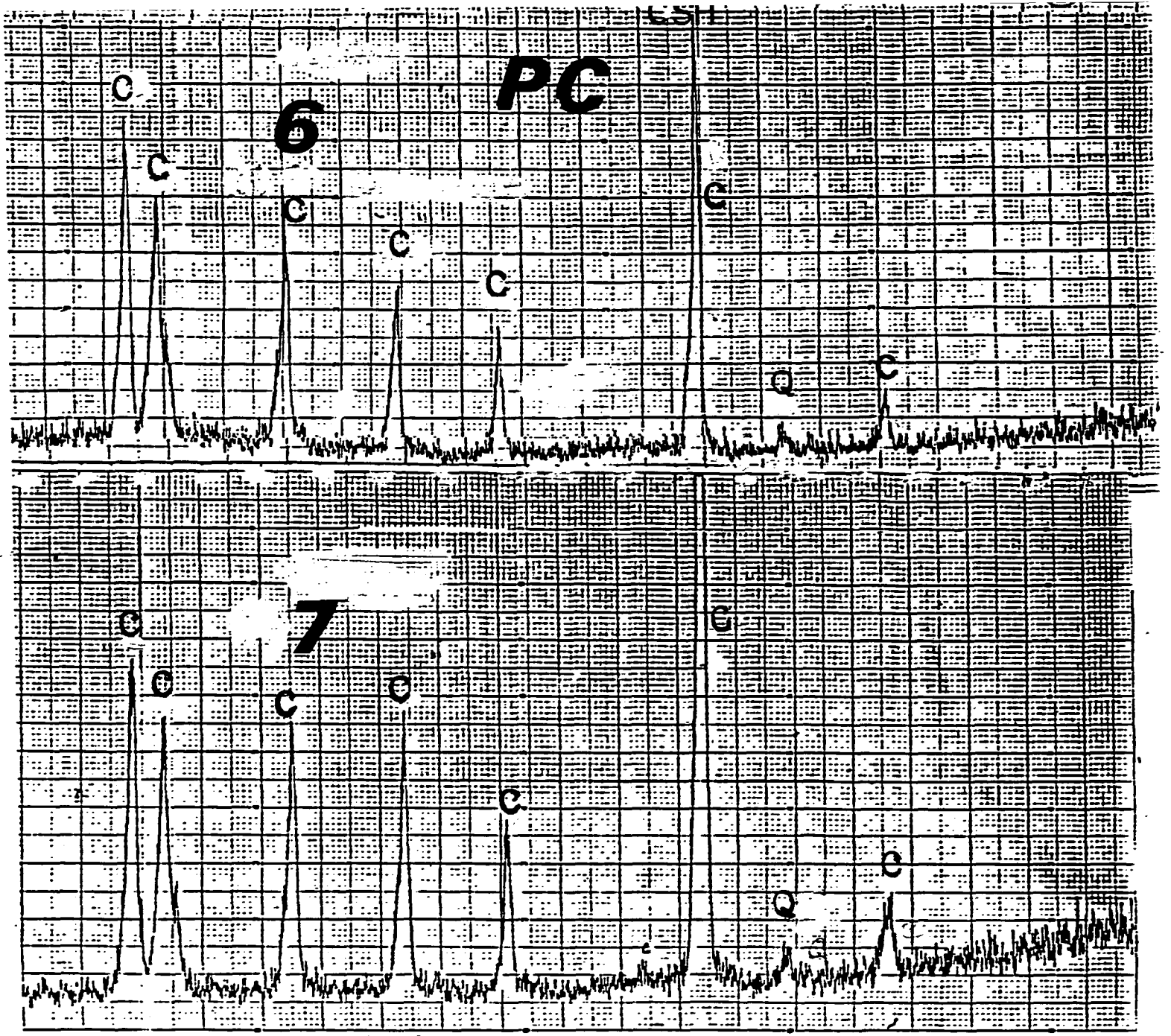

Figure B-1. Limestone-portland cement specimen

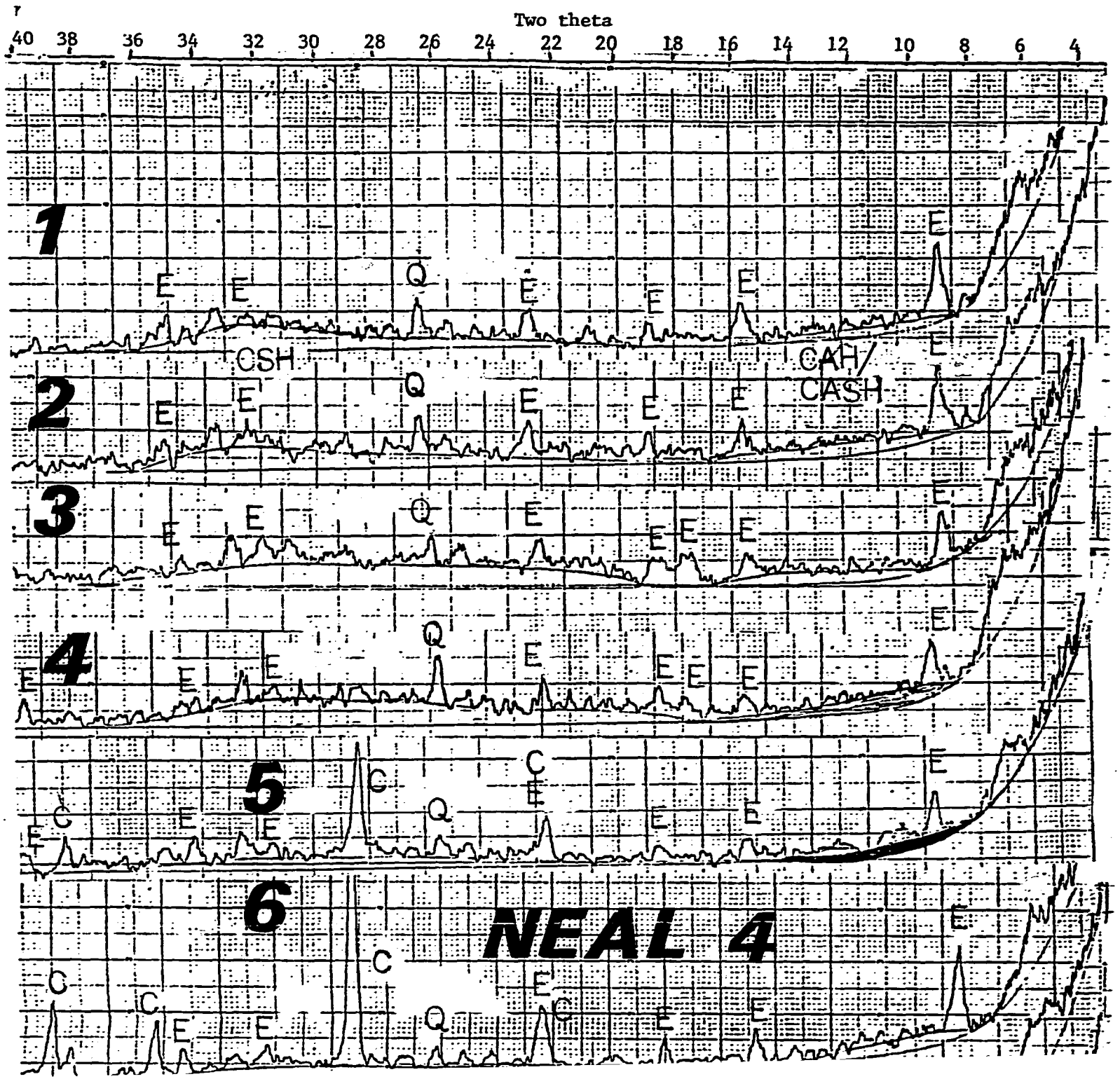
Two theta
40 38 36 34 32 30 28 26 24 22 20 18 16 14 12 10 8 6 4
1
2
3
4
5
6
CSH
CAH/
CASH
NEAL 4

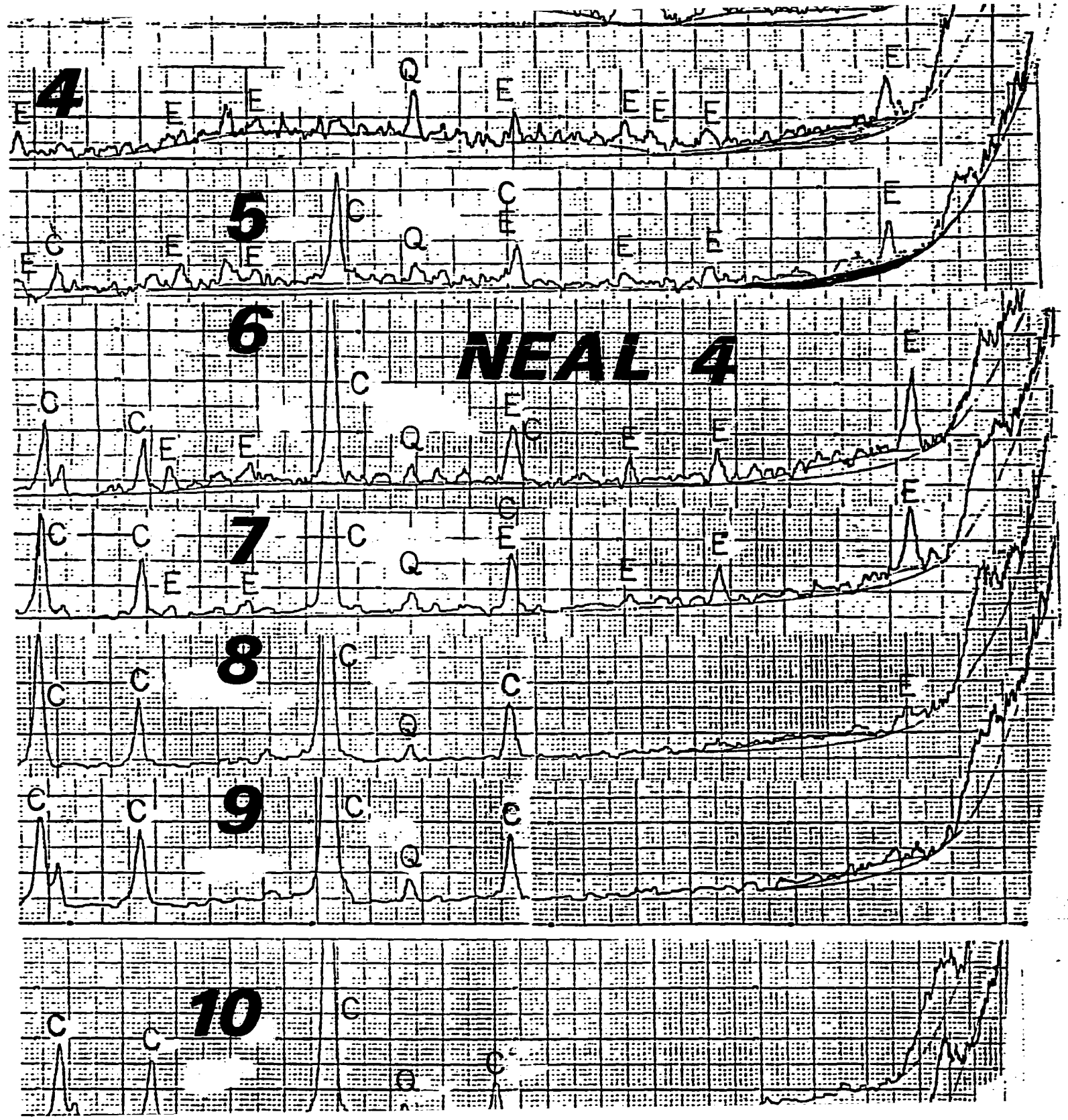
4
5
6
7
8
9
10
NEAL 4

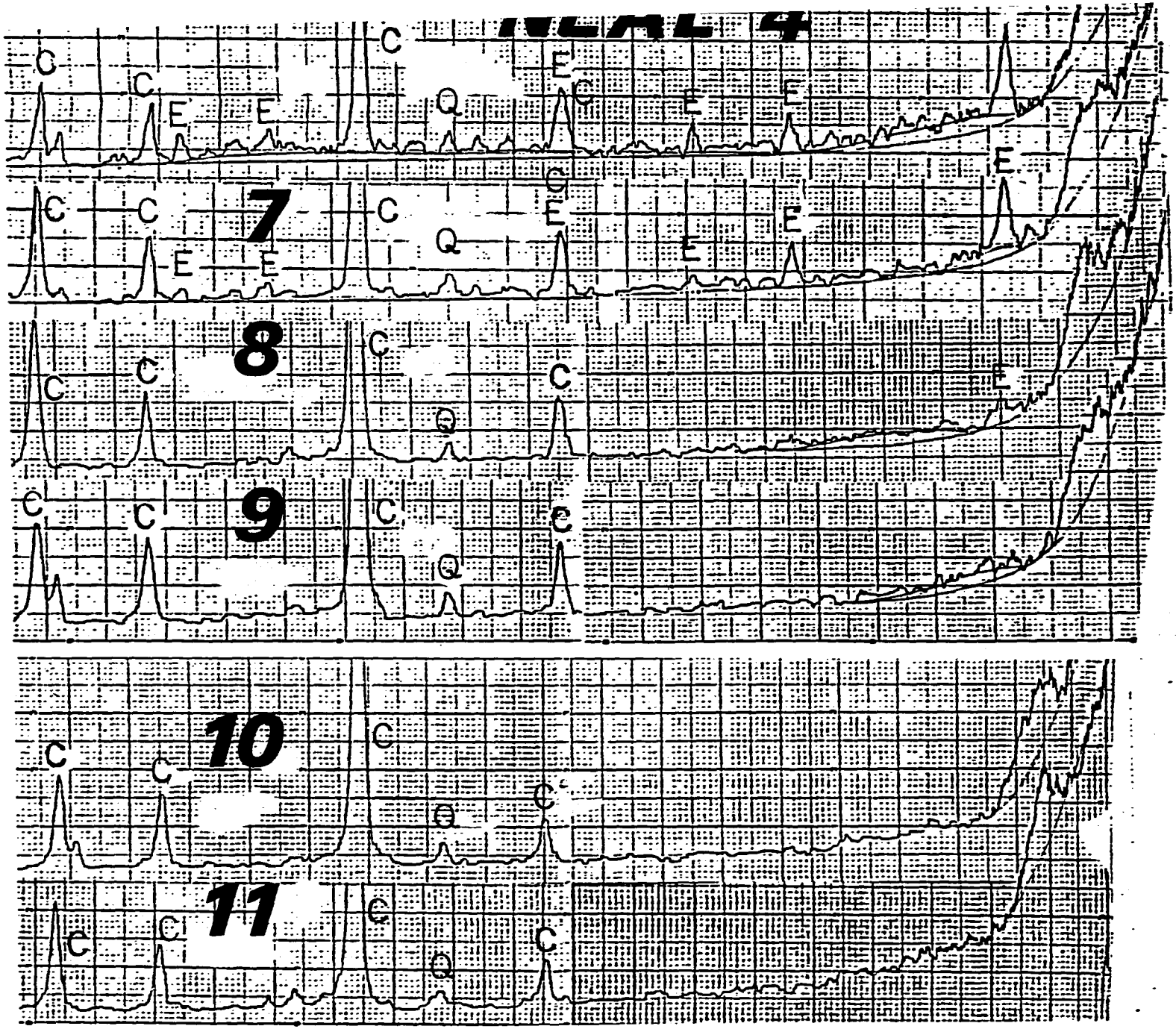

Figure B-2. Limestone-Neal #4 fly ash specimen

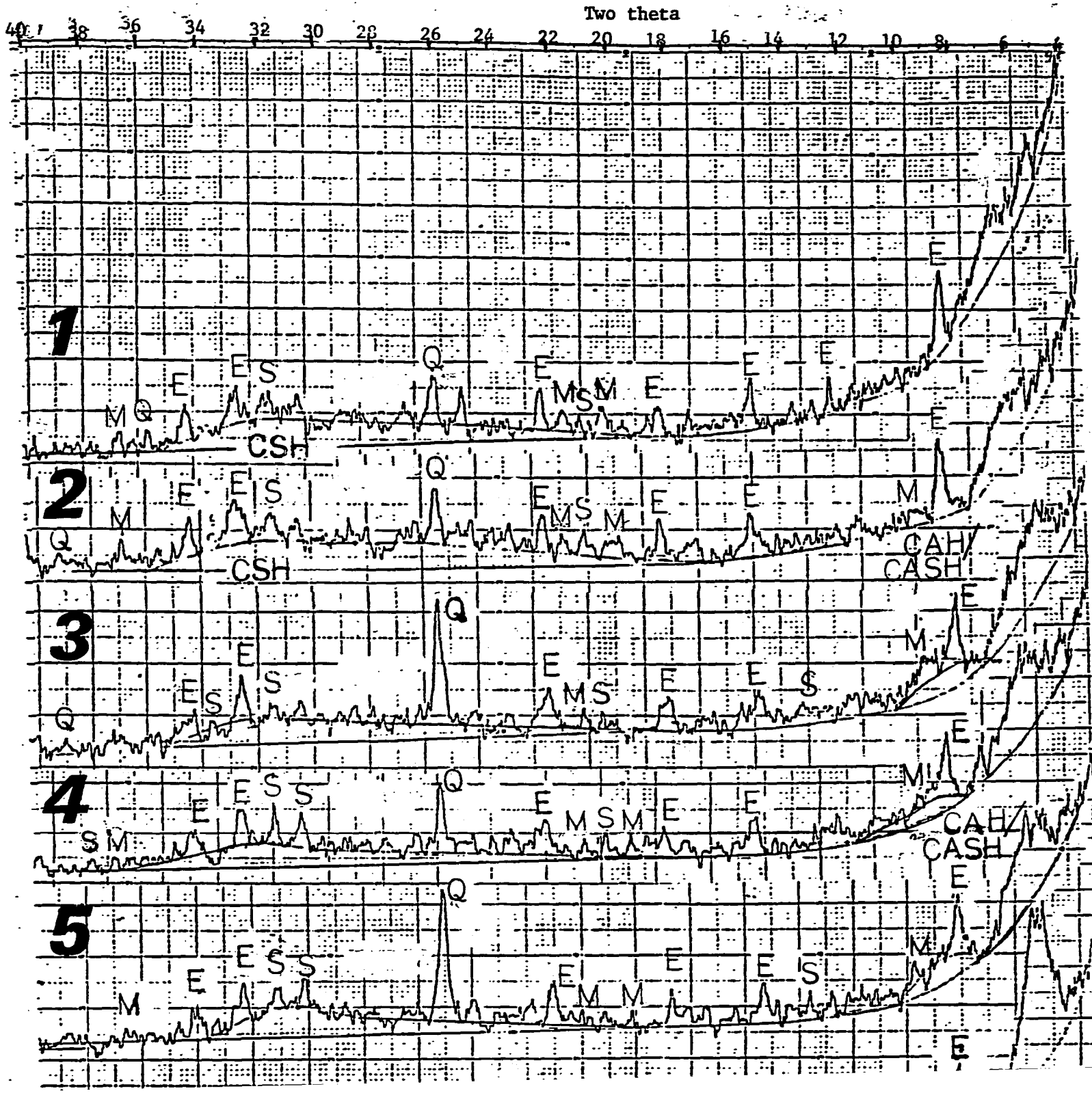
Two theta
40
38
36
34
32
30
28
26
24
22
20
18
16
14
12
10
8
6
1
2
3
4
5
CSH
CAH
CASH

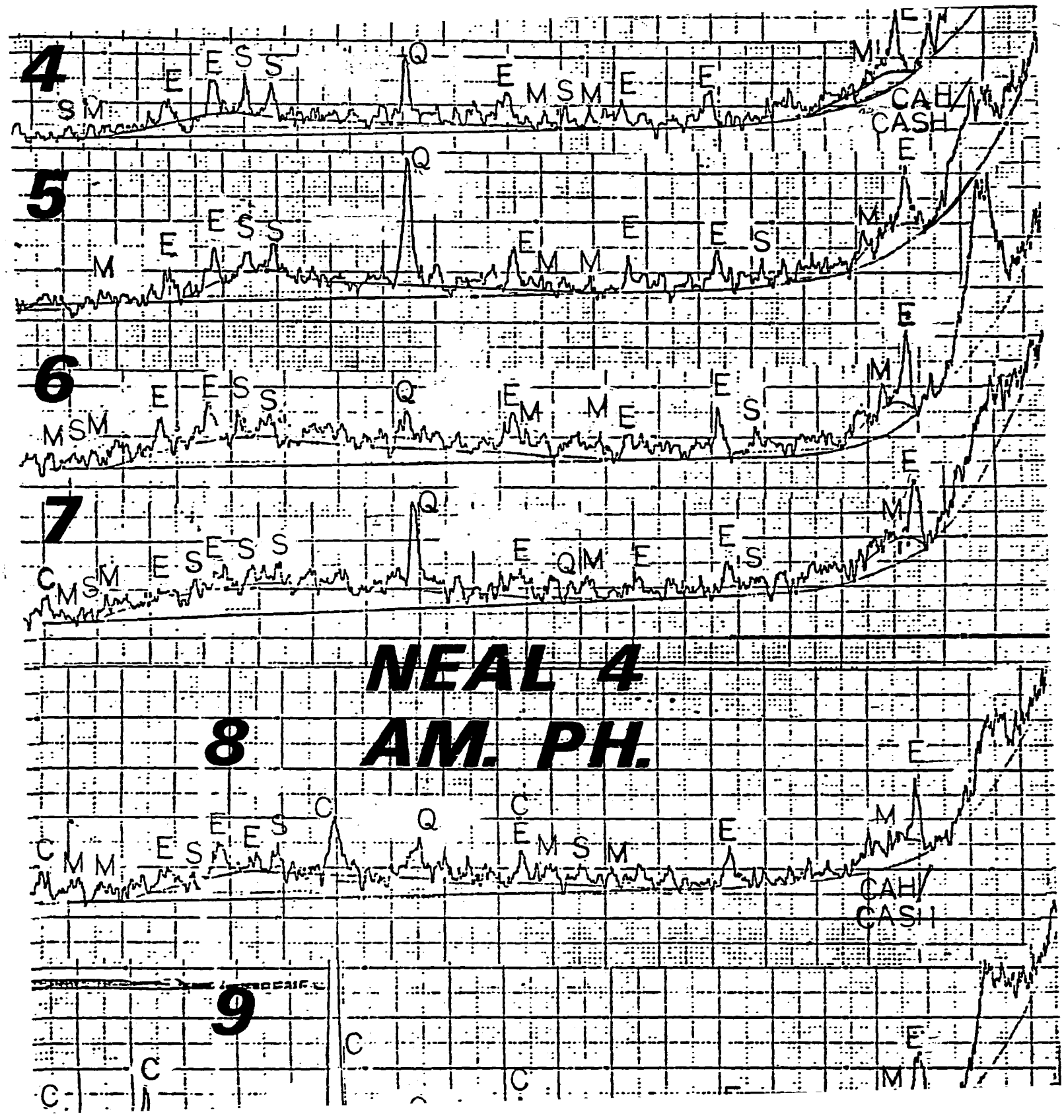
4
5
6
7
8
9
NEAL 4
AM. PH.
CAH/
CASH

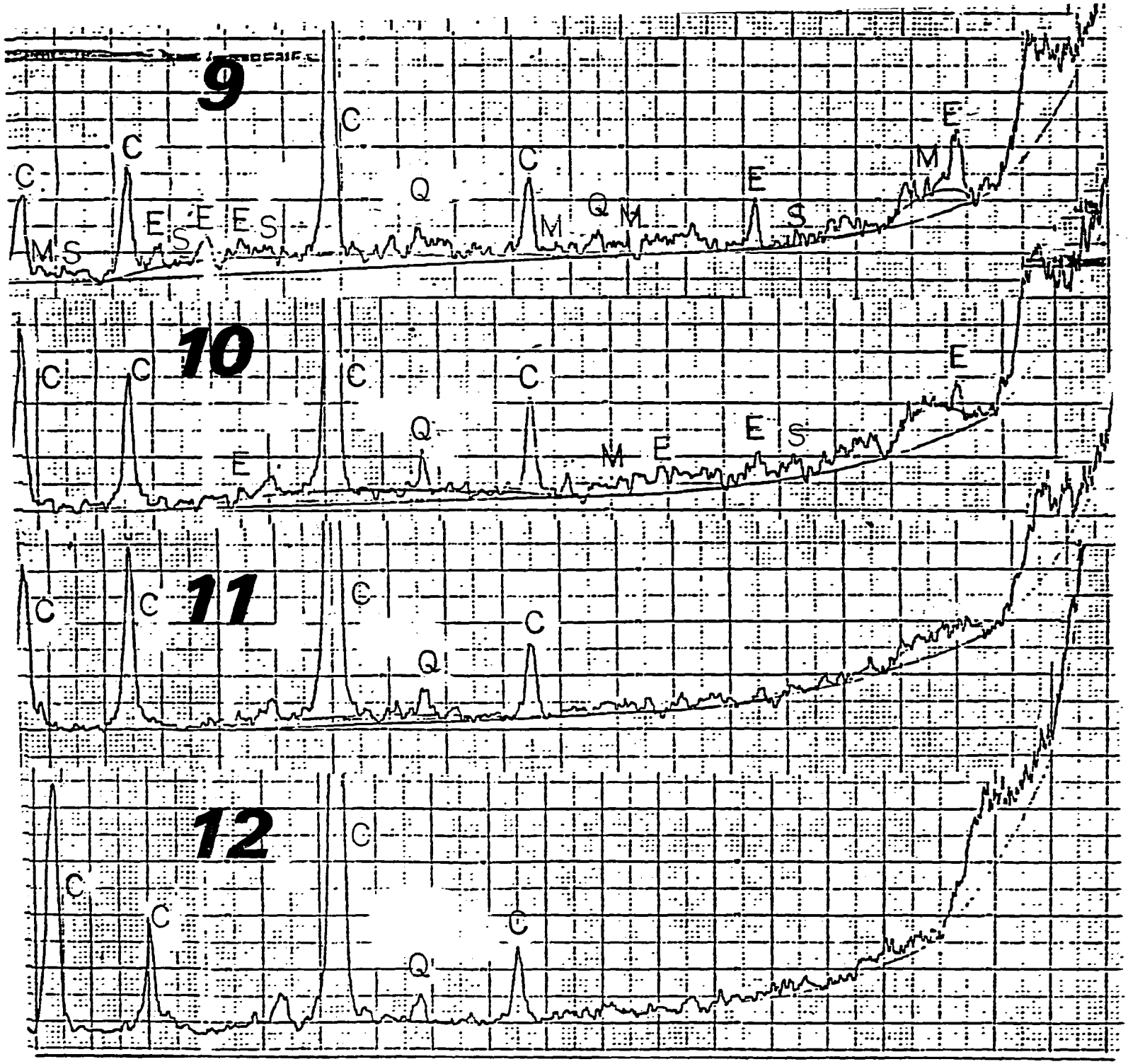

Figure B-3. Limestone-ammonium phosphate treated Neal #4 fly ash specimen

APPENDIX C

CRYSTALLOGRAPHY

CRYSTALLOGRAPHY

A single crystal is a solid throughout which the atoms or molecules are arranged in a regularly repeating pattern. Most crystalline solids are made up of millions of tiny single crystals and are said to be polycrystalline. These crystals are oriented randomly with respect to one another.

The geometric pattern of crystals can be established by dividing the space they occupy by three sets of two parallel planes into a repeating sets of parallelepipeds. Each parallelepiped is called a unit cell. The space-dividing planes intersect each other in a set of lines, and these lines in turn intersect in a set of points called point lattice as shown below.

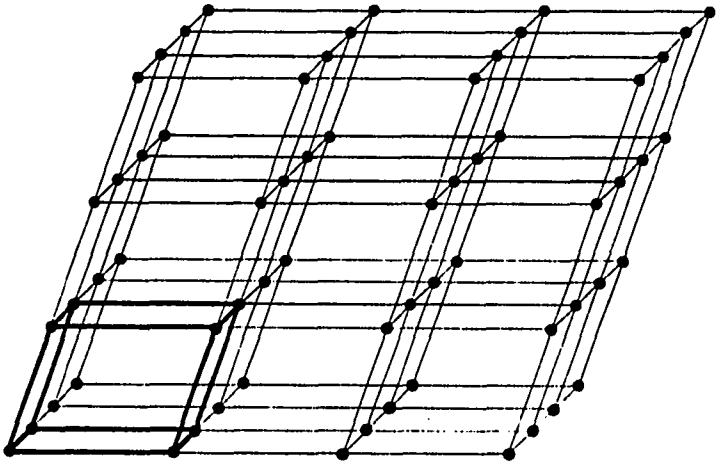

A point lattice.

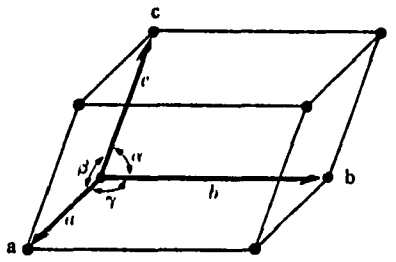

A unit cell

After Cullity [9]

The size and shape of the unit cell can be described by three vectors a, b, and c drawn from one of the cell taken as origin. These vectors define the cell and are called the crystallographic axes of the cell. The unit cell may also be described in terms of their lengths (a, b, c) and the angles between them (α, β, γ). These angles and lengths are the lattice parameters or lattice constants of the unit cell. By varying the lattice parameters various geometric shapes are obtained. There are 14 different possible space lattices (called Bravais lattice) as shown in Figure C-1.

A crystal plane can be characterized by the co-ordinates of its intercept with the crystallographic axes. In general, the Miller indices, defined as the reciprocal of the fractional intercepts which the plane makes with the crystallographic axes, are used to describe crystal planes. For example, if the Miller indices of a plane are (hkl), written in parentheses, then the plane makes fractional intercepts of 1/h, 1/k, 1/1 with the axes, and, if the axial lengths are a, b, c, the plane makes actual intercepts of a/h, b/k and c/1 as shown below.

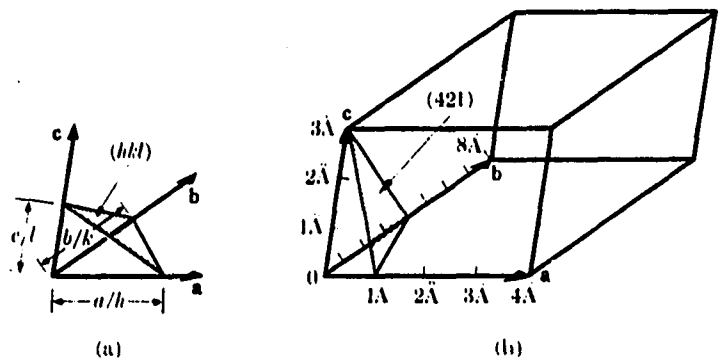

Plane designation by Miller indices, after Cullity [9]

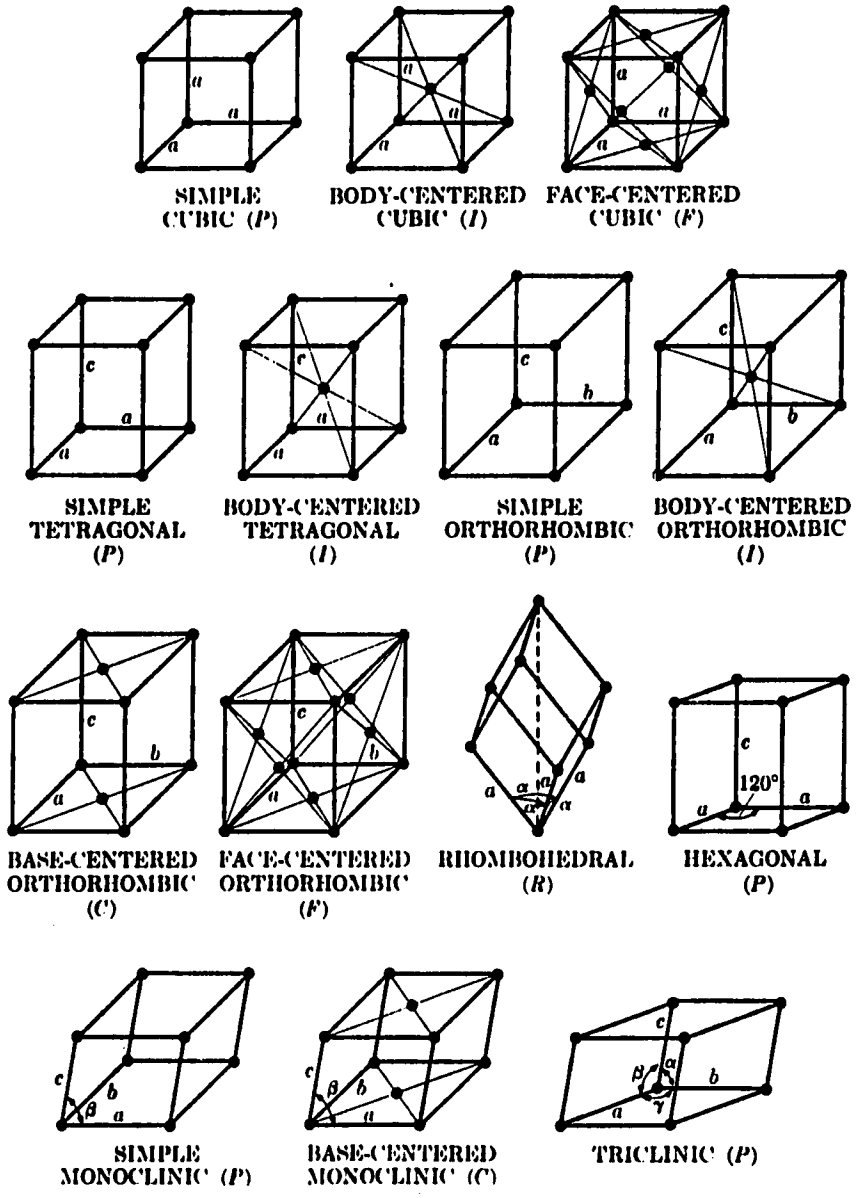

Figure C-1. The fourteen Bravais lattice, after Cullity [9]

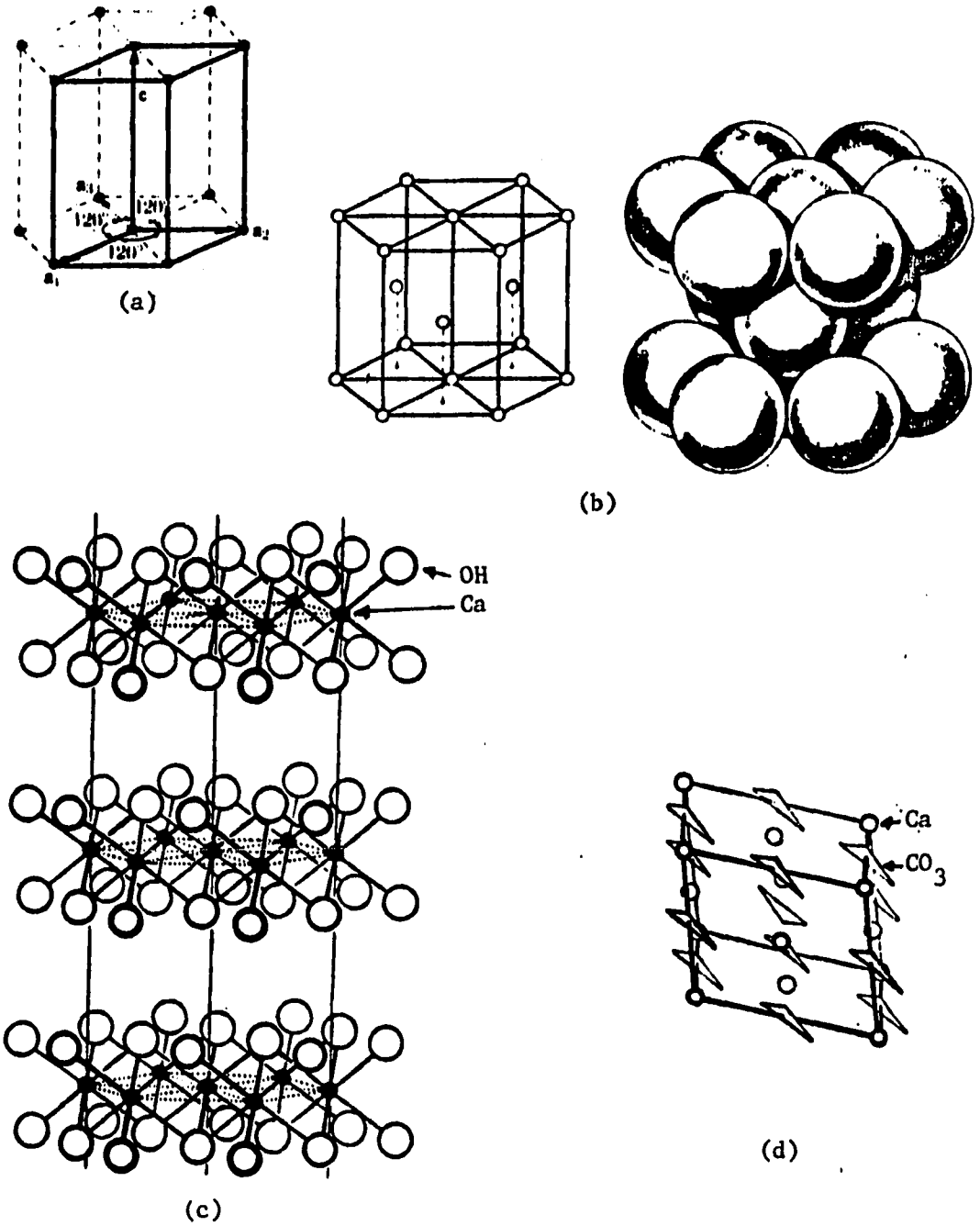

Figure C-2. Some pertinent crystal structures: (a) The hexagonal unit cell (heavy lines), after Cullity [9], (b) the hexagonal close-packed structure, after Cullity [9], (c) the hexagonal close-packed structure of $Ca(OH)_2$; a = 3.11 and c = 4.91 A^o, after Lea [19], and (d) The hexagonal structure of $CaCO_3$; a = 4.99 and c = 17.06 A^o, after Rao [30]

A number of crystal structures, pertinent to this research, is shown in Figure C-2. These include a typical hexagonal unit cell (Figure C-2a), a typical hexagonal close-packed structure (Figure C-2b), the hexagonal close-packed structure of $Ca(OH)_2$ (Figure C-2c), and the hexagonal structure of $CaCO_3$ (Figure C-2d).

APPENDIX D

ELECTRON MICROPROBE TEST RESULTS

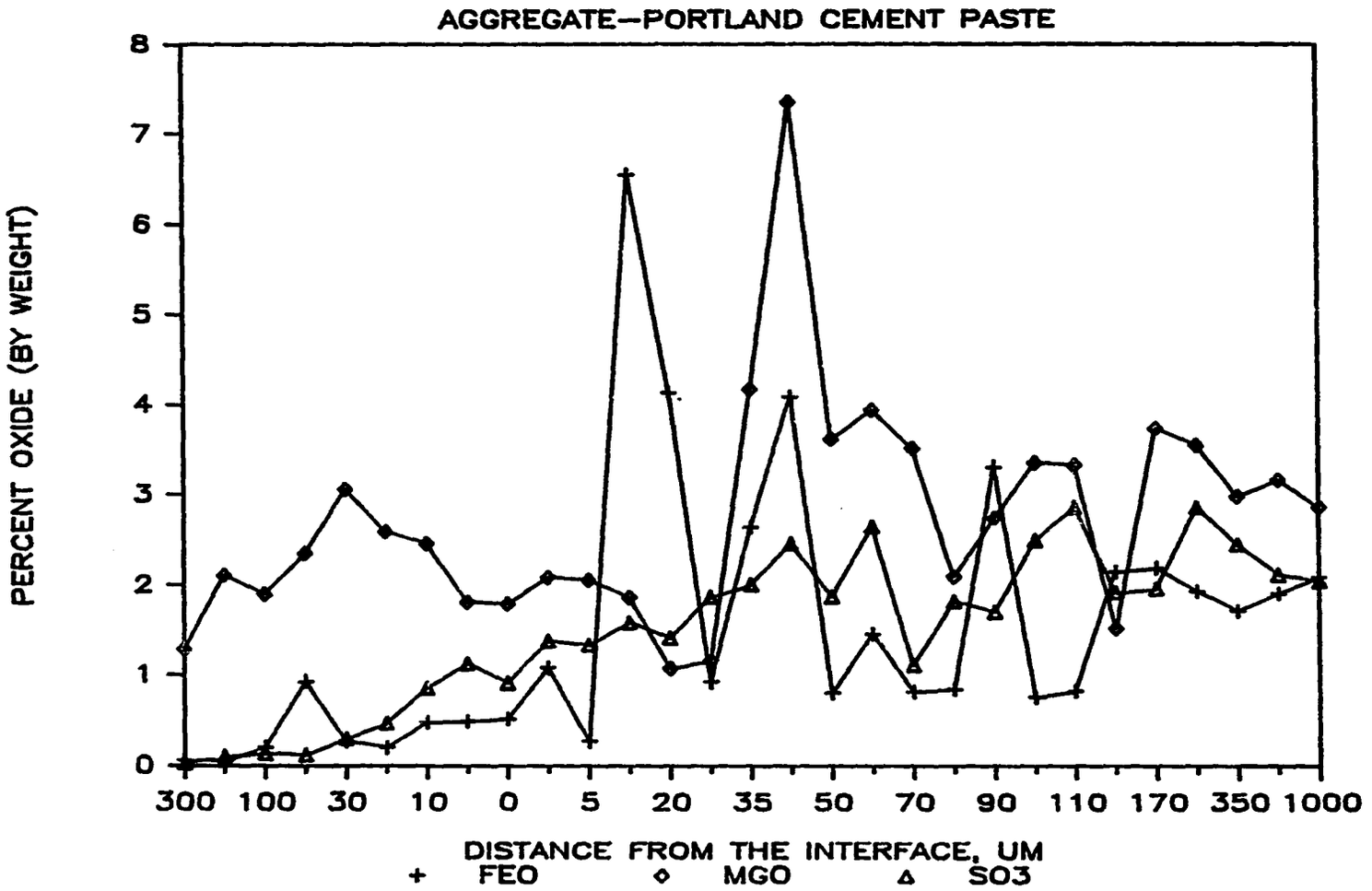
AGGREGATE—PORTLAND CEMENT PASTE
PERCENT OXIDE (BY WEIGHT)
0
1
2
3
4
5
6
7
8
300 100 30 10 0 5 20 35 50 70 90 110 170 350 1000
DISTANCE FROM THE INTERFACE, UM
+ FEO
◇ MGO
△ SO3

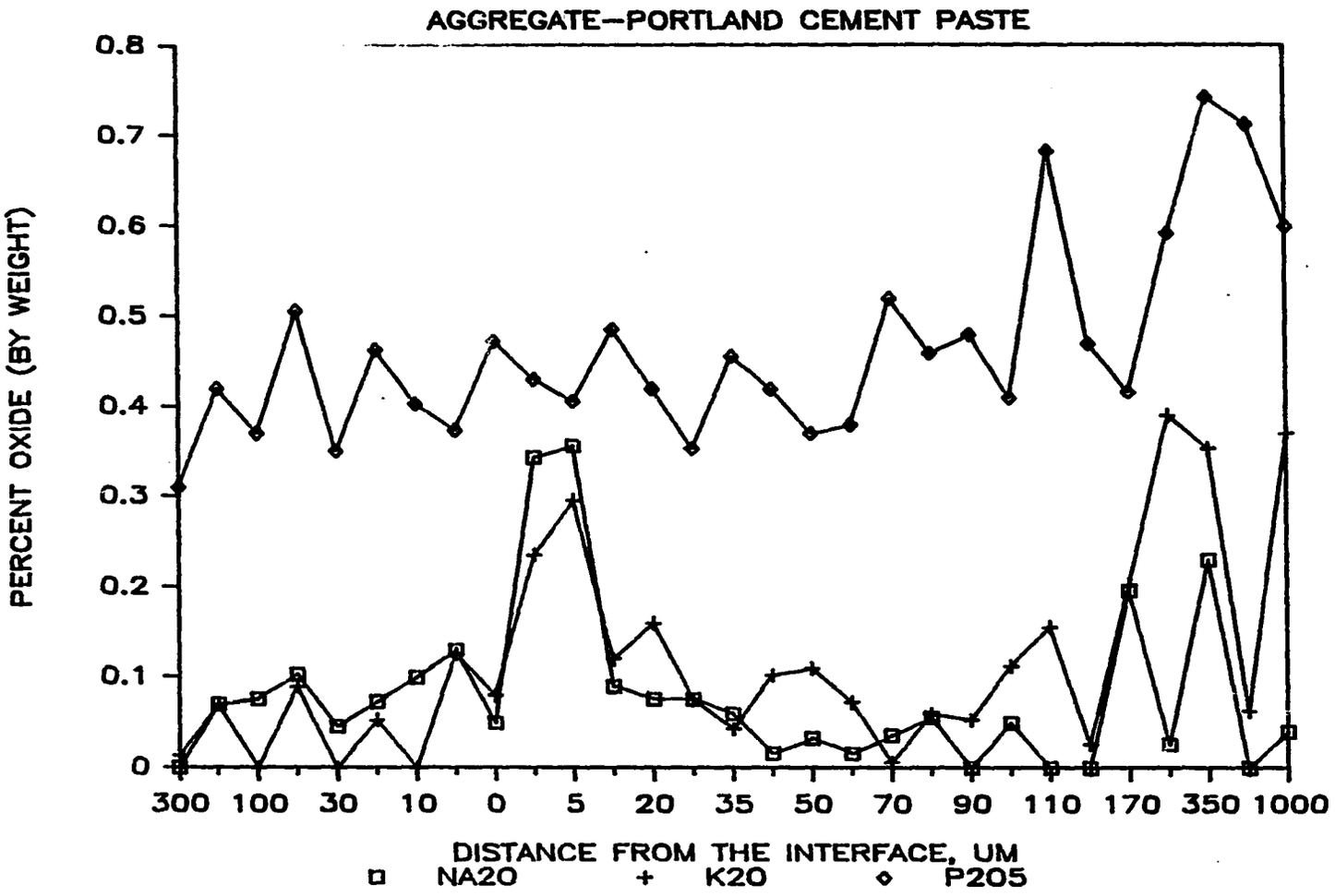
AGGREGATE—PORTLAND CEMENT PASTE
PERCENT OXIDE (BY WEIGHT)
0.8
0.7
0.6
0.5
0.4
0.3
0.2
0.1
0
300 100 30 10 0 5 20 35 50 70 90 110 170 350 1000
DISTANCE FROM THE INTERFACE, UM
NA2O
K2O
P2O5

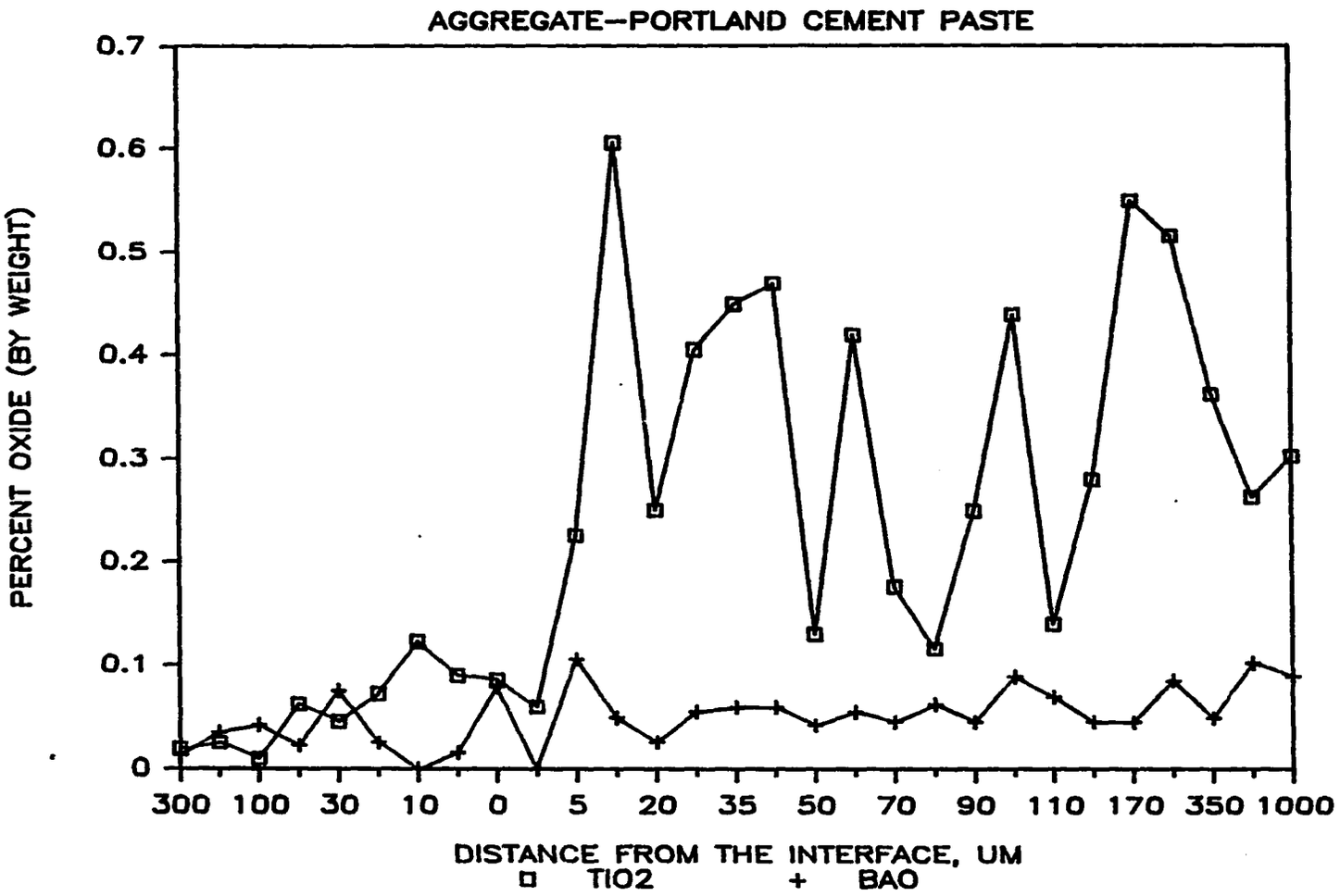
AGGREGATE--PORTLAND CEMENT PASTE
PERCENT OXIDE (BY WEIGHT)
0.7
0.6
0.5
0.4
0.3
0.2
0.1
0
300 100 30 10 0 5 20 35 50 70 90 110 170 350 1000
DISTANCE FROM THE INTERFACE, UM
TIO2
BAO

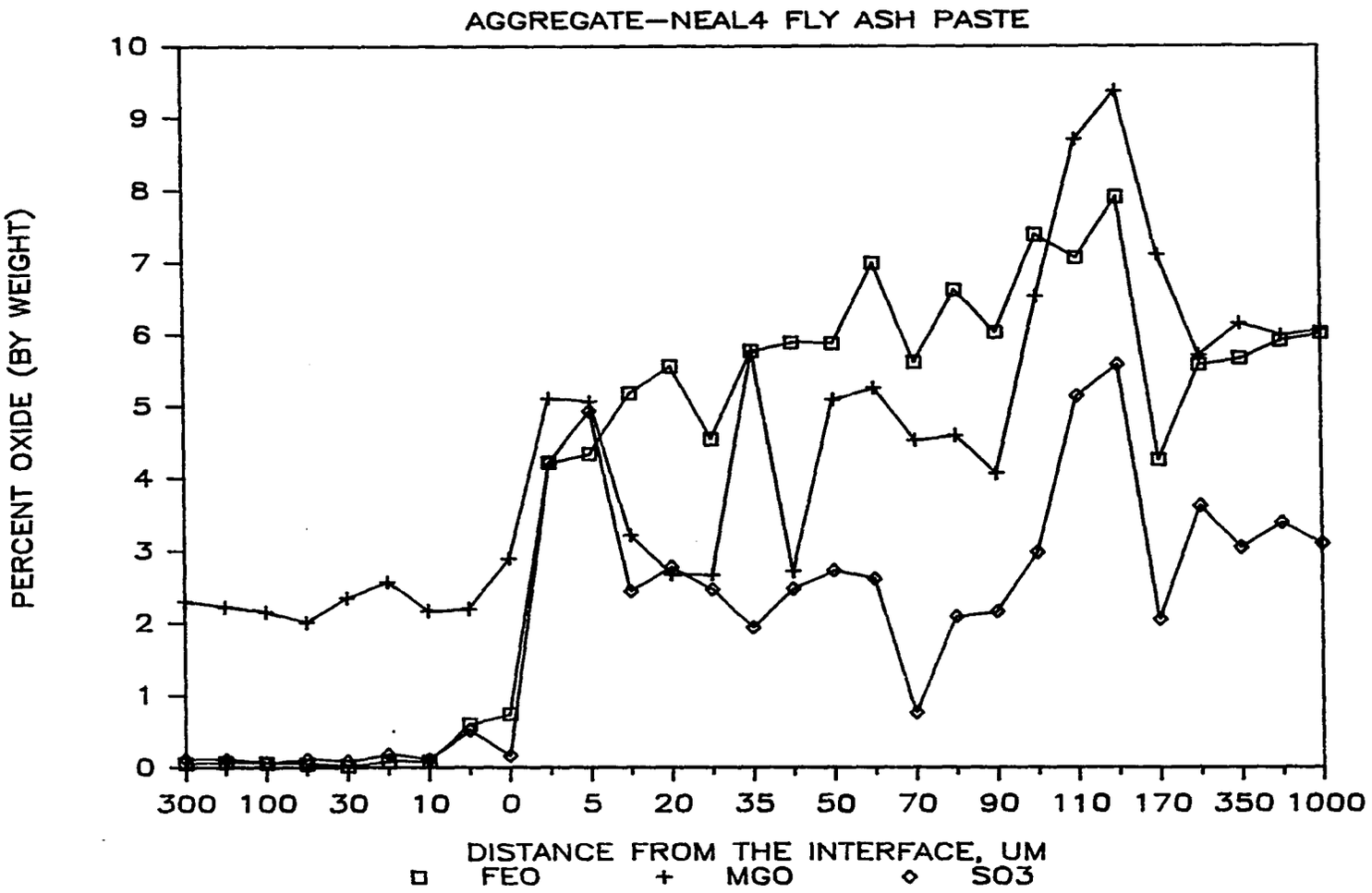
AGGREGATE—NEAL4 FLY ASH PASTE
PERCENT OXIDE (BY WEIGHT)
10
9
8
7
6
5
4
3
2
1
0
300 100 30 10 0 5 20 35 50 70 90 110 170 350 1000
DISTANCE FROM THE INTERFACE, UM
FEO
MGO
SO3

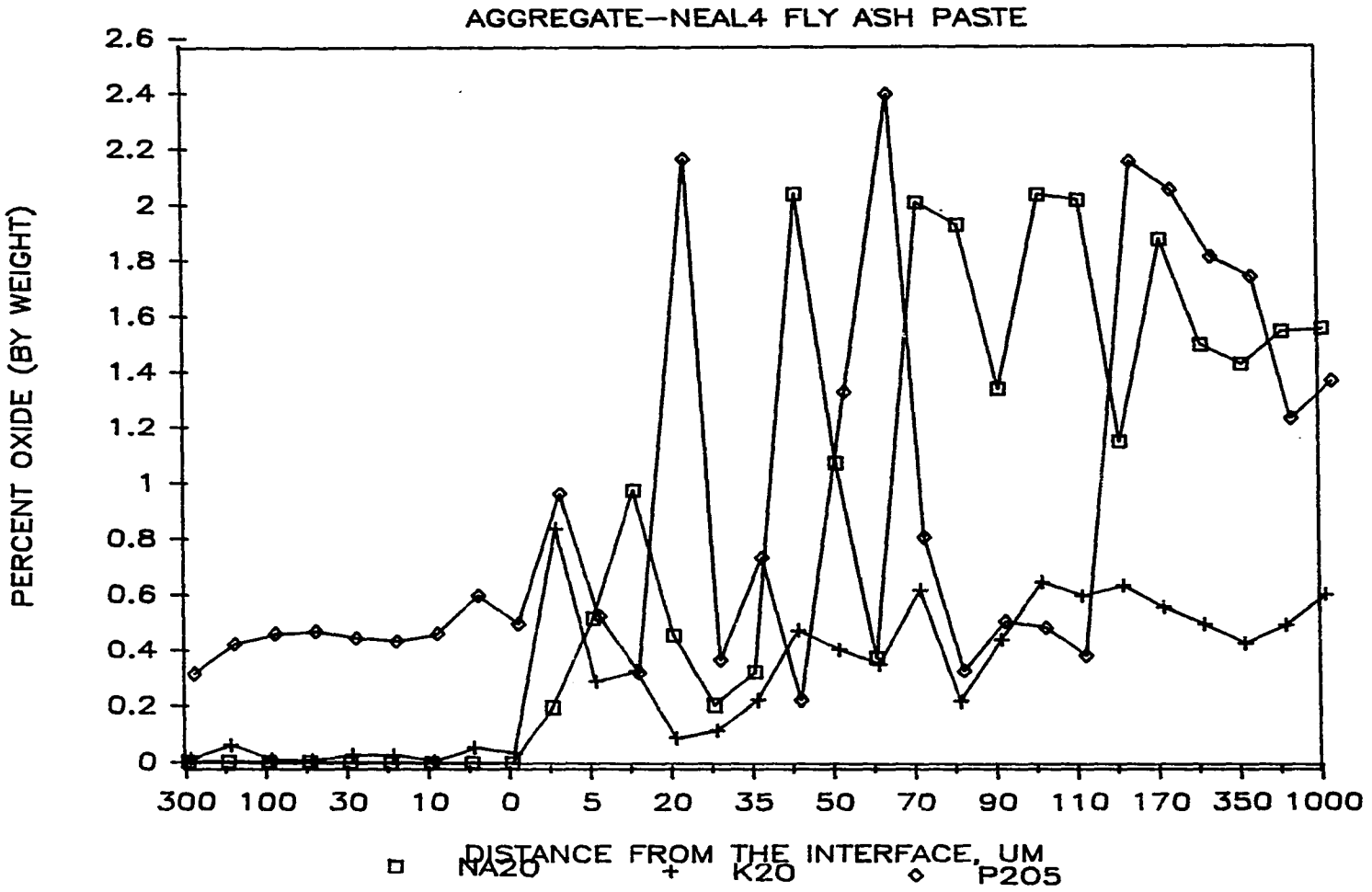
AGGREGATE—NEAL4 FLY ASH PASTE
PERCENT OXIDE (BY WEIGHT)
2.6
2.4
2.2
2
1.8
1.6
1.4
1.2
1
0.8
0.6
0.4
0.2
0
300 100 30 10 0 5 20 35 50 70 90 110 170 350 1000
DISTANCE FROM THE INTERFACE, UM
NA2O
K2O
P2O5

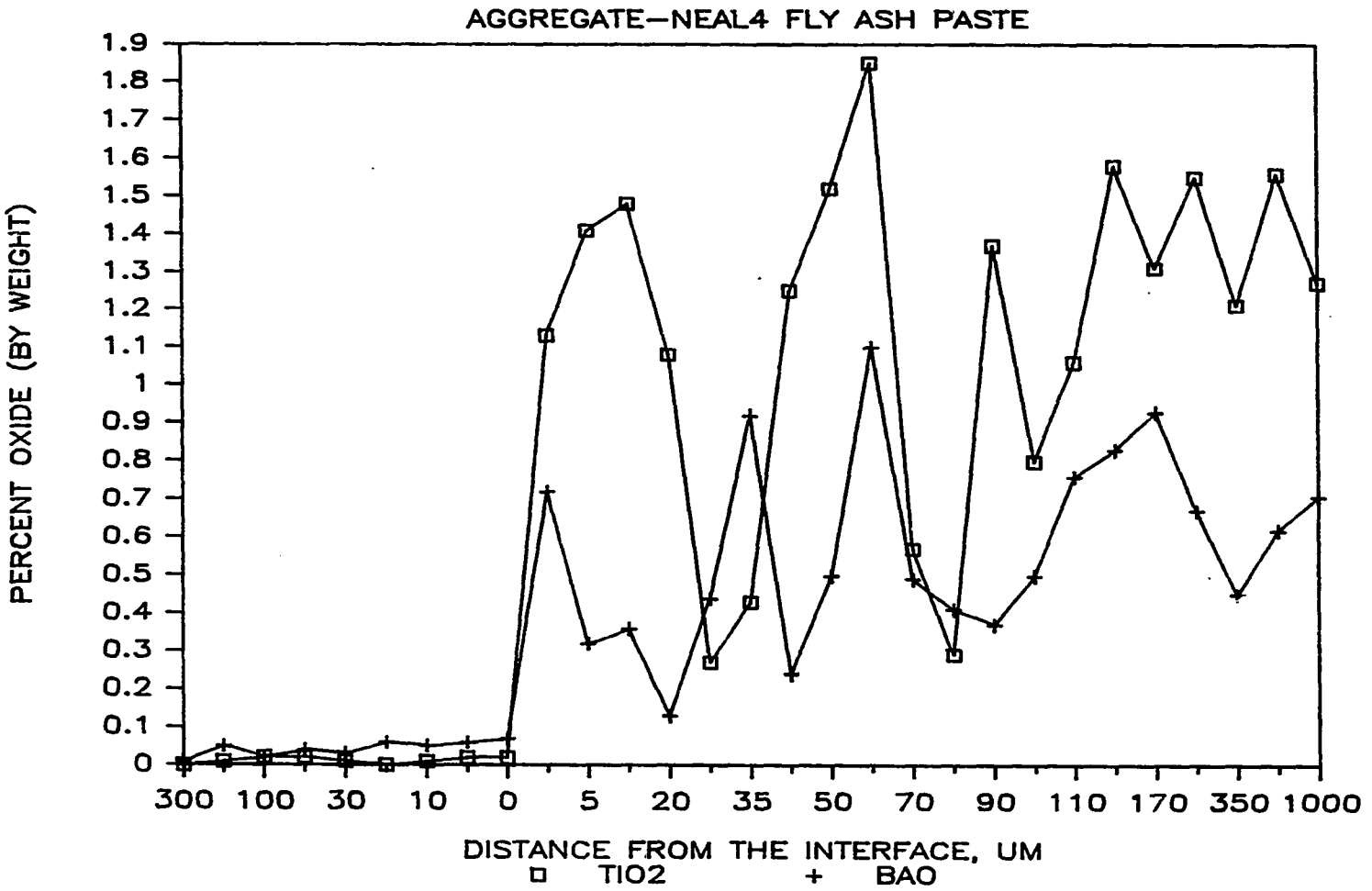
AGGREGATE—NEAL4 FLY ASH PASTE
PERCENT OXIDE (BY WEIGHT)
1.9
1.8
1.7
1.6
1.5
1.4
1.3
1.2
1.1
1
0.9
0.8
0.7
0.6
0.5
0.4
0.3
0.2
0.1
0
300 100 30 10 0 5 20 35 50 70 90 110 170 350 1000
DISTANCE FROM THE INTERFACE, UM
□ TIO2 + BAO

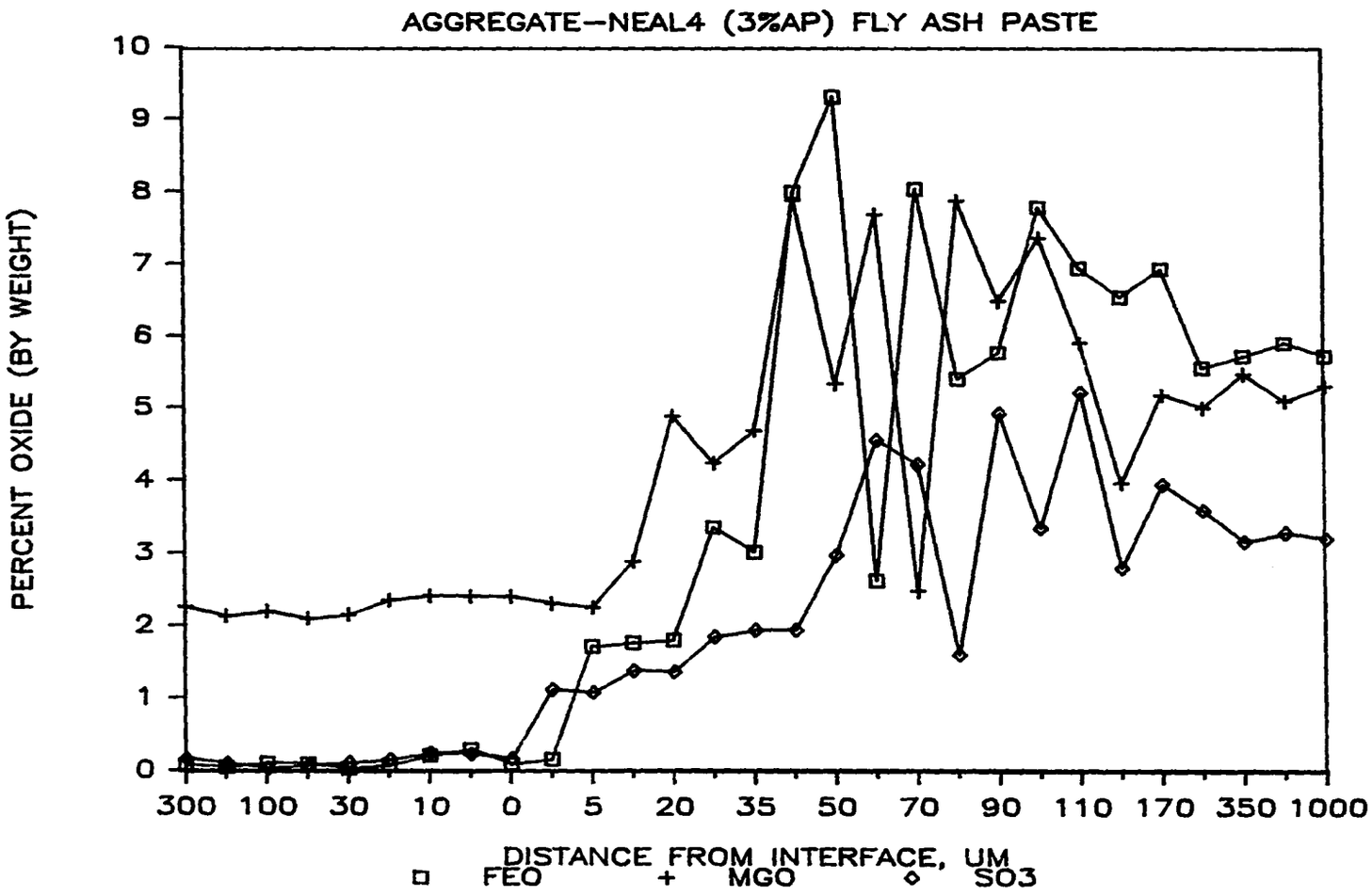
AGGREGATE—NEAL4 (3%AP) FLY ASH PASTE
PERCENT OXIDE (BY WEIGHT)
10
9
8
7
6
5
4
3
2
1
0
300 100 30 10 0 5 20 35 50 70 90 110 170 350 1000
DISTANCE FROM INTERFACE, UM
FEO
MGO
SO3

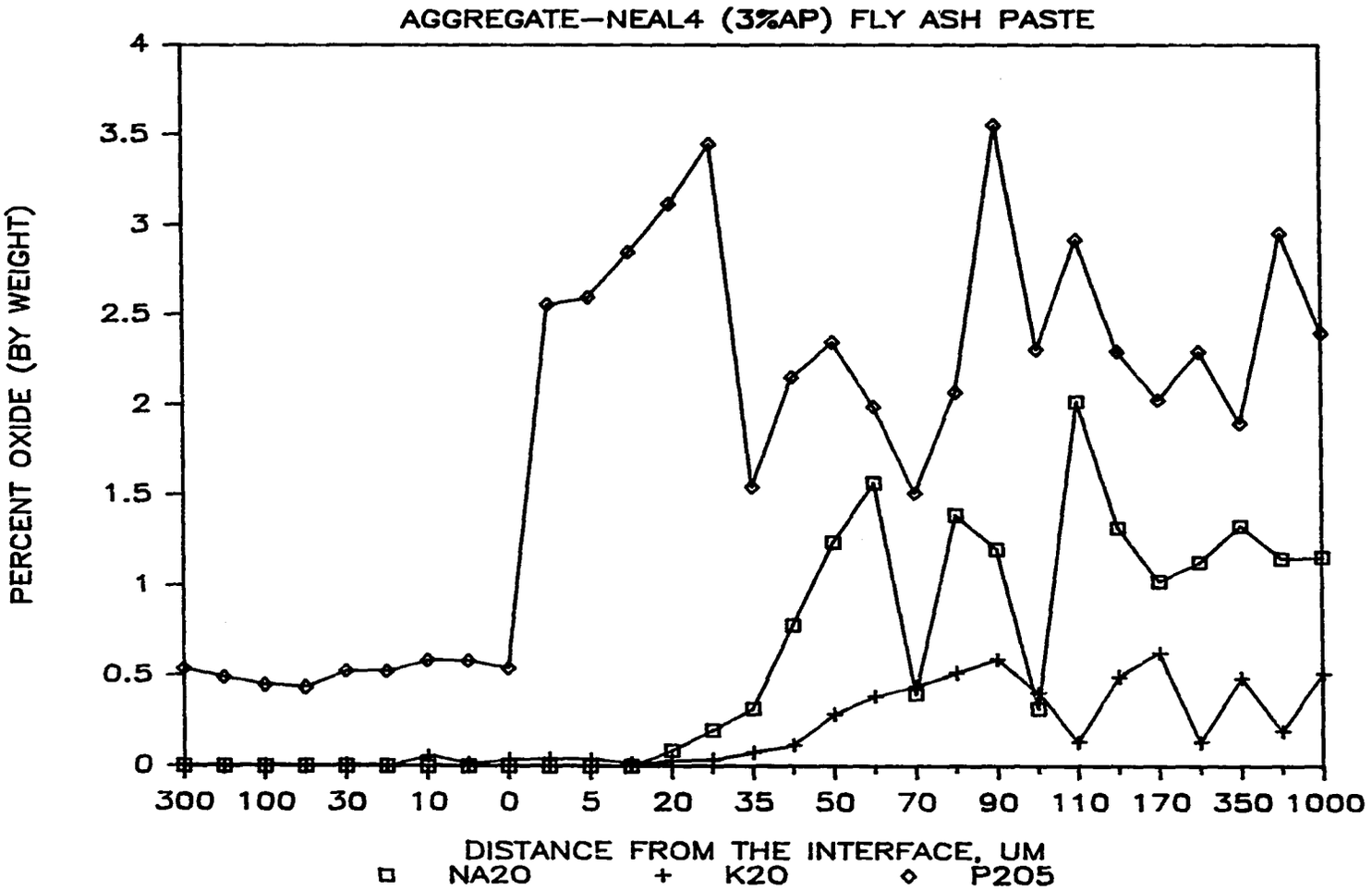
AGGREGATE—NEAL4 (3%AP) FLY ASH PASTE
PERCENT OXIDE (BY WEIGHT)
4
3.5
3
2.5
2
1.5
1
0.5
0
300 100 30 10 0 5 20 35 50 70 90 110 170 350 1000
DISTANCE FROM THE INTERFACE, UM
NA2O
K2O
P2O5

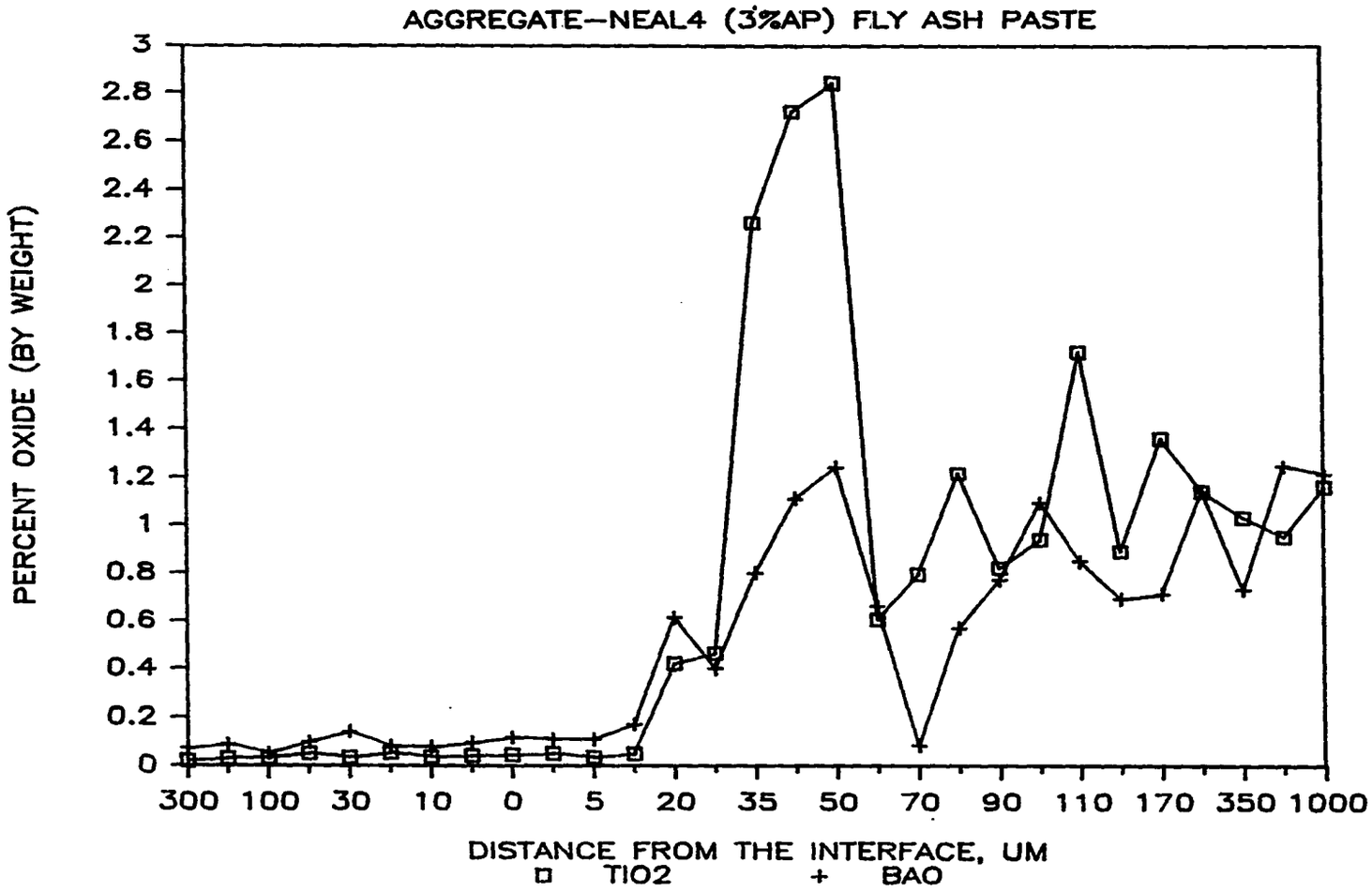
AGGREGATE--NEAL4 (3%AP) FLY ASH PASTE
PERCENT OXIDE (BY WEIGHT)
3
2.8
2.6
2.4
2.2
2
1.8
1.6
1.4
1.2
1
0.8
0.6
0.4
0.2
0
300 100 30 10 0 5 20 35 50 70 90 110 170 350 1000
DISTANCE FROM THE INTERFACE, UM
TIO2
BAO

APPENDIX E

MERCURY POROSIMETER TEST RESULTS

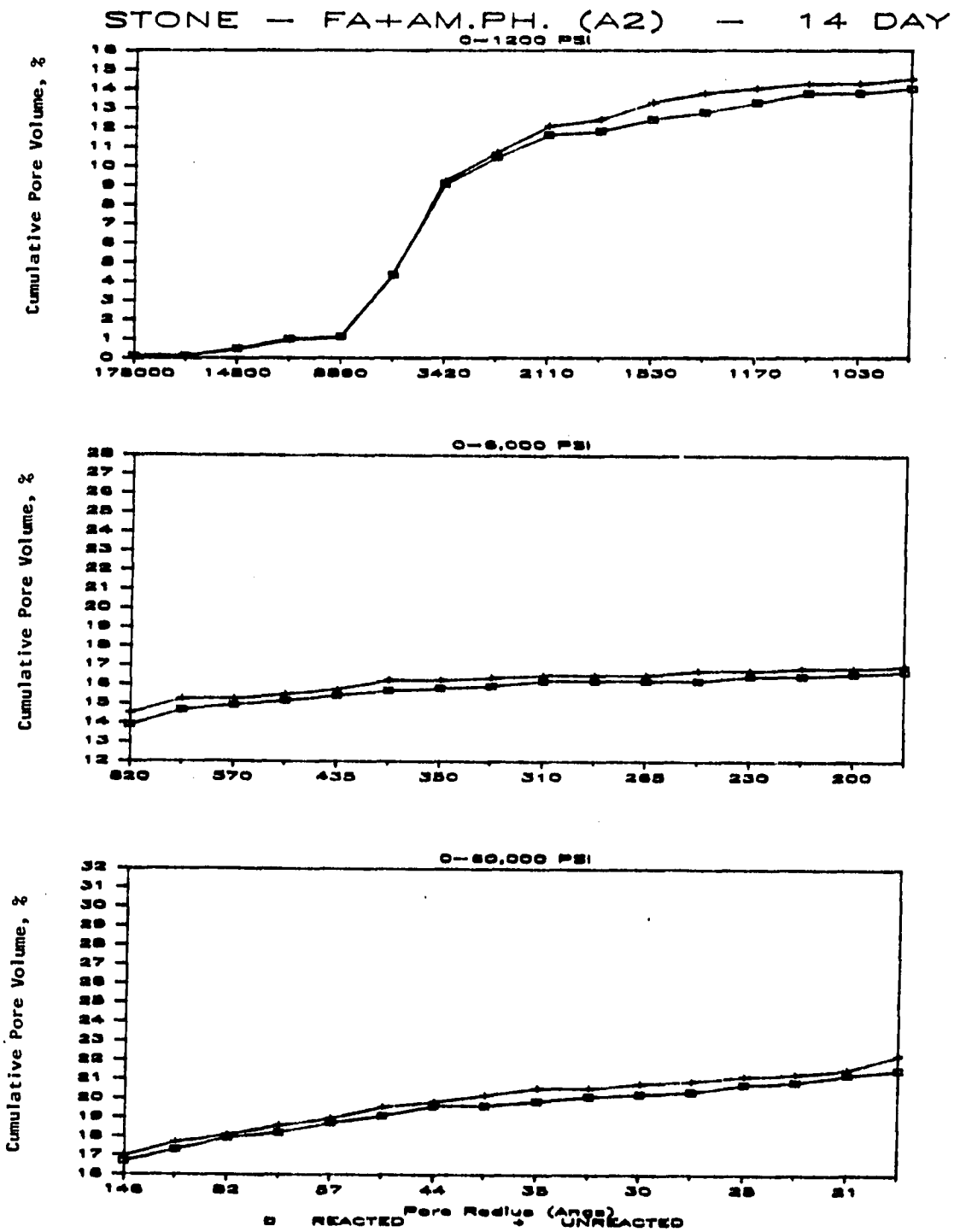
STONE — FA+AM.PH. (A2) — 14 DAY
0—1200 PSI
Cumulative Pore Volume, %
178000
14800
3420
2110
1530
1170
1030
0—6,000 PSI
Cumulative Pore Volume, %
820
570
435
350
310
265
230
200
0—60,000 PSI
Cumulative Pore Volume, %
148
82
57
44
35
30
25
21
Pore Radius (Angs)
REACTED
UNREACTED

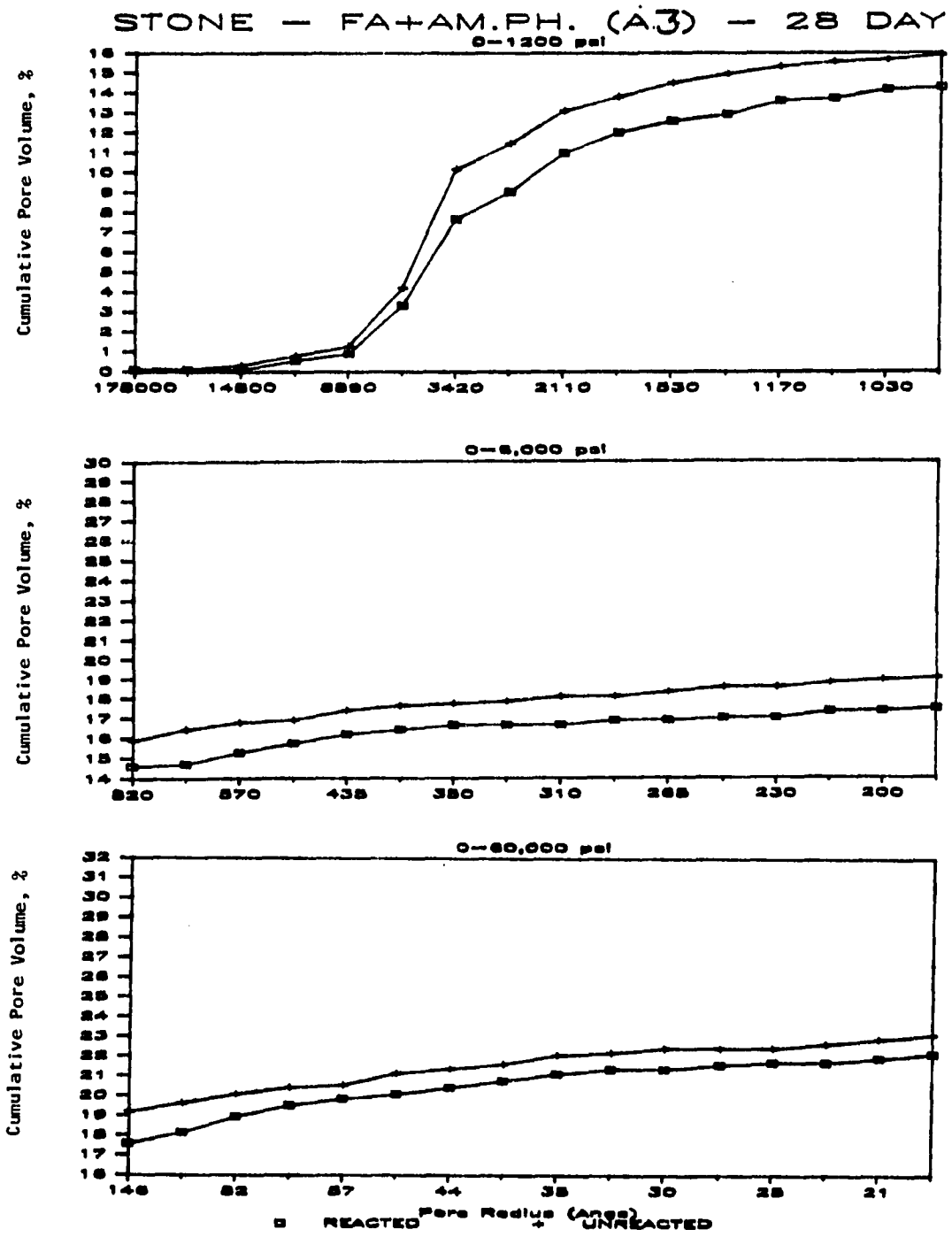
STONE — FA+AM.PH. (A3) — 28 DAY
0—1200 psi
Cumulative Pore Volume, %
178000 14800 6890 3420 2110 1530 1170 1030
0—6,000 psi
Cumulative Pore Volume, %
820 570 435 350 310 265 230 200
0—60,000 psi
Cumulative Pore Volume, %
146 82 57 44 35 30 25 21
Pore Radius (Angs)
REACTED
UNREACTED

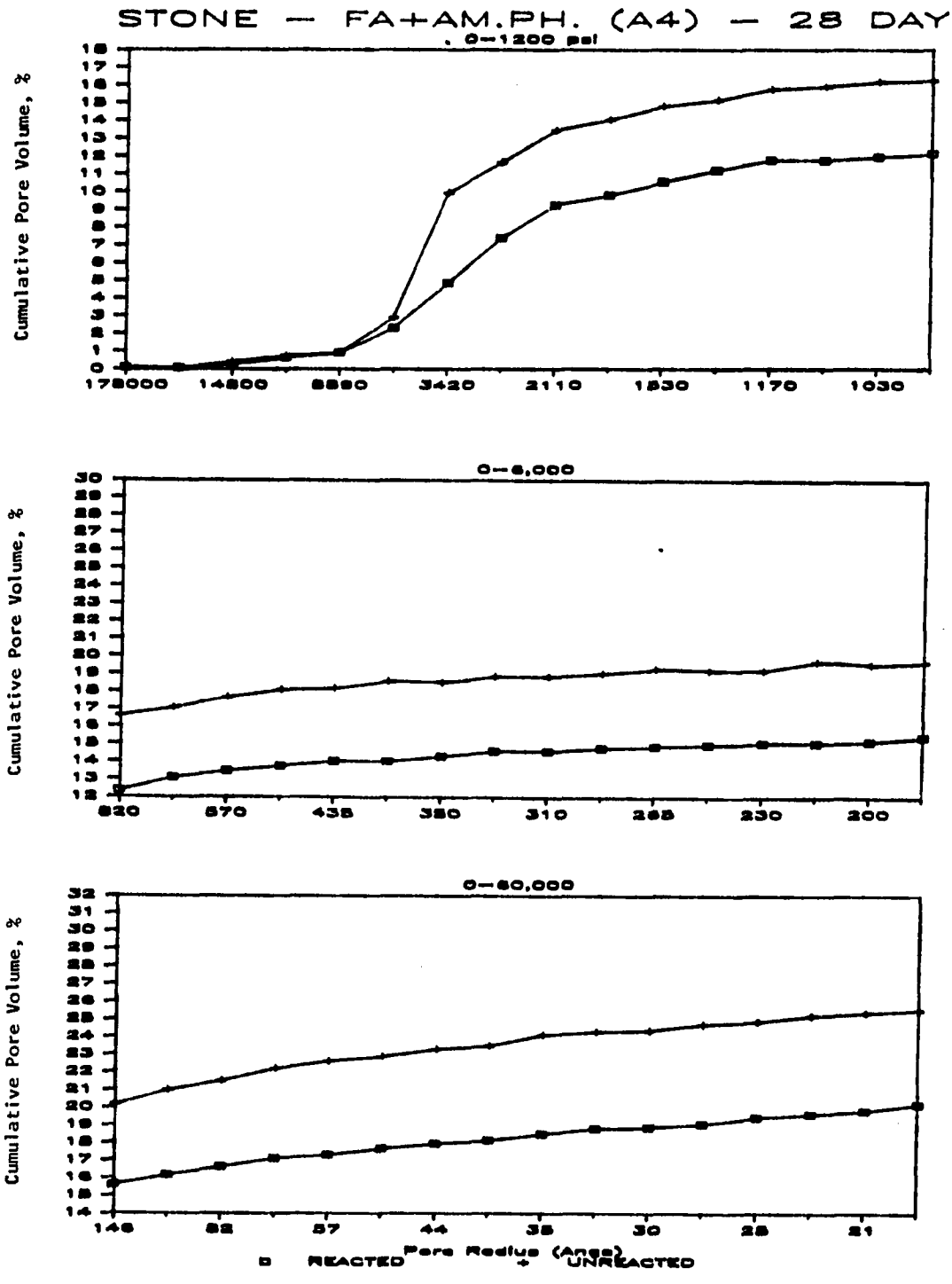
STONE — FA+AM.PH. (A4) — 28 DAY
0—1200 psi
Cumulative Pore Volume, %
178000
14800
6890
3420
2110
1530
1170
1030
0—6,000
Cumulative Pore Volume, %
820
570
435
350
310
265
230
200
0—60,000
Cumulative Pore Volume, %
148
82
57
44
35
30
25
21
Pore Radius (Angs)
REACTED
UNREACTED

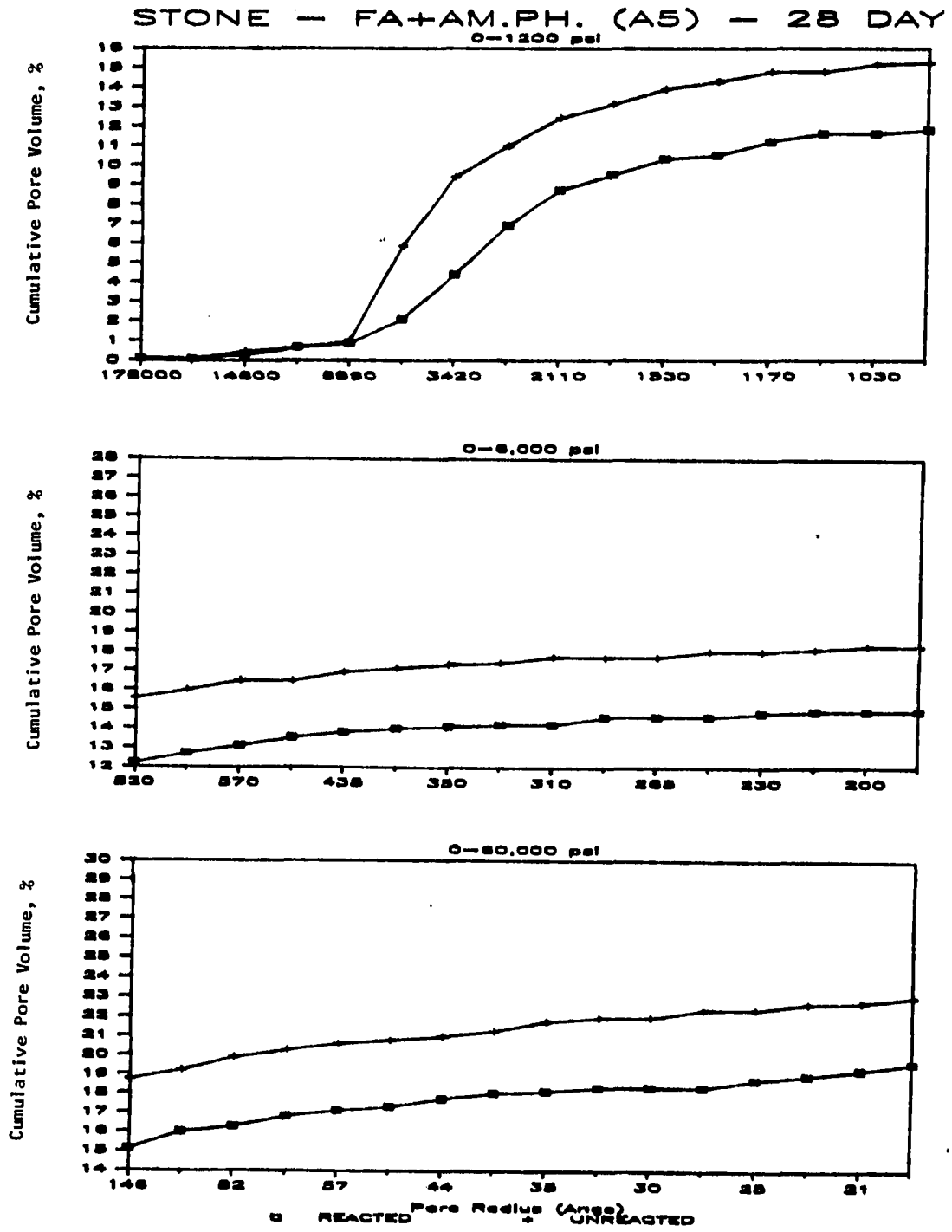
STONE — FA+AM.PH. (A5) — 28 DAY
0—1200 psi
Cumulative Pore Volume, %
178000
14800
6890
3420
2110
1530
1170
1030
0—6,000 psi
Cumulative Pore Volume, %
820
570
438
350
310
268
230
200
0—60,000 psi
Cumulative Pore Volume, %
146
82
57
44
38
30
25
21
Pore Radius (Angs)
REACTED
UNREACTED

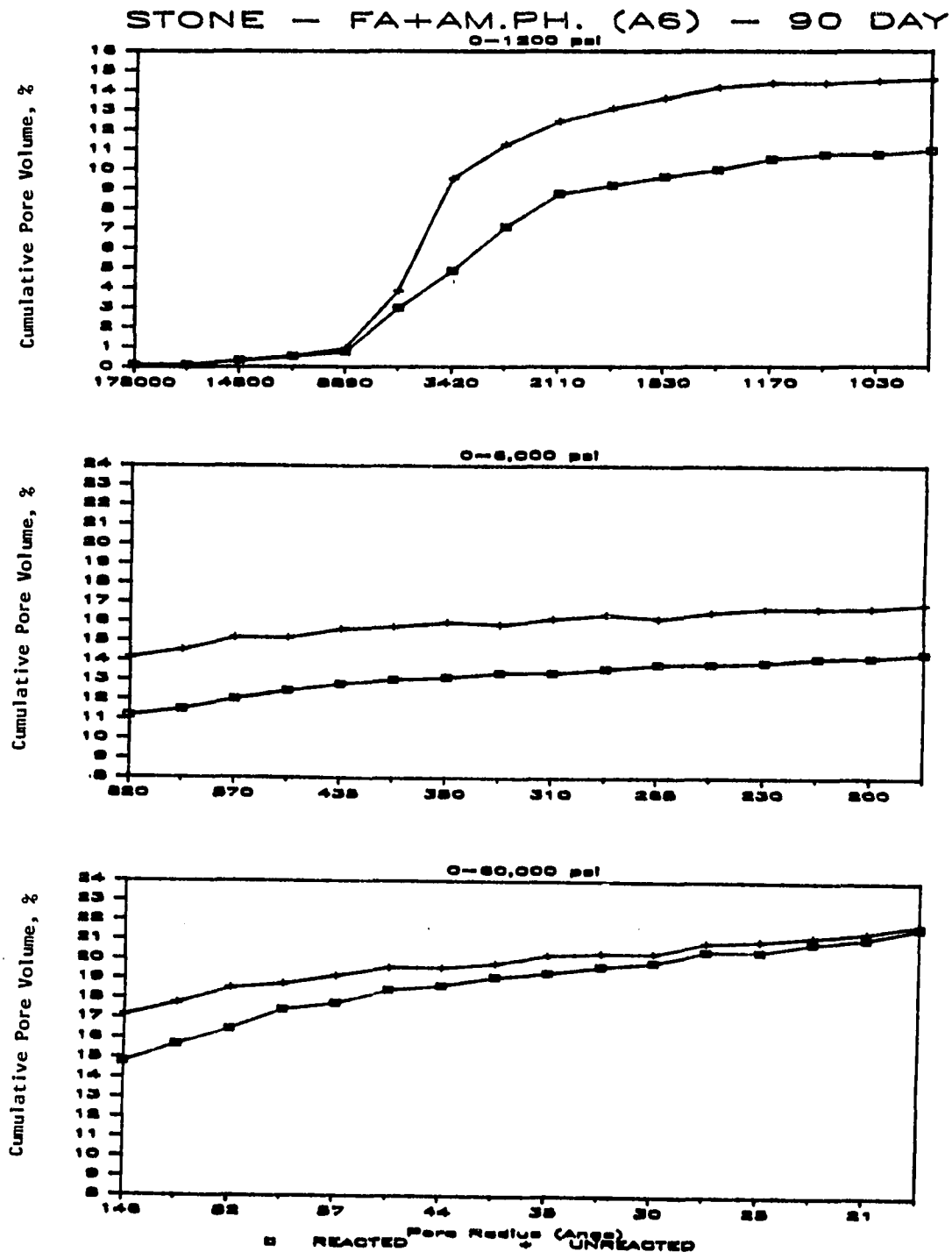
STONE — FA+AM.PH. (A6) — 90 DAY
0-1200 psi
Cumulative Pore Volume, %
178000
14800
3420
2110
1830
1170
1030
0-6,000 psi
Cumulative Pore Volume, %
870
435
380
310
230
0-60,000 psi
Cumulative Pore Volume, %
148
87
44
35
30
25
21
Pore Radius (Angs)
REACTED
UNREACTED

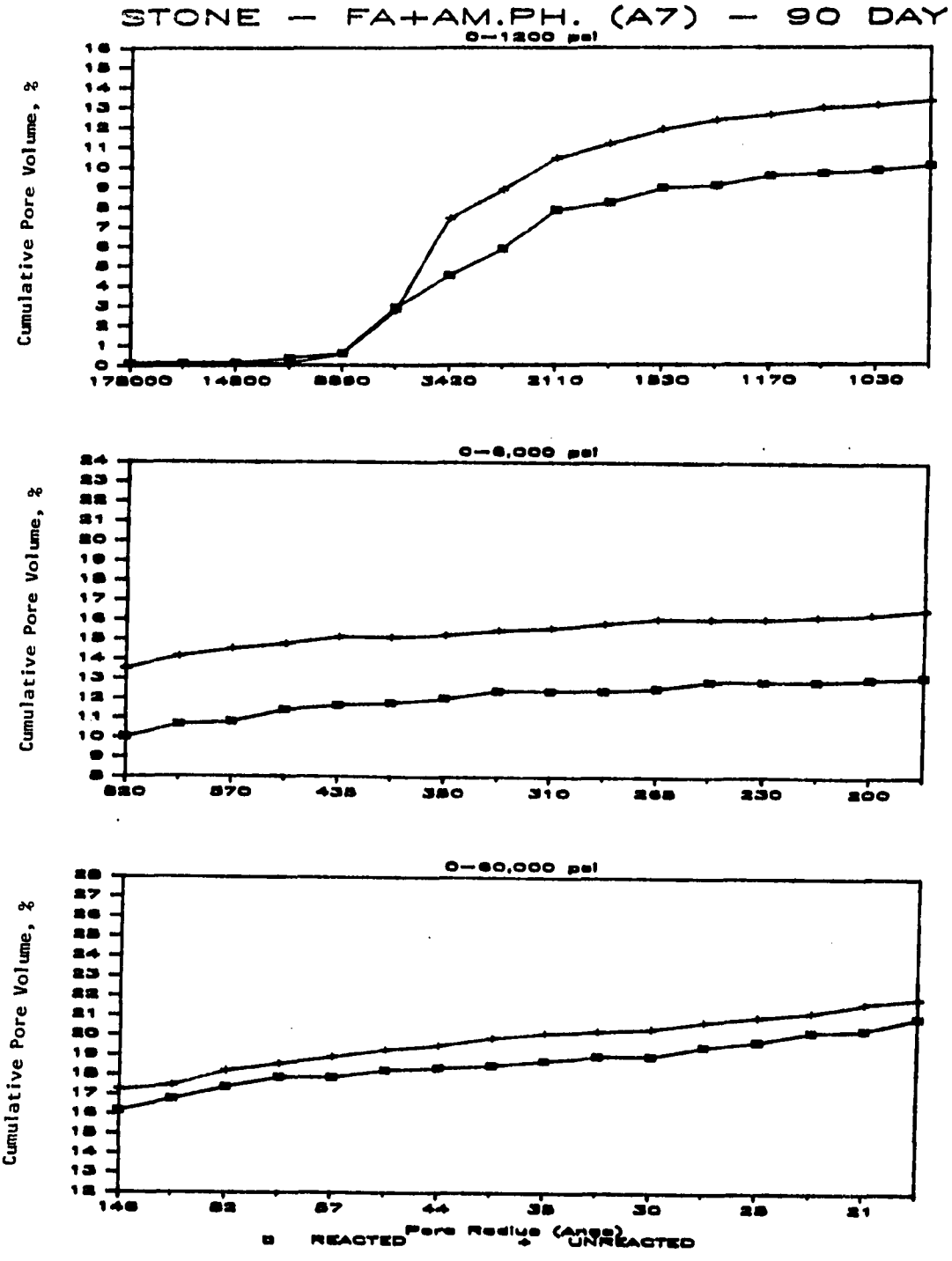
STONE — FA+AM.PH. (A7) — 90 DAY
0—1200 psi
Cumulative Pore Volume, %
178000
14800
8890
3420
2110
1830
1170
1030
0—6,000 psi
Cumulative Pore Volume, %
820
570
435
350
310
265
230
200
0—60,000 psi
Cumulative Pore Volume, %
148
82
57
44
35
30
25
21
Pore Radius (Angs)
REACTED
UNREACTED

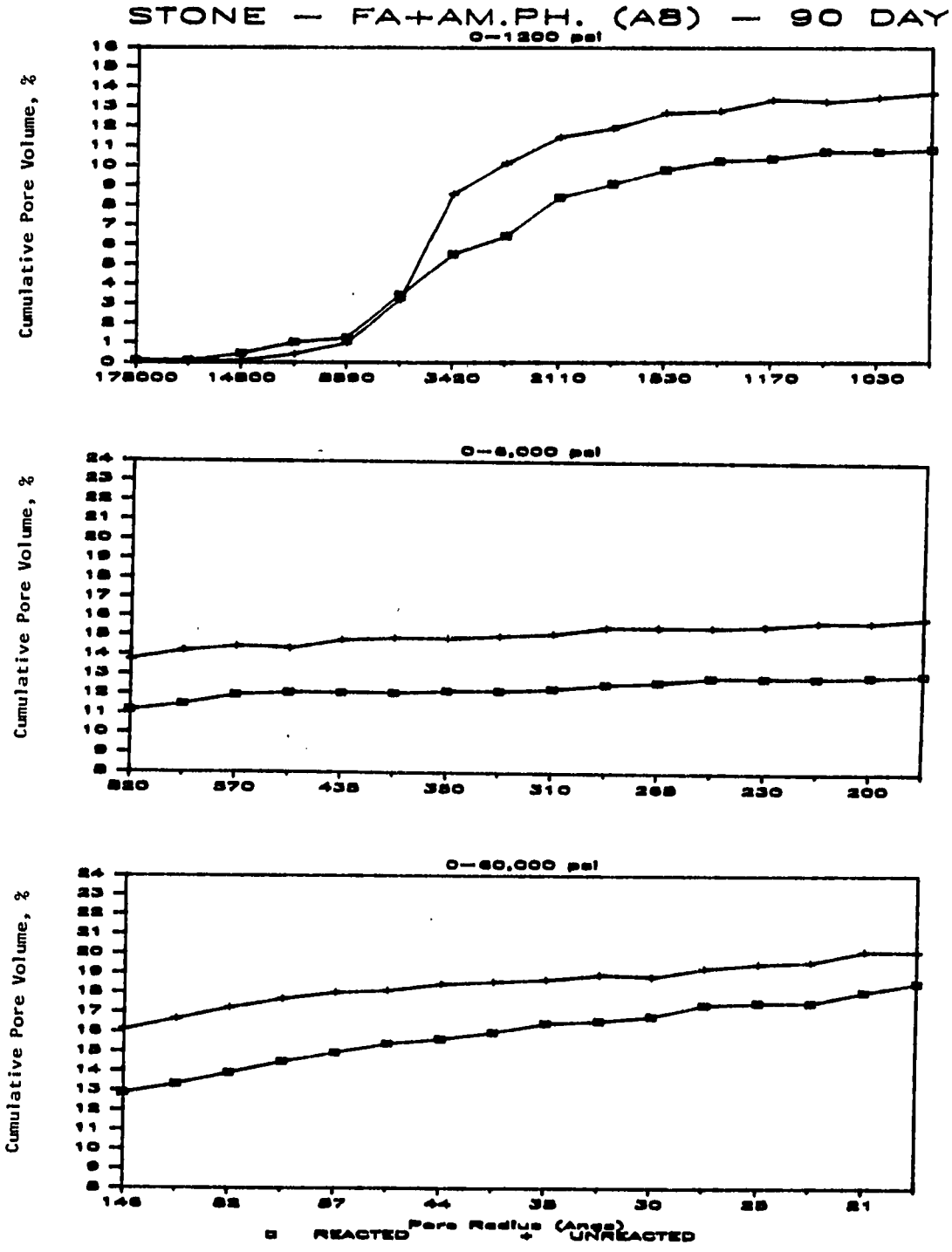
STONE — FA+AM.PH. (A8) — 90 DAY
0—1200 psi
Cumulative Pore Volume, %
178000 14800 8890 3420 2110 1830 1170 1030
0—6,000 psi
Cumulative Pore Volume, %
820 570 438 360 310 268 230 200
0—60,000 psi
Cumulative Pore Volume, %
148 82 57 44 35 30 28 21
Pore Radius (Angs)
REACTED
UNREACTED

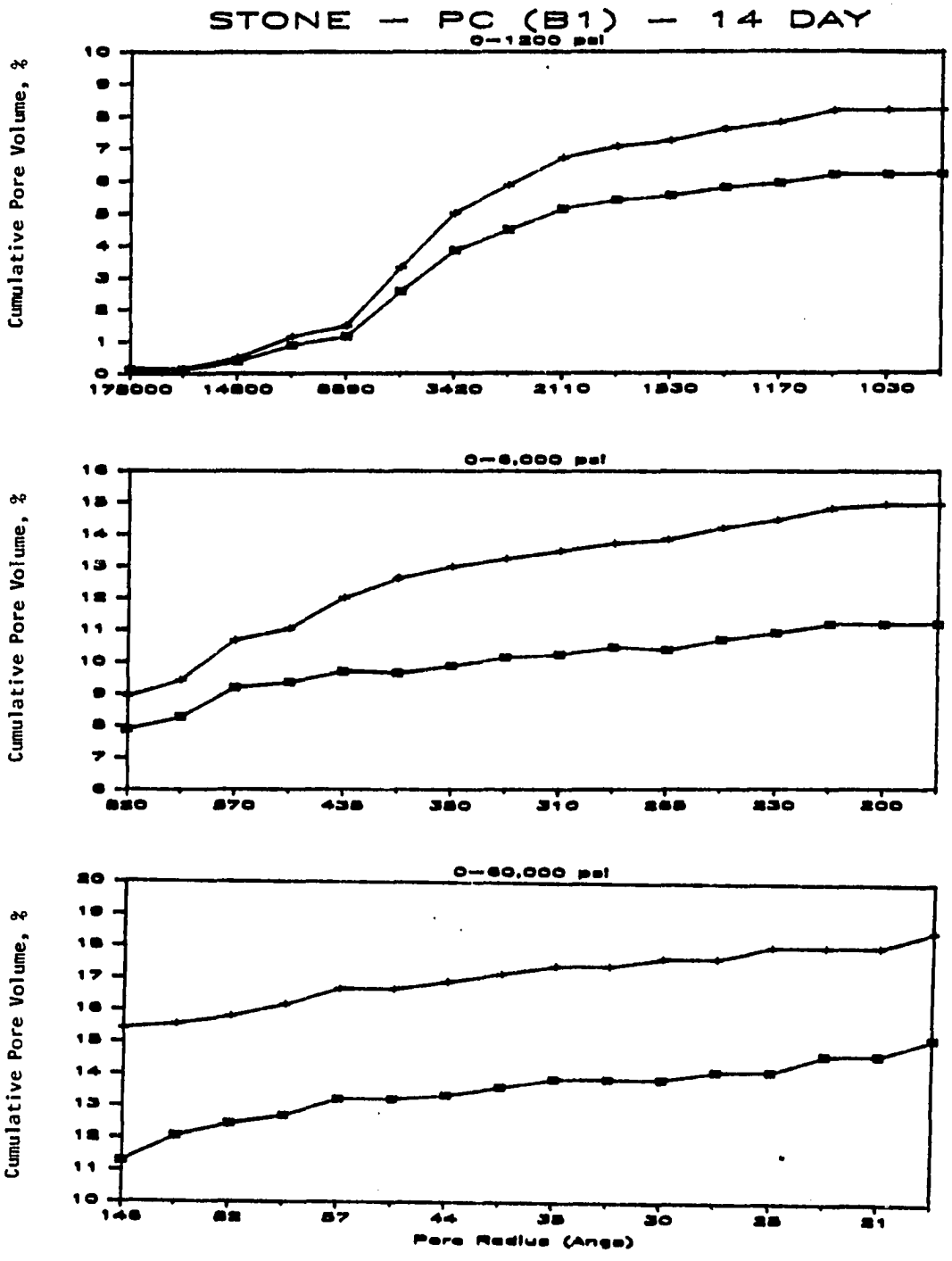
STONE — PC (B1) — 14 DAY
0—1200 psi
Cumulative Pore Volume, %
0
1
2
3
4
5
6
7
8
9
10
178000
14800
6890
3420
2110
1530
1170
1030
0—6,000 psi
Cumulative Pore Volume, %
6
7
8
9
10
11
12
13
14
15
16
870
438
310
200
0—60,000 psi
Cumulative Pore Volume, %
10
11
12
13
14
15
16
17
18
19
20
148
87
44
35
30
25
21
Pore Radius (Angs)

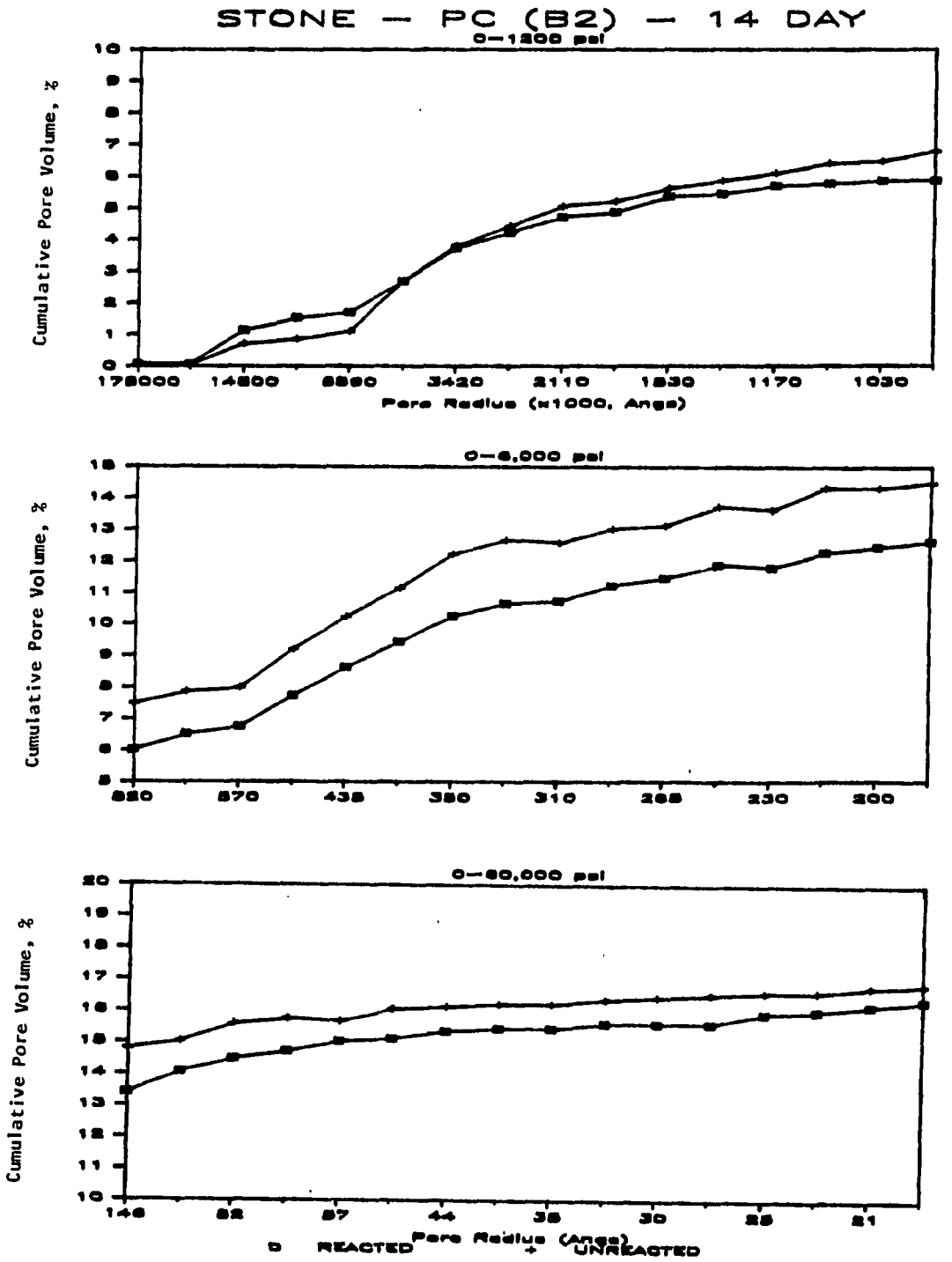
STONE — PC (B2) — 14 DAY
0—1500 psi
Cumulative Pore Volume, %
178000
14800
8890
3420
2110
1830
1170
1030
Pore Radius (x1000, Angs)
0—6,000 psi
Cumulative Pore Volume, %
850
570
435
350
310
265
230
200
0—60,000 psi
Cumulative Pore Volume, %
148
82
57
44
35
30
25
21
Pore Radius (Angs)
REACTED
UNREACTED

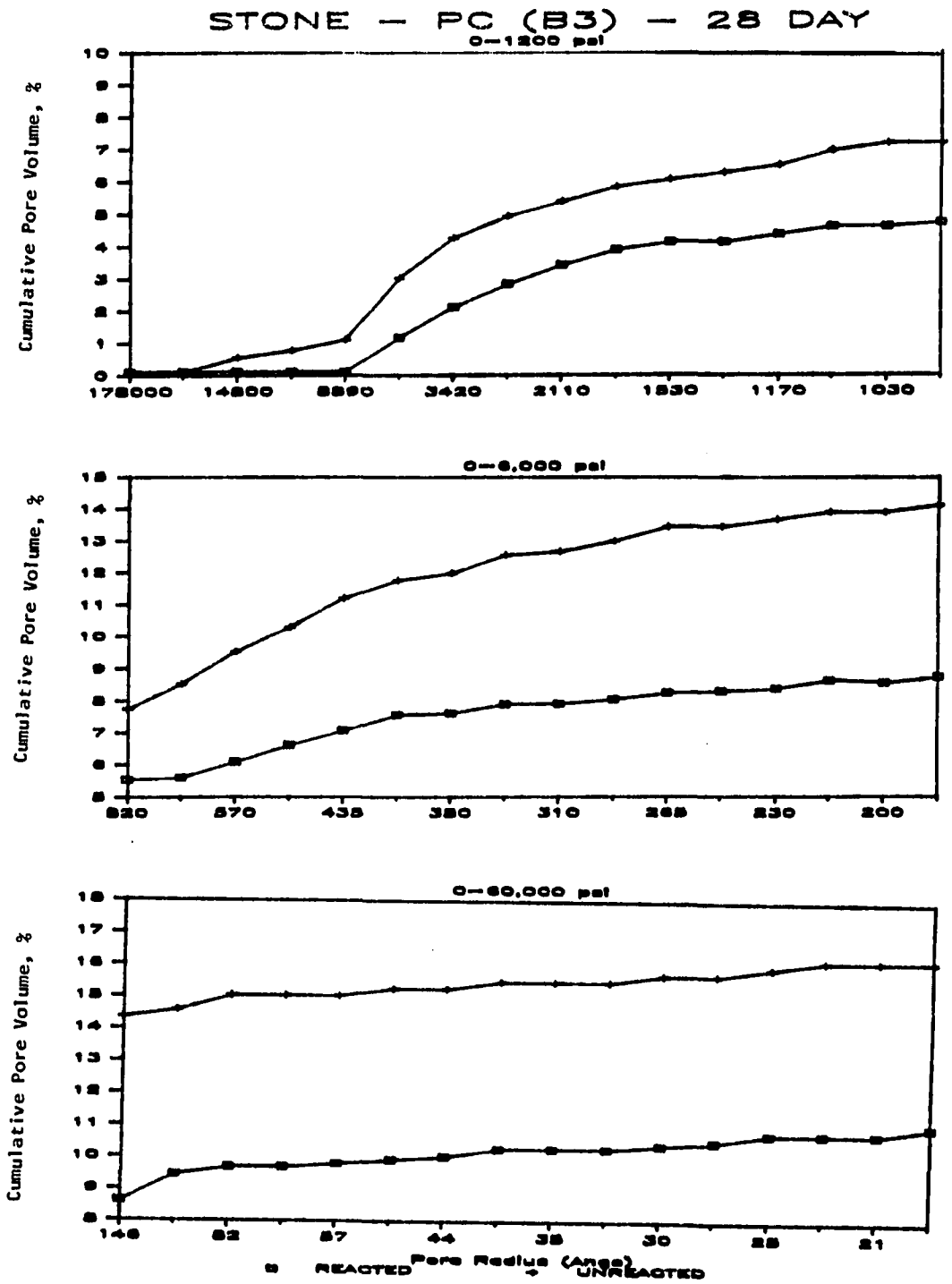
STONE — PC (B3) — 28 DAY
0—1200 psi
Cumulative Pore Volume, %
178000
14800
8890
3420
2110
1530
1170
1030
0—6,000 psi
Cumulative Pore Volume, %
820
570
435
350
310
265
230
200
0—60,000 psi
Cumulative Pore Volume, %
148
82
57
44
35
30
25
21
Pore Radius (Angs)
REACTED
UNREACTED

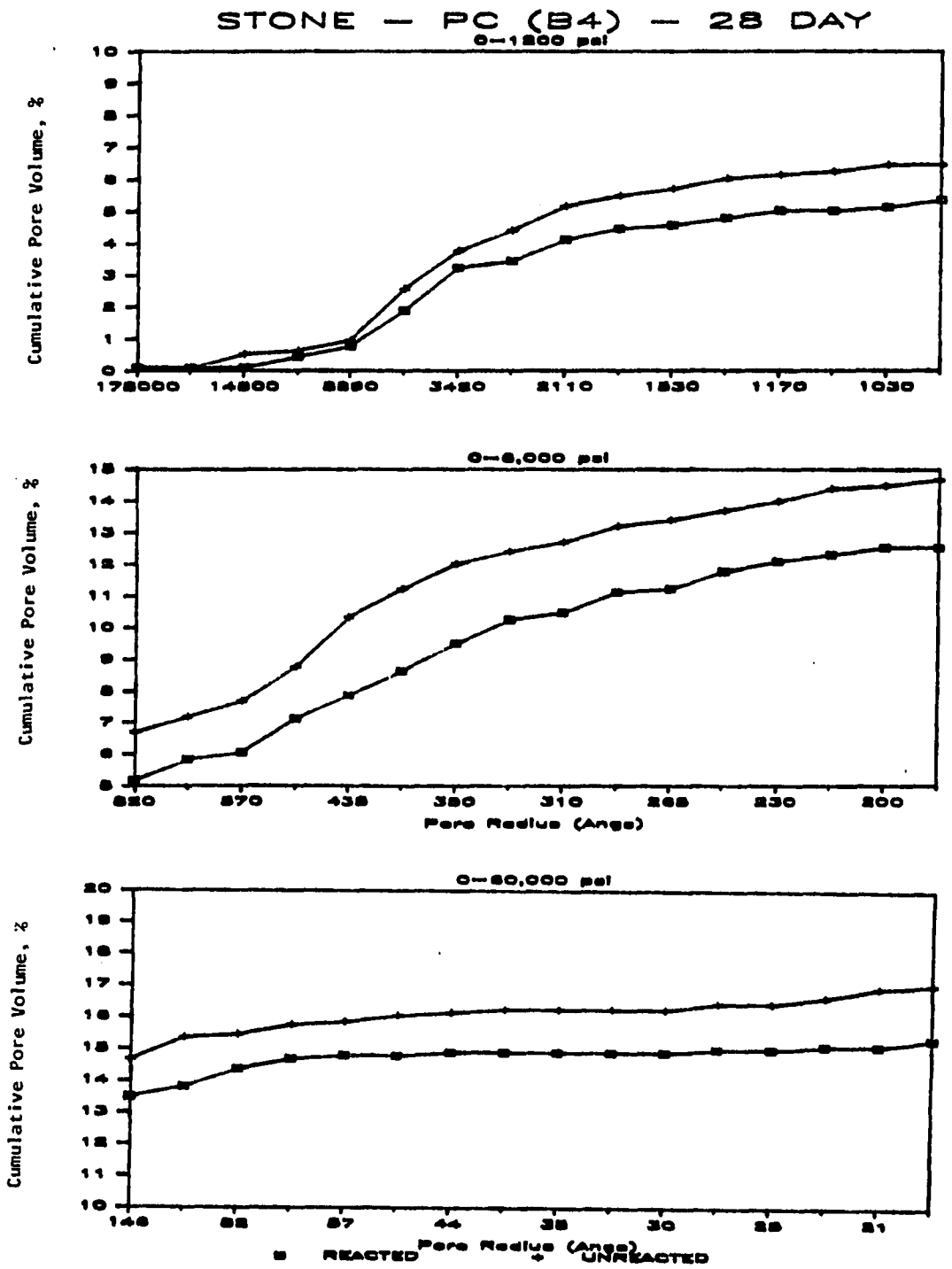
STONE — PC (B4) — 28 DAY
0—1200 psi
Cumulative Pore Volume, %
178000
14800
8890
3420
2110
1530
1170
1030
0—6,000 psi
Cumulative Pore Volume, %
820
570
438
350
310
268
230
200
Pore Radius (Angs)
0—60,000 psi
Cumulative Pore Volume, %
148
88
57
44
38
30
25
21
Pore Radius (Angs)
REACTED
UNREACTED

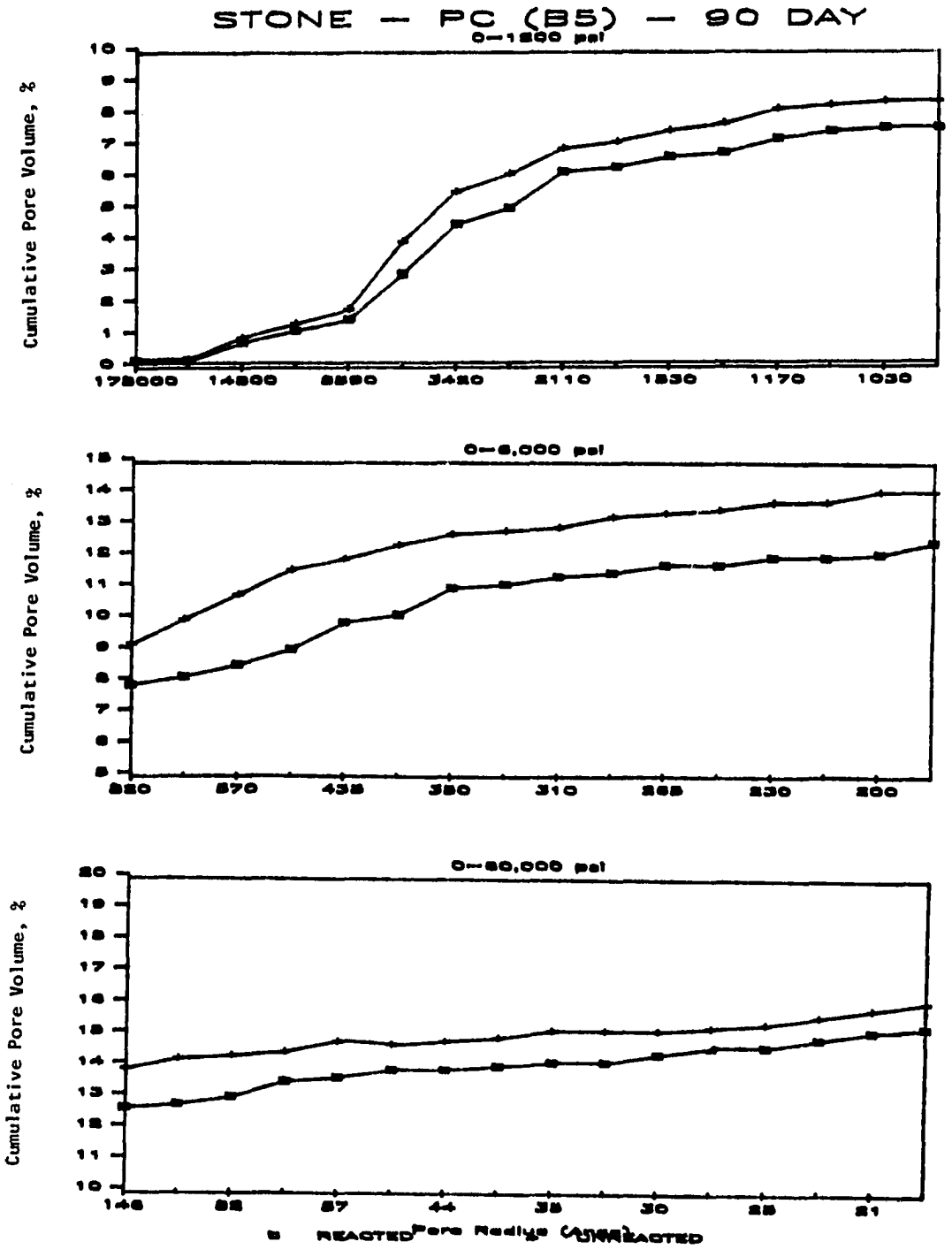
STONE — PC (B5) — 90 DAY
0—1,500 psi
Cumulative Pore Volume, %
0—6,000 psi
Cumulative Pore Volume, %
0—60,000 psi
Cumulative Pore Volume, %
% REACTED
Pore Radius
UNREACTED

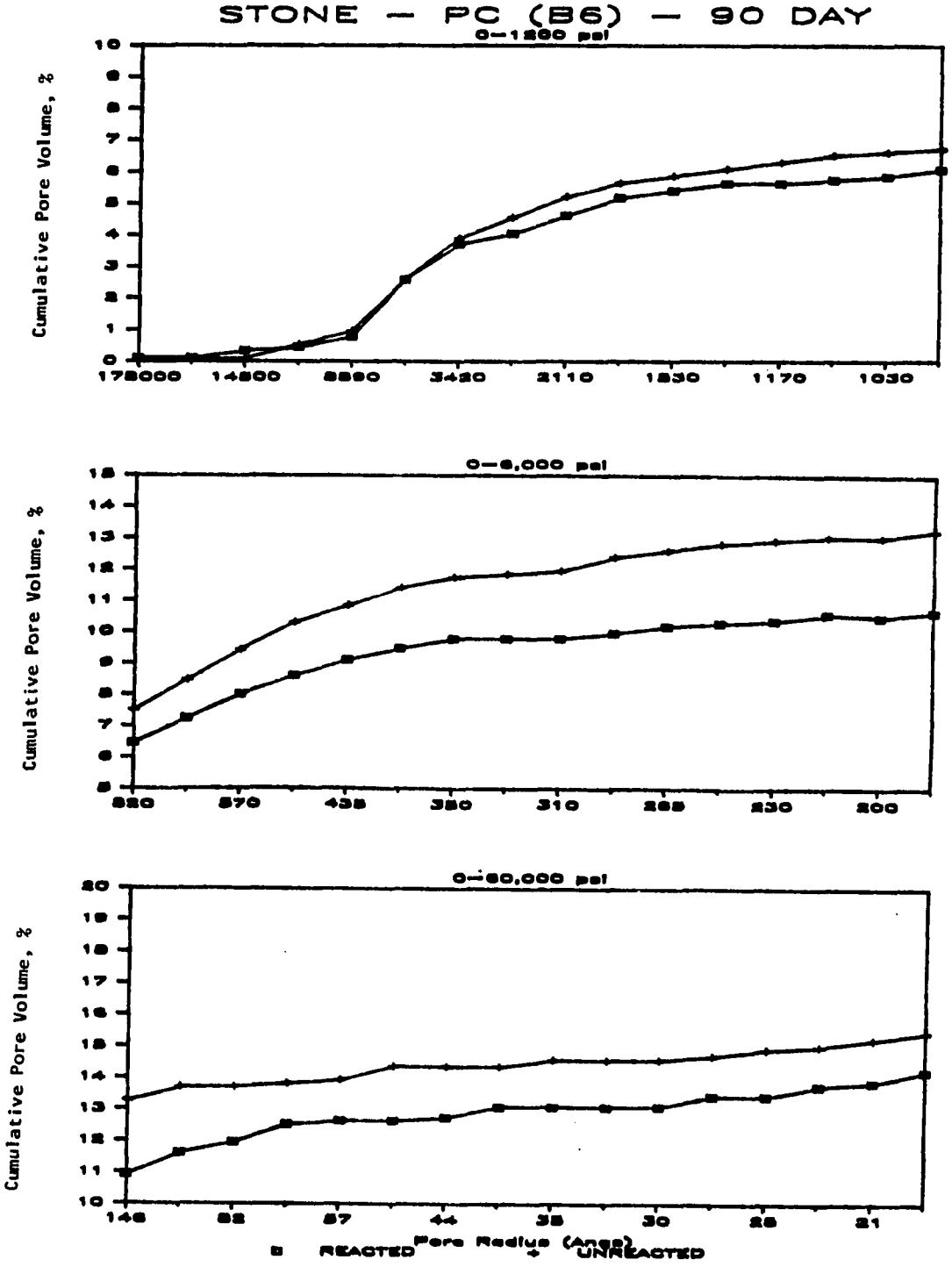
STONE — PC (B6) — 90 DAY
0—1,200 psi
Cumulative Pore Volume, %
178000
14800
8890
3420
2110
1830
1170
1030
0—6,000 psi
Cumulative Pore Volume, %
820
570
435
350
310
265
230
200
0—60,000 psi
Cumulative Pore Volume, %
146
82
57
44
35
30
25
21
Pore Radius (Angs)
REACTED
UNREACTED